GEDIZ UNIVERSITY ★ GRADUATE SCHOOL OF SCIENCE ENGINEERING AND TECHNOLOGY

IN VITRO ASSESSMENT OF ANTIBODY CONJUGATED GOLD NANORODS FOR BIOMEDICAL APPLICATIONS

M.Sc. THESIS

Gülşah MALGIR

Institute of Science

Nanotechnology Graduate Programme

Thesis Advisor: Assistant Prof. Dr. Hadi M. ZAREIE

DECEMBER, 2013

GEDIZ UNIVERSITY ★ GRADUATE SCHOOL OF SCIENCE ENGINEERING AND TECHNOLOGY

IN VITRO ASSESSMENT OF ANTIBODY CONJUGATED GOLD NANORODS FOR BIOMEDICAL APPLICATIONS

Msc. THESIS

Gülşah MALGIR

(60071104)

Institute Of Science

Nanotechnology Graduate Programme

Thesis Advisor: Assist. Prof. Dr. Hadi M. ZAREIE

DECEMBER, 2013

GEDİZ ÜNİVERSİTESİ ★ FEN BİLİMLERİ ENSTİTÜSÜ

BİYOMEDİKAL UYGULAMALAR İÇİN ANTİKOR BAĞLI GOLD NANORODLARIN *IN VITRO* DEĞERLENDİRİLMESİ

YÜKSEK LİSANS TEZİ

Gülşah MALGIR
(60071104)

Fen Bilimleri Enstitüsü

Nanoteknoloji Yüksek Lisans Programı

Tez Danışmanı: Yrd. Doç. Dr. Hadi M. ZAREIE

ARALIK, 2013

Gülşah Malgır, a **M.Sc.** student of GU **Institute of Science** student ID 60071104, successfully defended the **thesis** entitled *"IN VITRO* ASSESSMENT OF ANTIBODY CONJUGATED GOLD NANORODS FOR BIOMEDICAL APPLICATIONS" which she prepared after fulfilling the requirements specified in the associated legislations, before the jury whose signatures are below.

Thesis Advisor : Assistant Prof. Dr. Hadi M. ZAREIE   ....
                    Izmir Institute of Technology

Jury Members : Assistant Prof. Dr. Hadi M. ZAREIE   ....
                    Izmir Institute of Technology

                    Prof. Dr. M. Emin Şengün ÖZSÖZ   ....
                    Gediz University

                    Assoc. Prof. Dr. Yusuf BARAN   ....
                    Izmir Institute of Technology

To my parents and brother,

ACKNOWLEDGEMENT

December 2013   Gülşah MALGIR
                                                                         Bioengineer

TABLE OF CONTENTS

ABBREVIATIONS

CTAB	:	Cethyltrimethyl Ammonium Bromide
DLS	:	Dynamic Light Sacttering
DMSO	:	Dimethyl Sulfoxide
EDC	:	1-ethyl-3-(3-dimethylaminopropyl)carbodiimide) hydrochloride
GNR	:	Gold Nanorod
MHDA	:	Mercaptohexadecanoic acid
MM	:	Multiple Myeloma
MTT	:	1-(4,5-dimethylthiazol-2-yl)-3,5-diphenylformazan
NHS	:	N-hydroxysulfosuccinimide
PAGE	:	Polyacrylamide gel electrophoresis
PBS	:	Phosphate Buffer Saline
PEG	:	Polyethylene glycol
SDS	:	Sodium dodecyl sulfate
UP	:	Ultra Pure
TEMED	:	Tetramethylethylenediamine

LIST OF TABLES

LIST OF FIGURES

IN VITRO ASSESSMENT OF ANTIBODY CONJUGATED GOLD NANORODS FOR BIOMEDICAL APPLICATIONS

ABSTRACT

The strong absorption and scattering light of gold nanorods in near infrared region (650-900 nm) have gained a great deal of interest in biomedicine. The optical properties of gold nanorods with controllable aspect ratios, enable researchers to utilize them for phothermal cancer therapy selectively. In other words, they are capable of converting light to heat and in this manner, selectively targeted gold nanorods open a new window into the cancer treatement by taking advantages over current therapy techniques that are detrimental to healthy cells while treating cancer. For these reasons, the main focuse of this research is the use of actively targeted gold nanorods for photothermally destruction of Multiple Myeloma, one of the most common cancer types worldwide.

First, gold nanorods were fabricated via seed mediated method and functionalized with polyethylene glycol (PEG) (MW 1000) which is FDA approved molecule, prior to cellular assays. The characterization of original and PEG coated gold nanorods was performed via AFM, SEM, ultraviolet visible spectroscopy and dynamic light scattering (DLS) measurements.

Anti-CD138 (anti-Syndecan-1) monoclonal antibodywhich has affinity to CD138 receptors over expressed on the cytoplasmic membrane of multiple myeloma cells, was used to conjugate to gold nanorods for active targeting. Nanorods were examined in the cell culture with two different multiple myeloma cell lines (CD138 positive U266 cell line and CD138 negative ARH-77 cell line) to observe the impression of gold nanorods in specifically targeted therapy.

The cytotoxic effects of original and PEG modified gold nanorods on both cell lines were tested via MTT assay. Further, the apoptotic effects of originally prepared gold nanorods were tested via Annexin V assay. The number of PEG coated and anti-CD138 conjugated gold nanorods internalized by U266 and ARH-77 cell line was measured by ICP-MS.

Finally, both cell lines exposed to PEG coated gold nanorods and anti-CD138 conjugated gold nanorods were irradiated with 633 nm red laser for selective photothermal therapy. The results found in this preliminary research will shed light on the cure of Multiple Myeloma *in vivo* and clinic based therapy as a novel approach.

Keywords : Gold nanorods; Multiple myeloma; Photothermal Therapy; Seed mediated method

BİYOMEDİCAL UYGULAMALARDA ANTİKOR BAĞLI GOLD NANORODLARIN *IN VITRO* DEĞERLENDİRİLMESİ

ÖZET

Gold nanorodların NIR bölgede (650-900 nm) ışığı güçlü bir şekilde içlerine hapsetmeleri ve saçmaları bu eşsiz nanoparçacıkların son zamanlarda biyomedikal uygulamalarda kullanımı açısından önem arz etmektedir. Eşsiz optik özellikleri ve istenilen boyutlarda üretilebilmesi nedeniyle, gold nanorodlar, kanserin spesifik olarak fototermal tedavisinde, araştırmacılara olanak sağlamaktadır. Bir başka deyişle, gold nanorodlar ışığı ısıya dönüştürme potansiyelindedirler ve bu bağlamda spesifik olarak hedeflenerek, günümüzde uygulanan ve kanserli hücreleri tedavi ederken çevredeki sağlıklı hücrelere de zarar veren tedavi yöntemlerine nazaran kanser tedavisinde oldukça avantajlı hale gelmektedir.

Bu araştırmanın temel amacı; dünya genelinde oldukça yaygın bir kanser türü olan plazma hücre kanserinin fototermal tedavisi için aktif hedeflenmiş gold nanorodların kullanılmasıdır. Bunun için öncelikle gold nanorodlar, çekirdek aracılıklı metot ile sentezlenmiş ve hücre kültürü çalışmalardan önce yüzeyleri biyouyumlu ve FDA (Food Drug Association) onaylı bir polimer olan bifonksiyonel PEG ile modifiye edilmiştir. Sentezlenmiş ve PEG ile modifiye edilmiş gold nanorodların karakterizasyonu ise SEM, AFM, DLS ve UV spektroskopisi ile yapılmıştır.

Plazma kanser hücrelerinin sitoplazmik membranında aşırı üretilen CD138 reseptörlerine karşı afinitesi olan anti-CD138 monoklonal antikoru, aktif hedefleme için gold nanorodlara bağlanmıştır. Seçici hedeflemedeki etkinliğini gözlemek amacıyla iki farklı plazma kanseri hücre hattı (CD138 üreten U266 hücre hattı ve CD138 üretmeyen ARH-77 hücre hattı) kullanılarak gold nanorodların hücre kültüründe inkübasyonu yapılmıştır. Sentezlenmiş olan ve yüzeyi PEG ile modifiye edilen gold nanorodların her iki hücre hattı üzerindeki sitotoksik etkileri MTT analizi ile test edilmiştir. Aynı zamanda çeşitli konsantrasyonlarda sentezlenmiş olan orjinal gold nanorodların her iki hücre hattı üzerindeki apoptotik etkisini görmek için ise Annexin V analizi yapılmıştır.

PEG modifiye ve anti-CD138 monoklonal antikoru bağlı gold nanorodların hücresel alımı da ICP-MS cihazı kullanarak analiz edilmiştir. Son olarak, PEG modifiye ve anti-CD138 antikoru bağlı gold nanorodlara maruz bırakılan her iki hücre hattı, seçici fototermal terapi için 633 nm dalga boyunda kırmızı lazer ile radyasyona maruz bırakılmıştır.

Bu ön çalışmada bulunan sonuçlar yeni bir yaklaşım olarak, plazma hücre kanserinin *in vivo* çalışmalarına ve klinik tedavisine ışık tutacaktır.

Anahtar kelimeler: Gold nanorod; Plazma hücre kanseri; Çekirdek aracılıklı metot; Fototermal terapi.

1. INTRODUCTION

1.1 Literature Review

In recent years, there has been a remarkable increase in the use of metal nanoparticles for biomedical applications. The nanoparticles with plasmon resonance property can be modified with biological molecules to provide both diagnostic and photothermal treatment advantages. For instance; iron oxide nanocrystals have been used for magnetic resonance imaging (Harisinghani, Barentsz et al. 2003, McCarthy, Kelly et al. 2007). Furthermore, magnetic nanoparticles conjugated to small interfering RNA (siRNA) are substantial materials for SiRNA delivery (Woodle and Lu 2005, Medarova, Pham et al. 2007).

Since nanoparticles have mesoscopic size range of 10-100 nm diameter and have significantly larger surface areas with respect to larger size particles, they are advantageous in diagnosis and treatment of diseases in early phase.

Among metal particles, gold is the most preferable metal because of its non-toxic nature and unique size–shape dependent properties (C, Kumar et al. 2012). Gold nanoparticles can be produced by applying different preperation techniques to obtain various kinds of shapes including spheres (Turkevich, Stevenson et al. 1951, Frens 1972), nanorods (Jana, Gearheart et al. 2001).

Gold nanorods, which show strong absorption and scattering of light in the near-infrared region depending on their surface plasmon oscillations have been investigated as potential therapeutic agents (Jana, Gearheart et al. 2001). The more strong absorption of the light, the higher the thermal energy is. In other words, the strong absorption of light in the near infrared region enables nanorods to emit more heat. This emitted heat can be used effectively for drug release at a targeted site without damaging surrounding tissues (Kim, Ghosh et al. 2009). Several studies have proved that longitudinal surface plasmon resonance is prone to change due to the aspect ratio which is the ratio of length to width. With the increase in the aspect ratio, red shift occurs in the longitudinal absorption band of gold nanorods (Link and El-Sayed 1999, Lee and El-Sayed 2006) When gold nanorods are compared with gold nanospheres, longitudinal surface plasmons are affected from local dielectric field more than those of spherical nanoparticles.

Gold nanorods exhibit two plasmon resonances, one is transverse peak due to the transverse electronic oscillation and the other is longitudinal peak due to the longitudinal oscillation of conduction band electrons (Papavassiliou 1979) (Link and El-Sayed 2000). This property enables the photothermal ablation of cancer cells using gold nanorods: If laser is applied to the cancer tissue containing gold nanorods, the nanorods absorb the light and convert it to heat energy killing the surrounding cancer cells through photothermal effect.Theoretical calculations through temperature distribution in photothermal active threapy have shown the significance of pulsed laser source for effective heating (Prasad, Mikhailovsky et al. 2005, Keblinski, Cahill et al. 2006). The interaction of gold nanorods with femtosecond laser results in photothermal impacts such as (1) an increase in the electron temperature, through electron-electron scattering, within several hundred fs; (2) an increase in the lattice temperature, distribution of heat from the gold nanorods to the surrounding media to reach thermal equilibrium within 100 ps to several ns, relevant to the particle size, thermal properties of the surroundings, and laser intensity (Huang, Neretina et al. 2009, Hartland 2011).

1.2 Synthesis Of Gold Nanorods

Several synthesis methods have been developed in order to synthesize gold nanorods at high yields.

The first method for the production of gold nanorods was template method, introduced first by Martin and his colleagues (Foss Jr, Hornyak et al. 1994, Martin 1996). This method depends on the collection of golds within the porous membrane which is mostly made of polycrbonate or alumina. Briefly, gold nanoparticles are deposited on porous membranes and after deposition of golds, porous membranes, Cu or Ag are dissolved in a polymeric stabilizer such as poly (vinylprolinone). As it is shown in Figure 1.1, in order to enable electrodeposition, it is necessary to use a conductive template such as Cu or Ag metals. Finally, gold nanorods are dispersed in water or organic solvents by using sonication or agitation (Perez-Juste, Pastoriza-Santos et al. 2005).
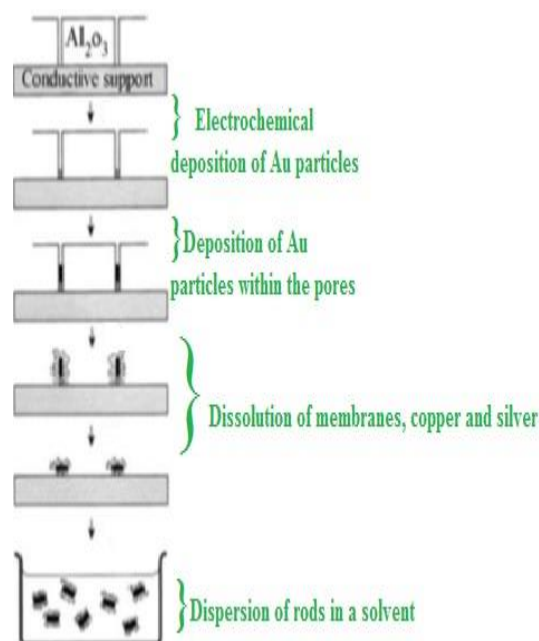
Figure 1.1 : Shematic representation of growth of gold nanorods with template method (van der Zande, Böhmer et al. 2000).

It is possible to form nanorods with different size and lengths via template method (see Figure 1.1) Size and diameter of synthesized gold nanorods can be tuned by adjusting the diameter of the pores of the membrane (van der Zande, Böhmer et al. 2000). But, in this technique one challenging issue is that the preperation of rod clusters are very difficult in terms of production yield.

The second synthesis approach is electrochemical approach which was first reported by Wang and his co-workers, is based on the use of two-electrode type electrochemical cell in which the gold source is used as a supporter for the reaction, while platinum plate is used as cathode. In this technique, $C_{16}TAB$ with its hydrophobic regions and tetradodecylamonium bromide ($TC_{12}AB$) as a rod inducing surfactant are used as a mixed surfactant system. Small ammounts of reagents are added to the mixed solution. Acetone is used for cylindyrical reshaping of nanorods whereas cyclohexane is used for the increase in the elongation of rod like micelles (Toernblom, Henriksson et al. 1994).

Gold nanorods generated by using electrochemical method is shown in Figure 1.2.
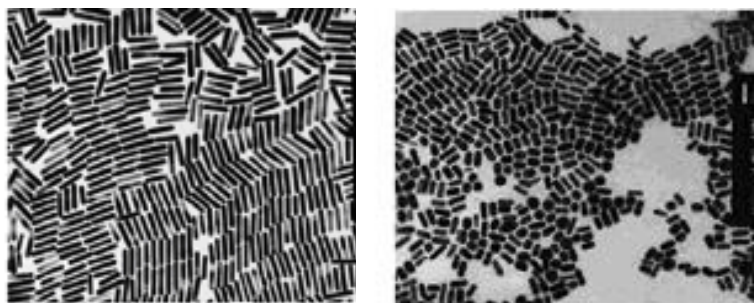
Figure 1.2 : TEM images of gold nanorrods with different aspect ratios synthesized by electrochemical method (Chang, Shih et al. 1999).

It was proved that silver plate behind platinum cathode was substantial for obtaining different aspect ratios of gold nanorods (Aspect ratio: length/width). The redox reaction occured from gold anode to silver plate leaded to the formation of silver ions. It was also illustrated by Wang and co-workers that concentration and formation rate of silver ions within the electrolytic solution were effective on the length of gold nanorods (Perez-Juste, Pastoriza-Santos et al. 2005).

Electrochemical process needs sonication stage. It was therefore limited to determine the exact effect of silver on gold nanorod synthesis. Also, control of the electric field makes this process complex and difficult (Kim, Song et al. 2002).

The most commonly used approach for the formation of gold nanorods at high yields is the seed-mediated method also known as wet chemical technique (Figure 1.3). This method has been reported by several authors with modifications on some steps.
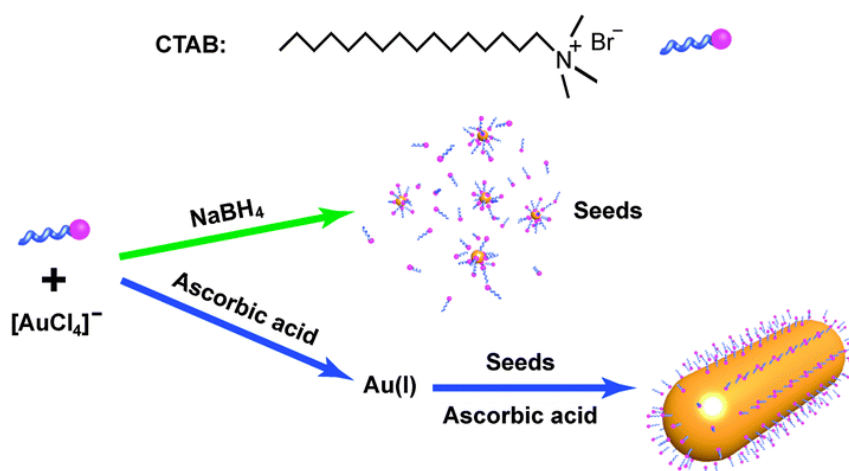
Figure 1.3 : Schematic illustration of the synthesis of gold nanorods in the existance of chemicals shown above (Chen, Shao et al. 2013).

This technique allows to produce nanorods at low cost. Further, it is possible to prepare nanoparticles in terms of well-controlled composition, shape and size (Perez-Juste, Pastoriza-Santos et al. 2005). Although wet chemistry technique has some advantages over other existing methods, scientists who study on nanoparticles, cast doubt on the accurate growth mechanism (Sau and Murphy 2004). Anyway, it has received a great deal of attention in nanotechnology field.

Wet chemistry technique was first demonstrated by Murphy et al. (Jana, Gearheart et al. 2001). In their studies, Murphy and co-workers modified electrochemical technique by using gold as chloroauric acid instead of gold electrode. CTAB was also used as a stabilizing agent with the addition of acetone and cyclohexane chemicals for reshaping of gold nanorods. Ascorbic acid is used as a weak reducing agent which only reduces Au^{+3} to Au^{+1}. Complete reduction of metallic gold can be provided by using seed particles which are 3 nm in diameter. Seed particles are formed in the presence of sodium borohydrate as strong reducing agent added to CTAB-chloroauric acid mixture (Perez-Juste, Pastoriza-Santos et al. 2005).

External factors such as temperature and pH are effective parameters which should be controlled during growth process. In one study, it was shown that at low pH conditions, ascorbic acid was not capable of reducing gold salt (Pal, De et al. 1998).

High temperature conditions also led to the formation of high aspect ratio of gold nanorods during growth process. Perez- Juste et al. showed that reduction of temperature and CTAB concentration gave rise to the synthesis of gold nanorods with short aspect ratio (Hubert, Testard et al. 2010). It was also found that changes in the concentrations of the reactants during growth progress yielded gold nanorods in various size and diameters (Vigderman, Khanal et al. 2012) Researchers have investigated the rod formations either in the absence or presence of silver nitrate. Murphy and co-workers experimented that the presence of small amount of silver nitrate triggered to the formation of spheroid and shorther nanorods (Figure 1.4) (Jana, Gearheart et al. 2001).
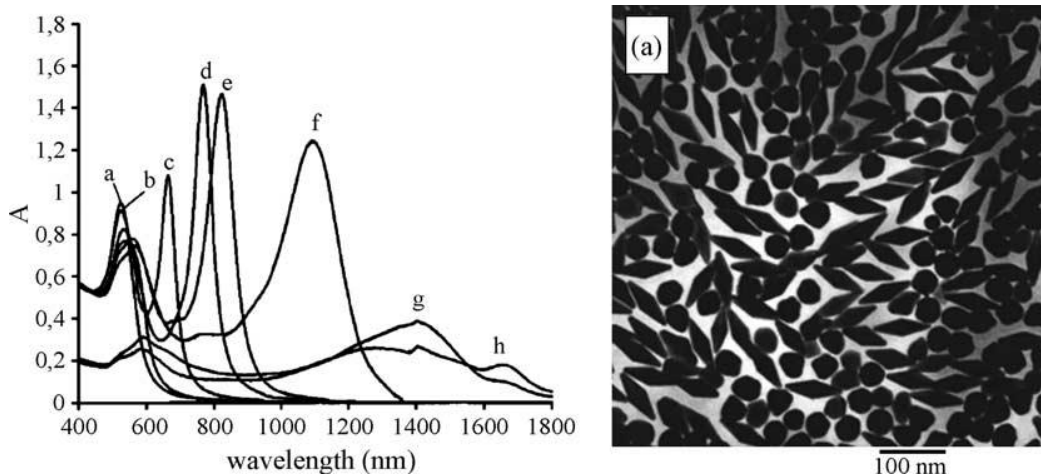
Figure 1.4 : UV spectrum of gold nanorods synthesized with increasing aspect ratios by decreasing seed amount added to the growth solution and TEM images of gold nanorods synthesized in the presence of small amount of silver nitrate (Jana, Gearheart et al. 2001).

Photochemical approach for the synthesis of gold nanorods was first demonstrated in 2002 by Kim and his colleagues. These researchers found that it was possible to produce uniform gold nanorods in the presence of silver nitrate. This process has some similarities with electrochemical approach. The main difference is the use of UV-light to enable reduction reactions (Kim, Song et al. 2002). Briefly, silver nitrate in the growth solution was exposed to UV light at 254 nm for 30 h. Solution was centrifuged and redispersed in water. The colour of the solution was indicative for gold nanorods with different aspect ratios.
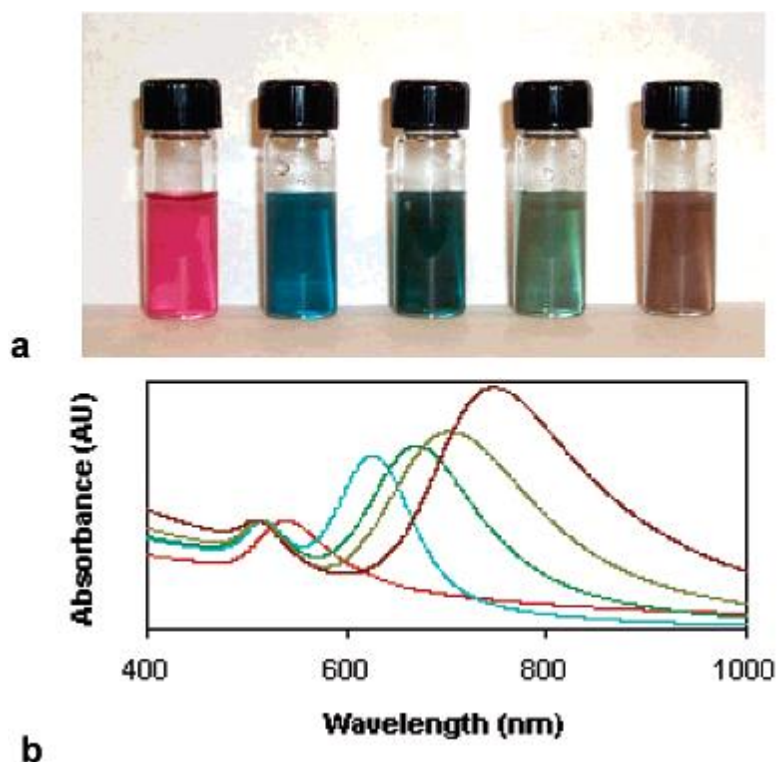
Figure 1.5 : (a) Image of photochemically prepared gold nanorods solution, and (b) corresponding UV-vis spectrum. The left solution was prepared with no silver ion addition. The other solutions were prepared with the addition of 15.8, 31.5, 23.7, 31.5 *i*L of silver nitrate solution, respectively. The middle solution was prepared with longer irradiation time (54 h) compared to that for all other solutions (30 h), and the transformation into shorter rods can be seen (Kim, Song et al. 2002).

UV-spectral data obtained by Kim et al. showed that in the absence of silver ions, there was only transverse peak which proved that there were several spherical nanoparticles with a very small amount of gold nanorods (Figure 1.5) (Kim, Song et al. 2002).

Placido et al. also demonstrated that silver nitrate added at various amounts during growth process was an important reactant for obtaining shorter or longer gold nanorods (Figure 1.5) (Placido, Comparelli et al. 2009).
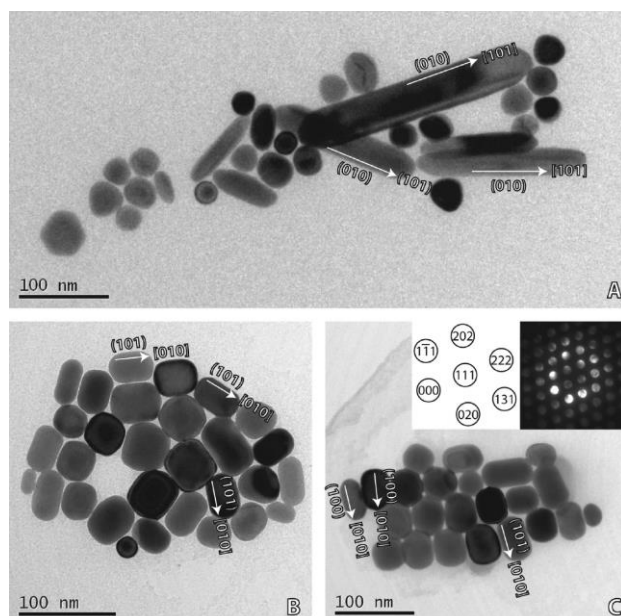
Figure 1.6 : Bright-field TEM images of small groups of AuNRs:(A) NRs prepared in the absence and (B and C) in the presence of Ag ions (Placido, Comparelli et al. 2009).

In photochemical method, formation of nanospheres and nanorods occur in the same reaction medium regarding to seedless growth. In this method, cyclohexane is used as a reagent which promotes the formation of micellar shape. Acetone is required as a reductant which reduces Au^{+3} to Au. Niidome, Nishioka et al. showed that in the absence of acetone, UV-light was limited to produce rod shaped gold nanoparticles (Niidome, Nishioka et al. 2003).

In order to synthesize gold nanorods at high yield, there are several methods other than the ones mentioned above. For example; El- Sayed and his co-workers used a similar method to the photochemical, electrochemical and seed mediated methods with some modification. In this method, silver ion was used to show that it is necessary for controlling the shape of gold nanorods. In the existance of silver ions, one dimensional gold nanorod formation (Figure 1.6) occurs in terms of providing crystal face stabilization. Silver ion was the most indicative component to form adjustable gold nanorods with their size and shape (Esumi, Hara et al. 1998, Leontidis, Kleitou et al. 2002).

The other methods performed by several researchers are the combination of the existing methods. For instance, Yamada and co-workers illustrated that if

photochemical and electrochemical methods were performed together, it gave rise to increase in the rate of nanorod growth (Niidome, Nishioka et al. 2003).

In another method applied by Wei et al., it was shown that gold nanorods could be easily grown on glass surface and gold salt concentration was the important reactant to form gold nanostructures (Wei, Mieszawska et al. 2004).

1.3 Surface Modification Of Gold Nanorods

Cetyltrimethylamonium bromide (CTAB) is used as a shape controlling agent during sythesis process (Alkilany, Nagaria et al. 2009). CTAB is substantial for the stabilization of gold nanorods. It makes them stable in the aqueous dispersant such as water or any other buffers. Because CTAB is positively charged, gold nanorods stabilized with CTAB do not tend to agregate in solution due to electrical repulsion.

Although the presence of CTAB provides stability, it is a highly toxic reagent and deteorites the membrane integrity of living cells. To reduce the toxicity of CTAB surfactant, excess CTAB can be removed by centrifugation (Nikoobakht and El-Sayed 2003) . However this process does not eliminate the toxicity problem as there are still CTAB molecules left on the surface of gold nanorods. The important point is to reduce the toxicity by removing the CTAB, while providing the stabilization of gold nanorods without CTAB.

Researchers have shown that in *in vitro* conditions, gold nanorods with CTAB surfactant, damaged cells whereas CTAB passivated gold nanorods were non- toxic (Connor, Mwamuka et al. 2005). The main approach for this should be the use of biocompatible counterparts which do not only enable particle stability (Gu, Cheng et al. 2009) but also enables detoxification of gold nanorods (Boca and Astilean 2010).

For *in vitro* and *in vivo* studies, ligand exchange procedure by using biocompatible reagents such as phosphatidylcholine, poly (styrene sulfonate) and thiolated poly (ethylene glycol) which considerably lessen the toxicity of gold nanorods with CTAB molecules, is an alternative approach (Takahashi, Niidome et al. 2006, Takahashi, Niidome et al. 2008).

The surface chemistry of gold nanorods should be taken into account for the utilization in biomedical field. Fuctionalization of gold nanorods' surface is carried out for the following reasons: Gold nanoparticles such as nanorods are prone to

interact with serum proteins in biological medium non-specifically (Strickland and Batt 2009). This results in the formation of larger aggregates of gold nanorods, which is undesirable for most biological applications. Surface modification of gold nanorods with poly (ethylene glycol) (PEG) may reduce the non-specific protein binding and thus enhance colloidal stability in biological medium (Boca and Astilean 2010). Moreover, immune system cells such as macrophages can recognise and eliminate gold nanorods which do not have a suitable surface chemistry. This prevents these nanoparticles to circulate in blood stream long enough to reach target tissues or cells. Modification of gold nanorods with non-immunogenic polymer, PEG, prevents the recognition of gold nanorods by immune system cells and thus prolongs their blood circulation half-life (Roberts, Bentley et al. 2012).

There are several ligands or molecules that have been used for reducing the toxicity of gold nanorods for *in vitro* and *in vivo* use. The most widely techniques used for the functionalization of gold nanords are PEGylation, layer by layer technique and silica coating (see Figure 1.7). Among these, the most common used polymer is PEG. Proteolytic enzymes in reticuloendotelial systems recognize and destroy molecules come from outside of the cell. In this regard, PEG overcoating inhibits the recognition and degradation by proteolytic enzymes and reticuloendothelial systems (Roberts, Bentley et al. 2012).

Thiol terminated PEG makes nanoparticles stable not only in phosphate buffer saline (PBS) but also under high or low pH conditions (Pelicano, Martin et al. 2006) and also in the neutral conditions. It enhances the circulation time of nanoparticles in blood by reducing the recognition by reticuloendothelial system cells (Wang, Wang et al. 2009).

Liopo et al. modified the gold nanorod surface with thiolated PEG molecule and performed cellular toxicity analysis using MTT and LDH (lactate dehydrogenasis) assays on SKBR3 and MDCK cell lines exposed to CTAB coated GNRs or PEGylated GNRs. It was obviously determined that PEG-GNRs conjugates did not show any toxicity on both cell lines (Liopo, Conjusteau et al. 2012).

In a study performed by Grabinski et al., the influence of PEG coated gold nanorods and mercaptohexadecanoic acid (MHDA)-coated gold nanorods on the viability of human keratinocyte cell line (HaCaT) were evaluated.The results showed that these two functionalized gold nanorods were not highly toxic to cells and also they

25

influenced the expression of genes corresponding to stress response and toxicity (Grabinski, Schaeublin et al. 2011).

Another technique for the surface functionalization of the gold nanorods is layer by layer technique using polyelectrolytes. Initially, gold nanorods are overcoated with anionic polyelectrolytes. Then, cationic polyelectrolytes are attached to this layer (KyuáLee, YoungáShin et al. 2009, Alkilany, Thompson et al. 2012). The main goal for the use of anionic and cationic polyelectrolytes in combination is to make nanorods dispersable in biological media and reduce the cellular recognition. Polystyrenesulfonate is the most widely used anionic polymer as it avoids CTAB by using filtration or centrifugation. Hence, PSS-coated gold nanorods are available for the absorbtion of cationic polyelectrolyte.Qui et al. used poly(diallydimethylammonium chloride) (PDDAC) to attach to the PSS-gold nanorod layer. They found that PDDAC-PSS-gold nanorod showed strong internalization and less toxicity on human breast adenocarcinoma cell line (MCF-7) (Qiu, Liu et al. 2010).

There is a new coating tool for functionalization process is mesophorous silica which has suprouted recently. Mesophorous silica which is capable of diminishing CTAB toxicity and providing gold nanorods dispersion easily, is also a promising tool. Despite this, there are limited applications related to its use (Zhang, Wang et al. 2013).
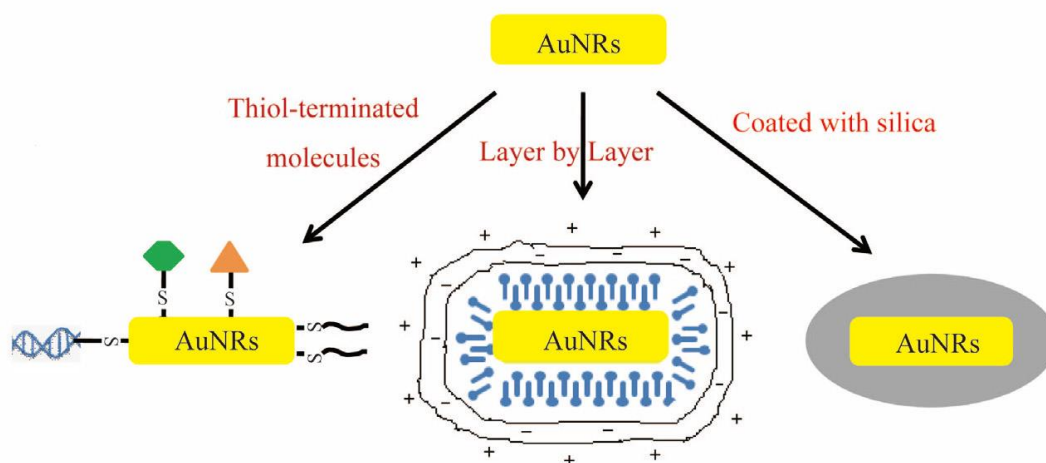
Figure 1.7 : Shematic representation of three common strategy for modification of gold nanorods surface (Zhang, Wang et al. 2013).

Beside the methods mentioned above, there are also alternative coating methods including amphipilic block copolymer or phospholipid coating. Yet, these methods have some limitations on the functionalization. In a desired coating agent, some specifications including good water solubility, physical and chemical efficiency through modification are needed (Basiruddin, Saha et al. 2010).

In addition to the stabilization of gold nanorods and prevention of toxicity, functionalization is mandatory for selective targeting and drug delivery. In a study by Black Kirkpatrick et al., gold nanorods were examined using two genetically engineered cells derived from human colon carcinoma, HCT-116. One of thes cells expressed delta opioid receptor, the other did not. In this research, delthorphin, an exogenous opioid heptopeptide which has a high affinity for delta opioid receptor expressed on human colon carcinoma cells, was conjugated to the overcoated gold nanorods through the distal end of PEG-SH molecule. The authors clearly showed that in a mixed population of cells, by using gold nanorods it was possible to make selective imaging and selective elimination of receptor expressing cancerous cells without damaging adjacent cells that do not express receptor (Black, Kirkpatrick et al. 2008).

Reuveni et al. investigated the efficiacy of passive and active targeted gold nanoparticle for CT imaging of cancer both in *in vitro* and *in vivo*. Head and neck squamose cell carcinoma was chosen as a model system. Two gold nanoparticle groups were used. Carboxylate-PEG-thiol functionalized gold nanoparticle was covalently attached to the anti-EGFR antibody for active targeting whereas other PEG coated gold nanoparticle (GNP) was covalently attached to the anti-rabbit IgG for passive targeting. In *in vitro* study, A431 cells with highly express EGFR were exposed to these GNPSs. In *in vivo* study, researchers injected actively and passiveley targeteted gold nanoparticles to the mice bearing from squamose cell carcinoma head and neck tumors derived from A431 cells.

Interestingly, 3-6 hours later anti-EGFR coated gold nanoparticles demonstrated contrast enhancement in CT imaging five times greater than anti-rabbit coated gold nanoparticles (Reuveni, Motiei et al. 2011). This research suggests that gold nanoparticles could be useful as molecular probes.

In a study by Rostro- Kohanloo et al, conjugation efficiacy of targeted gold nanorods was tested. Human breast cancer cell line SKBR-3 and normal epithelial mammary cell line MCF10A, KU7 bladder cell line were examined as *in vitro* model

systems. Carboxy-PEG-thiol was chosen which attached to gold nanorods from its thiol ends while carboxyl groups were for antibody bonding covalently. Gold nanorods were covalently conjugated to the anti-Her2 and anti-rabbit IgG as control group. Anti-Her2 conjugated and anti-rabbit IgG conjugated gold nanorods were incubated with Her2 overexpressing cell line SKBR-3 and normal epithelial cell line MCF10 respectively. Dark field imaging showed that actively targeted nanorods binded to the cancer cell line strongly.

On the other hand, this team also examined KU7 bladder cell line *in vitro*. KU7 blader cells were exposed to C225 antibody coated gold nanorods and anti-rabbit IgG conjugated gold nanorods. confocal reflectance spectroscopy results illustrated that actively targeted gold nanorods with C225 antibody had binded to KU7 cells where as anti-rabbit IgG conjuagted gold nanorods did not (Rostro-Kohanloo, Bickford et al. 2009).

Ramos and Rege used cationic poly (amine ether) for the functionalization and stabilization of gold nanorods. After the surface modification, gold nanorods were positively charged, which enabled negatively charged plasmid DNA to be complexed with the gold nanorod surface easily due to the electrostatic interactions (Ramos and Rege 2012).

1.4 Biomedical Applications Of Gold Nanorods

The unique properties of gold nanorods such as controllable size and shape, ease of surface functionalization, capability of absorbing and scatterring light in the near infrared region have made them potential candidates as contrast agents and therapeutic systems for diagnosis and treatment of diseases, respectively.

Plasmonic excitations of nanoparticles take advantages over other imaging methods using organic dyes. For instance, gold nanoparticles can absorb light five orders of magnitude higher than the best light absorbing organic dyes (Jain, Lee et al. 2006). This property increases the popularity of gold nanoparticles be useful as contrast agents in bioimaging systems (Wang, Xie et al. 2004) such as dark field imaging. Huang et al. demonstrated the possible use of anti-EGFR conjugated gold nanorods for the optical detection of oral epithelial cell lines (HOC 313 clone 8 and HSC 3).

Scattering red light from gold nanorods in dark field resulted in the visualisation of malignant and non-malignant cells distinguishably (El-Sayed, Huang et al. 2005). Gold nanorods are potentially useful in surface enhanced raman scattering (SERS) for biological species. Biological molecules have weak Raman signals. When laser is applied to biological molecules, enhanced Raman signals could be observed. In order to avoid detrimental results in biological molecules by using UV or visible lasers, SERS is a promising approach for understanding the molecular structure without making damage (Fleischmann, Hendra et al. 1974, Albrecht and Creighton 1977). Gold nanorods with their properties of scattering light stronger provide researchers to apply them as molecular probes. This is also advantageus to recognise small molecules targeted with gold nanorods even at low concentrations (Strickland and Batt 2009).

Gold nanorods have been attractive vehicles in gene delivery. Gene therapy is basicly known as therapeutic approach which enables genetic materials to penetrate into organism. It brings researchers to change damaged or overexpressed genes with new ones (Patel, Giljohann et al. 2010). To enhance the targeting efficiency of new genes, there are various mechanisms and approaches available. Recently, the use of nano based therapy has gained much attention for gene delivery. Engineered nanoparticles could provide to bring out gene pathways and functionality while reducing unselective targeting regarding to biological effects (Fox, Drury et al. 1998, Brown, Dickson et al. 2010). For instance, gold nanoparticles have been used for delivering of small oligonucleotids and small interferring RNA into cells (Kim, Schulz et al. 2012) to repair gene in effectiveness. Kim et al. explored that human peripheral blood mononuclear cells (PBMCs) which are restrained cell line were exposed to gold nanoparticles.

Gold nanoparticles modified with oligonucleotides accelerated the transcription potential towards immune system. In other words, this conjugate stimulated the signaling receptors which gave rise to activate the genes in signaling pathway and immune regulation (Kim, Schulz et al. 2012). Interestingly, AuNRs have been demonstrated to be able to pass blood brain barrier (BBB) and silence the expression of DARPP-32 by delivering specific short interfering RNAs (siRNAs) into the neuron cells (Zhang, Meng et al. 2011).

In therapeutic applications, gold nanorods have been used for thermal ablation of tumors in animals (Choi, Kim et al. 2011) Gold nanorods are capable of converting

light to heat energy, this property makes them strong candidates in targeted delivery systems respectively. Heat is an effective approach for the destruction of tumorous cells and providing macromolecules such as drugs to penetrate into cells efficiently. More heat is necessary to eliminate tumor tissue but it is unfortunetaley detrimental to cells located near tumor tissue. In other words, tumorous cells are more sensitive to hyperthermic effects than normal cells because of their higher level metabolic activities. For this reason, it is preferable to kill abnormal cells via localized hypertermia (Kapp, Hahn et al. 2000, Wust, Hildebrandt et al. 2002). It should be taken into consideration that current techniques consist of microvave radiation, ultrasound waves, radiofrequency pulses adversely influence surroding tissues while providing heat energy on abnormal tisues, (Huff, Tong et al. 2007). To figure out this problem, the use of nanotherapy, particularly gold nanorods as photothermal reagents have a great deal of attention in contemporary research area (Kreibig and Vollmer 1995). This particular application of gold nanorods has been described in detail in sections 1.5 and 1.6.

Gold nanorods are not only promising tools for cancer therapy but also are appealing tools for other therapeutic applications. It has been possible to selectively target and destroy pathogenic bacteria by using nano-based approach. Norman et al. found that gold nanorods attached to the anti- PA3 polyclonal antibody which is specific to gram-negative bacterium *Pseudomonas aeruginosa*, significantly reduced the cell viability in the presence of near infrared radiation (Norman, Stone et al. 2008).

1.5 Cancer Theraphy Via Gold Nanorods

Cancer is one the major causes of death all over the world. Current cure techniques are insufficient to treat cancer. Current trial methods are limited to the patients which are suffering from cancer. In addition, cancer drugs commonly used, have several side effects and complications on patients. Existing cure techniques are slow, time consuming and expensive. Particulary, cancer treatment techniques such as chemotherapy and immunotherapy which are being used up to now, require intense labour, budget and time for both diagnosis and therapy. These techniques may be also detrimental to cancer patients, as these approaches do not only kill cancerous cells, but also damage surrounding normal, healthy cells at the same time.

Furthermore, drug resistance occurs with conventional chemotherapy and immunotherapy methods due to the presence of drug resistance proteins inside the cells which minimizes the drug efficiacy (Kiziltepe, Ashley et al. 2012). To tackle all these problems of conventional methods, nanotechnology based therapies have been investigated.

The establishment of gold nanorod library with versatile number of aspect ratios in the near infrared region makes gold nanorods more attractive than their counterparts for cancer therapy and diagnosis strategies. As an example, Huang et al. investigated how gold nanorods could be used as diagnostic and imaging tool on malignant and nonmalignant cells. By conjugation of gold nanorods with anti-EGFR monoclonal antibody which selectively recognizes the EGFR expressing malignant cells, two malignant oral epithelial cells (HOC 313 clone 8 and HSC 3) and nonmalignant epithelial cells (HaCaT) were clearly distinguished from each other (Huang, El-Sayed et al. 2006).

Kuo et al. used gold nanorods for the delivery of paclitaxel to selectively treat breast cancer (Kuo, Hovhannisyan et al. 2010). In this study, Paclitaxel was attached to gold nanorods modified with a polyelectrolyte in order to illustrate how gold nanorods are effective for the release of paclitaxel in tumorous cells. When gold nanorods were irradiated with laser in the near infrared region, gold nanorods extracted heat and paclitaxel near gold nanorod absorbed more heat. In other words, more kinetic energy occured for the release of this anticancer drug for the treatement of MCF-7 breast cancer cell line (Kuo, Hovhannisyan et al. 2010).

Dickerson et al. reported that PEGylated gold nanorods were effective in photothermal therapy. They illustrated the efficiency of gold nanorods both *in vitro* and *in vivo*. Subcuteneous squamose cell carcinoma xenografts were grown in nude mice and modified gold nanorods were delivered into the mice via direct or intravenous injection in order to see the effect of injection site. The data showed that under the near infrared laser irradiation, gold nanorods could supress the tumor growth photothermally in an injection site-independent manner (Dickerson, Dreaden et al. 2008).

1.6 Active and Passive Targeting via Gold Nanorods

Effective targeting systems have been examined in nanomedicine. There are two kinds of targeting strategies, i.e.active and passive targeting, being used in this field. In passive targeting, nanoparticles can accumulate in the tumor site through enhanced permeability and retention effect of tumor. But this has obstacles by means of achieveness of effective targeting. Therefore, it is essential to modify the nanoparticle surface with specific targeting agents such as monoclonal antibodies to enhance selective tumor targeting (Matsumura and Maeda 1986, Jain 1999, José Alonso 2004). This is well-known as an active targeting strategy. For active targeting, modification of nanoparticle surface with targeting agents including aptamers (Eliaz and Szoka 2001), carbonhydrates (Li, Lai et al. 2010) and peptides (Singh, Grossniklaus et al. 2009) has been studied. On the other hand, antibodies and ligands which are specific to the markers located and over-expressed on the tumor cells have remarkably received attention from researchers. In this manner, active targeting is under intense work for gene and drug delivery and photothermal therapy systems for cancer treatment.

In a study reported by Xio et al., PEG-gold nanorods conjugated to Doxorubicin were functionalized with cRGD targeting peptide. According to the cellular uptake and cytotoxicity assay results, cRGD- gold nanorods enhanced the cellular uptake and had more cytotoxicity over cancer cells expressing $\alpha v \beta_3$ integrin when compared to gold nanorods-doxorubicin without targeting agent, cRGD. In other words, active targeting system was more effective than passive targeting system (Xiao, Hong et al. 2012).

Jing and his colleagues generated folate conjugated gold nanorods to target folate receptor bearing hepatocellular carcinoma cells. They illustrated that folate- gold nanorods conjugated to the cell membrane and entered into cytoplasm easily. They also showed that photothermal therapy approach with the use of folate conjugated gold nanorods could inhibit the proliferation of hepatocellular carcinoma cells, HepG2 (Jin, Yang et al. 2012)

1.7 Multiple Myeloma

Multiple myeloma is a heamatological plasma cell cancer type which causes remarkably high deaths worldwide (Picot, Cooper et al. 2011).

It occurs when B-lymphoctes also known as plasma cells differentiate into post germinal phase of malignancy. This malignancy is the result of plasma cells accumulated within bone marrow. It has been a big challenge to overcome drug resistance in multiple myeloma cells. Since multiple myeloma cells acumulate in the bone marrow microenvironment, their sensitivity to chemotherapy reagents diminish in terms of cell-adhesion mediated drug resistance (CAM-DR) (Damiano, Cress et al. 1999, Sanz-rodríguez and Teixidó 2001). The main point to achieve efficient targeting in multiple myeloma is usually to hinder the adhesion of these plasma cells to the bone marrow microenvironment (Kiziltepe, Ashley et al. 2012)

There are a number of current strategies used for the treatment of this important disease. The conventional method used nowadays is applying chemotherapy agents such as vincristin, dexametasone and melphalan. However, it is known that this therapy leads to increase in the malignancy reknown as therapy related myelodesplastic syndromes (Ishii, Hsiao et al. 2006). There is a substantial requirement for new strategies to treat multiple myeloma. Nanotechnology based therapy may be an alternative approach to cure this disease. Badr et al. illustrated that it was possible to cure multiple myeloma using silica nanoparticles. In this study, Badr and his co-workers used different multiple myeloma cell lines, U266 and RPMI 8226. It was demonstrated that combination of silica nanoparticle with snake venom enhanced the effectiveness of snake venom in cancer cell lines with increasing the induction of apoptosis in these cancerous cells (Badr, Al-Sadoon et al. 2012).

Kiziltepe et al. designed engineered nanoparticles functionalized with anti-very late antigen-4 (VLA-4) peptide- pH sensitive Doxorubucin conjugates to target multiple myeloma cells *in vitro*. The main goal in that sudy was not only to provide targeted Doxorubicin delivery into multiple myeloma (MM) cells, but also to hinder adhesion tendency of these cells towards bone marrow stroma cells by targeting very late antigen-4 (VLA-4) overexpressing MM cells. It was reported that nanoparticle binded VLA-4 initiated receptor mediated cellular uptake and efficient release of Dox because of pH sensitive bond hydrolysis in the acidic endocytic vesicles (Kiziltepe, Ashley et al. 2012).

33

In this thesis, gold nanorods were intended to be used as phototherapeutic agents for providing a new approach in the tratment of Multiple Myeloma via selective targeting. For selective targeting, anti-CD138 monoclonal antibody which has affinity to the CD138 antigen expressing Multiple Myeloma cells was conjugated to PEGylated gold nanorods. CD138 antigen positive and negative cell lines, U266 and ARH-77, were used to demonstrate the efficiacy of antibody conjugated gold nanorods for photothermal destruction of cancer cells selectively. To the best of the author's knowledge, this is the first study utilizing gold nanorods actively targeting Multiple Myeloma cell lines using anti-CD138 monoclonal antibody. Briefly, gold nanorods in a desired size range were synthesized using seed mediated method. To make gold nanorods stable and non-toxic, their surface was functionalized with PEG. Heterofunctional PEG mixture was used for the modification of the surface of gold nanorods via thiol linkage. MTT assay was carried out to show the toxic effects of CTAB or PEG coated gold nanorods on U266 and ARH-77 cell lines respectively. Meanwhile, characterization techniques, described in experimental section were also performed before and after functionalization of gold nanorods. Before conjugation of anti-CD138 antibody to gold nanorods, lysozyme was used as a model protein and nanodrop measurements and SDS-PAGE results were recorded after conjugation to the gold nanorods in order to determine the concentration of protein attached to gold nanorods. Cellular uptake of PEG coated and anti-CD138 conjugated PEG coated gold nanorods were carried out by using inductively coupled plasma mass spectroscopy (ICP-MS). Photothermal ablation of PEG coated and anti-CD138 conjugated gold nanorods on U266 and ARH-77 cell line was tested by using 633 nm red laser.

2. EXPERIMENTAL SECTION

2.1 Materials

Cethyltrimethylamonium bromide (CTAB, CAS number: 57-09-0, $C_{19}H_{42}BrN$, Sigma, Germany), L-Ascorbic acid (Lot No: 05878, Fluka Analytical, Germany), Chloroauric acid ($HAuCI_4$, Lot No:), Silver nitrate ($AgNO_3$, Lot No: 10K023, Alfa Aesar, Germany), Sodium Borohydrate ($NaBH_4$, Cat No: 48086, Sigma, Germany), N-ethyl- N'- (3-dimethylaminopropyl) carbodiimide hydrochloride (EDAC, Cat no: 25952-53-8, Merck, Germany), N-Hydroxysuccinimide (NHS, Cat No:6066-82-6, Merck, Germany), Polyethylene glycol (PEG-SH, MW 1000, Cat. No: 729108, Sigma, Germany), SH-PEG-COOH, MW 1000, Lot No:ZL25647, Creative PEGWORKS, USA), Disinfectant (Deconex, Reiniger, Germany) Anti-CD138 human monoclonal antibody azide free (Cat No:10-520, Abcore, USA), Lysozyme from chicken egg white (Cat No: 62971, Fluka, Germany), Amonnia Solution (NH_4OH,% 32, Cat.No:B0714426-136, Merck, Germany), Hydrogen Peroxide (H_2O_2, % 30, Cat. No: K42254197-119, Merck, Germany), Acrylamide, 99,9% (Cat. No: 161-001, Bio-Rad, USA), Bis (N, N'-Methylene- bis Acrylamide (Cat. No: 161-0201, Bio-Rad, USA), Tris (Cat. No: 161-0716, Bio-Rad, USA), Glycine (Cat. No: 161-0718, Bio-Rad, USA), SDS (Sodium Dodecylsulfate, Cat. No: 161-0301, Bio-Rad, USA), Ammonium Persufate (Cat. No: 161-0700, Bio-Rad, USA), TEMED (Cat. No: 161-0800, Bio-Rad, USA) Thermo-0671 protein ladder (Thermo Scientific) RPMI 1640 (+L-Glutamine, Lot. No: 1228417, Gibco, Utah, USA), Phosphate Buffer Saline (1X PBS, Cat. No: SH30256.01, Gibco, Utah, USA), Trypan Blue dye (Cat. No: 03-102-1, Biological Industries, Israel), MTT (Thiazol Blue Tetrazolium Bromide, Cat No: M5655, Sigma, Germany), Annexin V-FITC apoptosis kit (Cat. No:K101, Biovision, USA). All chemicals were used as received. Multiple myeloma cell lines ARH-77 and U266 were provided by Dr. Yusuf Baran at Izmir Institute of Technology.

2.2 Methods

2.2.1 Fabrication of gold nanorods via seed mediated method

Gold nanorods at various aspect ratios were synthesized using seed mediated technique according to a modified version of methods previously described by Nikooobaht et al. (Nikoobakht and El-Sayed 2003). and Green et al. (Green, Martyshkin et al. 2011).

2.2.3.1 Synthesis of GNRs (absorption maximum at 700 nm)

Step 1 : Preparation of Seed Solution

Prior to use all glassware was cleaned with disinfectant (5ml in 1 ml UP water) and rinsed twice with distilled water and dried under N_2 gas. All chemicals were freshly prepared and dissolved in 18 ohm ultrapure (UP) water. Au seeds which were 3-5 nm diameters, were prepared by the reduction of $NaBH_4$ in th presence of HAuCI4 using seed mediated method described by Nikoobaht et al. Briefly, $HAuCI_4.H_2O$ in UP water (250 µl, 0.01 M) was added into CTAB solution UP water (9,75 ml, 0,1 M) under magnetic stirring. ice-cold $NaBH_4$ solution in UP water (0.6 ml, 0,01 M) was added to the Au mixture. The color of the solution turned into brownish color within seconds. Afterwards, seed solution was kept at 30 ^{o}C for 15- 20 min in order to get rid of free Na ions.

Step 2: Preparation of Growth Solution (G1)

CTAB solution in UP water (9,75 ml, 0,1 M) and $HAuCI_4$ solution in UP water (0,5 ml, 0,01 M) were mixed under magnetic stirring. $AgNO_3$ solution in UP water (50 µl, 0,01 M) was added to this mixture. After addition of ascorbic acid as a mild reducing agent, the color of the solution immediately turned into colorless. Finally, seed solution (12 µl) was added. The solution was stirred for 2 minutes. Approximately 10 minutes later, the color of the growth solution changed to grey. Gold nanorods were kept in dark for further use.

2.2.1.2 Synthesis of gold nanorods (absorption maximum at 740-780nm)

Seed mediated method previously reported by Green et al. (Green, Martyshkin et al. 2011) was used for the fabrication of gold nanorods at 740-780 nm.

Step 1: Preparation of Seed Solution

$HAuCI_4$ solution in UP water (250 μl , 10 mM) was added into CTAB solution in UP water (5 ml, 0,2M.). Ice-cold $NaBH_4$ solution in UP water (0,6 ml, 0,01 M) was put into this mixture immediately (See Figure 2.1). The color turned into brownish. Seed solution was incubated at room temperature for at least 2 hours before use for the reduction of free Na^+ ions.

Step 2: Preperation of Growth Solution

G2 and G3 growth solutions were prepared as shown in Table 2.1. Typically, a growth solution containing CTAB solution in UP water (0,2 M)   and $HAuCI_4$ solution in UP water (0,01 M) were mixed with freshly prepared ascorbic acid solution in UP water (78,8 M) which was used as a mild reducing agent for the reduction of Au^{3+} to Au^+. The color of the solution turned from brow-yellow to colorless when ascorbic acid was added. After Au seeds were added (60 μl for G2, 80 μl for G3 growth solutions) to the growth solution, the color of the solution was turned into wine red within minutes. Growth solution was kept under dark for futher use. Growth solution was concentrated via centrifugation to obtain a gold nanorod concentration of 1000 μg/ml. Rod formation was schematically illustrated (See Figure 2.1).

Table 2.1 : Fabrication of gold nanorods using wet chemistry technique, seed mediated method (Green, Martyshkin et al. 2011).

Chemicals	##G2	##G3
CTAB (0,2 M)	17 mL	20 mL
AgNO$_3$ (32mM)	80 μL	120 μL
HAuCI$_4$ (0,01 M)	1,7 mL	2 mL
Ascorbic Acid (78,8 mM)	280 μL	360 μL
Seed Solution	60 μL	80 μL
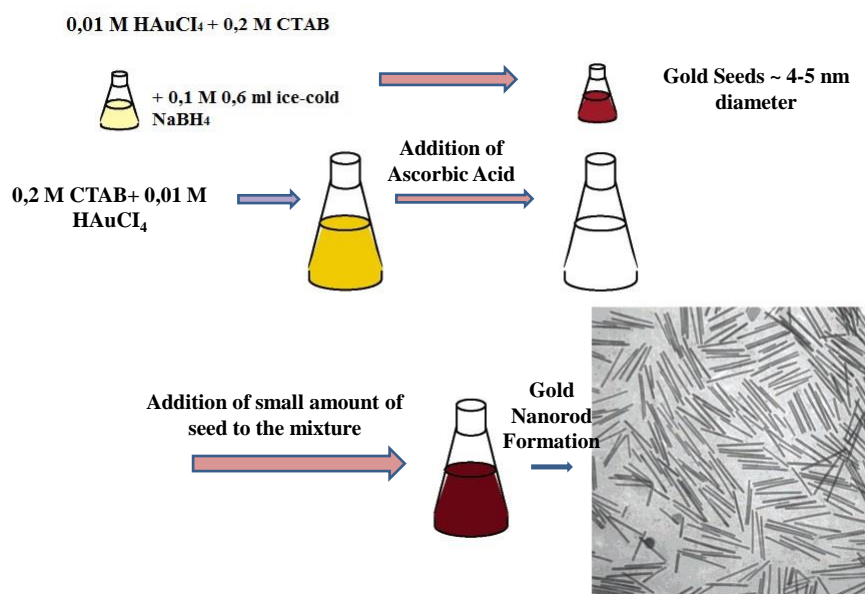
Figure 2.1 : Schematic illustration of the synthesis of gold nanorods (Rayavarapu 2010).

2.2.2 Surface modification of gold nanorods

Surface modification of gold nanorods was carried out using PEG-thiol and carboxy-PEG-thiol mixture. Prior to use, all glassware was cleaned with dezenfectan 5m in 1L UP water and rinsed twice with distilled water. To replace CTAB molecules on the surface of gold nanorods with a mixture of bi- and mono-functional PEG molecules, i.e. monomethoxy-PEG-thiol (PEG-SH) and carboxy-PEG-thiol (COOH-PEG-SH), gold nanorods (1 ml, 1000 μg/ ml) were first centrifuged at 9000 rpm and washed twice to reduce the CTAB concentration in solution. Mixed PEG solutions of COOH-PEG-SH/ PEG-SH in UP water) were prepared at varying PEG-SH: COOH-PEG-SH molar ratios of 1:1, 1:3 and 1:9. Gold nanorod pellets were dispersed in UP water at a concentration of 1000 μg/ ml. Mixed PEG solution (0,05 ml, 0.25 mg mixed PEG; 0,1 ml, 0.5 mg mixed PEG, 0,2 ml, 1 mg mixed PEG) was then added into gold nanorod solutions (1 ml, 1000 μg as Au atom). The solution was magnetically stirred for 30 minutes and left in dark overnight. Next day, the mixture was transferred into dialysis membrane with 10000 Da MWCO (Spectra/Por) in

order to remove unreacted PEG molecules. The dialysis was carried out against UP water which was changed frequently for 3 days. After the dialysis, the solution was transferred into falcon tubes and dried via liophiliser. After drying, the gold nanorods were redispersed in UP water and then sonicated for one minute before further use.

2.2.3 Characterization of PEG coated or CTAB coated gold nanorods

2.2.3.1   Scaning electron microscopy (SEM)

Before samples were prepared, silica wafers were exposed to the piranha solution. Piranha solution was prepared in in   ultra pure water containing H_2O_2 and NaOH with volume ratios 5:1:1. Piranha solution was heated up to 65 ^{o}C and silica wafers were exposed to the solution until bubbles were not observed on the wafers. Next, wafers were washed with distilled water and technique EtOH and dried under N_2 gas. All samples (1000 µg/ ml, gold nanorod solutions at varying PEG concentrations in PBS) were diluted 5 times and 10 µl of each sample was dropped onto the silica wafer for SEM imaging. High resolution SEM (Zeiss Ultra Plus) with 5.00kV was used.

2.2.3.2 Dynamic light scattering

Dynamic light scattering (DLS) was used in order to determine the surface charge and hydrodynamic diameter of GNRs before and after modifications. A High Performance Malvern Zeta Sizer (Malvern Instruments Ltd. Southborough, MA, USA) was used at 25 ^{o}C and 60 second runs were performed for each sample. Measurements   for each samples were done in triplicate and the average of these measurements were obtained with standard deviations   for the evaluation of the results.

2.2.3.3 UV-visible spectroscopy

18x18 mm glass surfaces were cleaned with technique EtOH and dried under N_2 gas. Lenses and the light density of the light mcirsocope was adjusted. 10 µl of each sample in PBS (1000 µg/ ml as gold atoms) was dropped on to the glass surface and

the absorbance value of CTAB coated, PEG-coated and lysozyme coated GNRs were obtained by using Nanodev UV spectrophotmeter (Nanodev, Turkey) in which 200 nm fiber optic was used as bridge between the spectra system and light microscope in 10X objective. Datas were obtained from Ocean Optics Spectra Suite Software programme.

2.2.4 Conjugation of gold nanorods with lysozyme as a model protein

Before conjugation of anti-CD138 antibody to PEGylated gold nanorods, binding efficiency of PEG capped gold nanorods was tested with a model protein, lysozyme (MW 14000, Sigma, Germany). For the preparation of a stock protein solution, lysozyme was dissolved in PBS at a concentration of 5 mg/ml. To target all of the carboxylate groups of COOH-PEG-SH molecules on the GNRs surface, 44,8 μl of lysozyme stock solution was diluted first with $NaCO_3$ buffer (55,2 μl, 100 mM) at pH 8,6. On the other hand, EDC solution in UP water (0,01 M as final concentration) and NHS solution in UP water (0,005 M as final concentration) were added into 100 μl of PEG coated GNR solution in PBS (1000 μg/ ml gold atoms) . After 5 minutes, the protein solution (100 μl, 44,8 mg) was added into the GNR solution. Meanwhile, gold nanorods treated with EDC and NHS without lysozyme were prepared as control. The reaction was continued at +4°C overnight. Next day, Lsysozyme conjugated GNR solution and GNR solution without lysozyme were centrifuged at 9000 rpm for 15 min and then washed with PBS twice in order to remove the unreacted agents and side-products. The final GNRs were dispersed in PBS.

2.2.4.1 Characterization of Lysozyme conjugated PEG-coated GNRs
2.2.4.1.1 Nanodrop measurement

Protein concentration datas of prepared samples were analyzed by using Vilber Lourmat UV based imager. Standart curve was obtained by making serial dilutions from initial stock lysozyme solution. To determine the protein conjugation yields, the absorbance values of the supernatant of conjugation mixtures after reaction and each wash were determined at 280 nm. As a background reading, the absorbance

measurements were also performed with PEG-gold nanorod without lysozyme solution. Absorbance values of each sample were converted to the concentration values using standart curve. The amount of protein conjugated with PEG coated GNR was calculated theoretically using the concentration data.

2.2.4.1.2. Polyacrylamide gel electrophoresis

A 12% separating gel was first prepared. Briefly, acrylamide stock solution in distilled water (containing 0,081 M acrylamide and 0,001 M, N, N'-Methylene-bis Acrylamide in 10 ml distilled water) , distilled water (8,375 ml) , 1,5 M Tris-HCl (pH:8,8) in distilled water (54,45 g, 300 ml) , % 10 (w/v) sodium dodesyl sulfate in distilled water (3,4 mM, 250 μl) as stabilizing buffer were mixed. Finally, ammonium persulfate (4,376 M in 125 μl distilled water) and tetramethylethylenediamine (TEMED) (12,5 μl) which trigger polymerization were added to the mixture. The solution was poured between the glass plates in the gel cassette systems until the top of the short plate. gel was allowed to polymerize for at least 45 minutes. Meanwhile, 4% stacking gel was prepared as follows. First, monomer solution including acrylamide stock solution (0,01 M acrylamide and 0,13 mM, 1,3 ml) in distilled water, 6,1 ml distilled water, Tris-HCl (0,5 M, 2,5 ml) in distilled water (pH:6.8), % 10 sodium dodecyl sulfate (0,01 g, 100 μl) in distilled water, ammonium persulfate (8,76 M, 50 μl) in ditilled water and 10 μl of TEMED, was prepared. Stacking gel was poured to cover the surface of seperating gel and a 10 well comb was put into the gel and left overnight. All the samples (10 μl) were diluted with loading buffer stock solution containing 3 ml distilled water, 0,5 M, ml Tris- HCl in 1ml distilled water, pH: 6,8 , 20 % (v/v) glycerol (1,6 ml), bromphenol blue (7,46 mM, 0,4 ml) in distilled water, 10 % SDS (0,35 M, 1,6 ml) 5% (v/v) β- mercaptoethanol (0,4 ml) (with a volume ratio of 1:1), and all samples were denatured in a water bath at 100ºC for 10 minutes. Prestained marker (3μl) (Page ruler prestained marker, with size range from 10kDa to 70kDa, 0671, Thermo Scientific) was first loaded on the gel. Each sample (10 μl) was loaded and the gel system was run at 100 V for 100 minutes. 5X electrode buffer containing Tris (125 mM , 45 g), Glycine (960 mM, 216 g), 0.5% SDS (15 g) in 3 L distilled water at pH 8.3 was prepared as stock solution. 300 ml, 5X stock solution was diluted with distilled water to 1,5 ml, 1X electrode buffer for one electrophoretic run.

At the end of running time, gel was taken up and put into a plastic plate containing 20 % (v/v) Trichloroacetic acid (60 ml pure TCA, 240 ml distileed water) for fixation. The gel was shaken at 50 rpm for 30 minutes. Next, gels were washed three times with UP water gently. 0,1 % G-250 coomassie blue solution (1 g, 1000 ml)   in 10 % acetic acid, 50 % methanol and 40 % distilled water was added to cover the gel. The gel was shaken for 10 minutes for staining. Afterwards, destaining solution containing 50 % (v/v) methanol,   10 % (v/v) acetic acid and 40 % distilled water (100 ml) was added onto the gel and incubated for 30 minutes. The solution was replaced with fresh destaining solution to remove excess stain. Finally, the gel was analyzed using a Bio-Rad imaging software.

In order to visualize the protein bands more clearly, an additional staining protocol, using silver staining was performed. In this procedure, initially, 50 % ethanol solution (300 ml absolute ethanol diluted with 300 ml distilled water) was added to cover the gel and shaken for 20 minutes. This step was repeated three times. Next, gel was washed with pre-treatment solution containing sodium thiosulfatepentahydrate (4,03x 10^{-5} M, 8 ml) in distilled water for 1 minute. The gel was then rinsed with deionized water for 20 seconds three times. The silver nitrate solution containing silver nitrate (0,01 M, 400 ml) in distilled water and 37 % formaldehyde (300 μl) was then added to cover the gel surface and the gel was shaken for 20 minutes. In order to remove excess stain from the gel, gel was washed twice with deionized water for 20 seconds. Finally, developing solution consists of potassium carbonate(0, 16 M, 408,3 ml) pre-treatment solution (8 ml), 37 % formaldehyde (300 μl) and distilled water (400 ml) to develop the background was added to the chamber and the final gel was shaken gently until the bands were visualized. Deionized water was then added to slow down the reaction. The gel was analyzed with a Bio-Rad imaging software.

2.2.5 Conjugation of anti-CD138 monoclonal antibody to gold nanorods

CD138   is a heperan sulfate bearing proteoglycan that is expressed on myeloma tumors. The high level expression of this antigen on myeloma tumors leads to be used in the antibody targeting approach for the treatment of myeloma tumors.

In this research, anti-CD138 monoclonal antibody with its high binding affinity to CD138 was used. Conjugation method was carried out for anti-CD138 attachment to the GNR. To target % 0,1 of COOH groups on PEG coated gold nanorods, anti-CD138 monoclonal antibody in PBS (100 μg, 48 μl) was diluted first in $NaCO_3$ (100 mM, 52 μl). EDC solution in UP water (0,01 M as final concentration) and NHS solution in UP water (0,005 M as final concentration) were added into 500 μl of PEG coated GNR solution in PBS (2000 μg/ ml gold atoms) to activate the carboxylic ends of PEG on the GNR surface. The mixture was allowed to sit for a while. The reaction continued at $+4^{o}C$ overnight. Next day, anti-CD138 conjugated GNR solution was centrifuged at 9000 rpm for 15 min and then washed with PBS twice in order to remove the unreacted agents and side-products. The final GNR pellets were dispersed in PBS as final concentration of GNR was 1000 μg /ml.

2.2.6 Cell viability assay via MTT

Cell Culture

U266 and ARH-77 cells were routinely cultivated in RPMI 1640 containing % 10 FBS and % 1 penicilin/streptomycin at 37 °C under 5% CO_2 atmosphere. Cells were passaged in every two days when they reach 80% confluency. Cells at logaritmic growth phase were collected for all experiments.
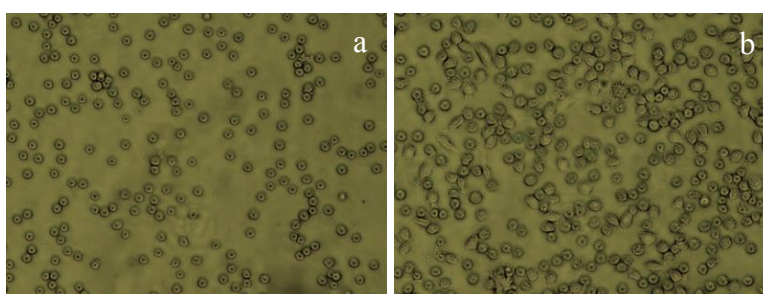
Figure 2.2 : Morphology of cells used in the study under light microscope Olympus CKX 41 in 20x objective. a) U266, b) ARH-77.

U266 which is a suspended cell line and ARH-77 which is a loose adherent cell line were collected separately into Falcon tubes. Cells were centrifuged at 800 rpm for 5 minutes in order to remove the culture medium. After centrifugation step, the medium was gently removed with pipette and cells were resuspended in 20 ml of

fresh RPMI-1640 cell culture medium by making serial pipetting. Before cell cultivation, Trypan Blue assay indicating dead cells in blue color was performed in order to determine the number of viable cells. Cells were counted with Neuber lam under light microscope. The cell suspensions were transferred into 96 well plates to yield a concentration of 10,000 cells/ well /190 μl.

Cells were exposed to different concentrations of gold nanorods (either CTAB capped or PEG-modified) (1 μg/ml, 2,5 μg /ml, 5 μg/ ml, 10 μg/ml) using a stock GNR solution at 1000 μg/ ml concentration. Before exposing to cells, gold nanorod solution in PBS (pH 7.4) was filtered using a 0,45 μm membrane filter. Final volume for each well was 200 μl. Cells containing only RPMI-1640 and cells containing only 5 % (v/v) RPMI-1640 and PBS were used as control groups. U266 and ARH-77 cells with samples were incubated at 37 ^{o}C in 5% CO_2 atmosphere for 24, 48, or72 h. After incubation time, MTT dye in PBS solution (5 mg, 1ml) was added to each well (20 μl per well) and the plates were further incubated for 3 h in a humidified incubator. Next, plates were centrifuged at 1800 rpm for 10 minutes to sediment the cells. The solution in each well was removed gently. Cells were treated with dimethylsulfoxide (DMSO) at a volume of 100 μl for each well in order to dissolve formazan crystals which were reduced from tetrazolium salts by oxidoreductase enzymes intracellularly. After addition of DMSO, plates were shaken at 125 rpm for 5 minutes. The absorbance values of solutions were obtained using a plate reader (Varioscan) at 570 nm.

2.2.7 Apoptosis assay via Annexin V-FITC

Annexin V binding method was used as described in Manufacturer's protocol. Cell staining was evaluated using Annexin V-fluorescein isothiocyanate (FITC) and simultaneously Annexin V with propidium iodide (PI) dye. Briefly, when U266 and ARH-77 cells reached 80-90% confluency in culture flask, they were collected in 50 ml falcon tubes for centrifugation. The cells were then centrifuged at 800 rpm for 5 min in order to remove the old medium. Cells were then resuspended in fresh RPMI 1640 (20 ml). Serial pipettings were done gently for resuspension. For each cell line, cell counting was performed using Trypan Blue assay. 500,000 cells/well/2 ml were plated in six-well plates. CTAB coated gold nanorods at various concentrations (2,5, 5, 10 and 25 μg/ml) were applied to cells using CTAB-GNR stock solution of 1000

μg/ ml. The PBS content of each well used as control was 5% of the total well volume 200 μl). Cells with only medium were used as control. After every addition of GNR to cells, serial pipettings in the wells were performed. After 24 h, cells in each well were collected in 15 ml Falcon tubes. Wells were washed with 1 ml of PBS and the washing solutions were also added to cell suspensions in tubes. Cells were centrifuged at 800 rpm for 5 min and the supernatants were removed gently. Cells were then washed with 1 ml of PBS. Next, cells in PBS were centrifuged at 800 rpm for 5 min again. After this step, PBS was removed and the cells were resuspended in 200 μl of annexin binding buffer which enables to detect phosphatydilserine exposure during apoptosis. Cells used as control group were resuspended in 800 μl of annexin binding buffer and suspension was divided into four glass tubes as each tube contained 200 μl solution.

After the addition of annexin V binding buffer to each glass tubes, 2 μl of Annexin V-FITC (except unstained and PI including tubes) and 2 μl of Annexin V-PI (except tubes only included unstained and FITC) were added to cells in glass tubes. Vortex was performed for homogenization for 1-2 seconds. Cells in the tubes were then incubated in the dark for 10-15 min in order to allow binding of protein to phosphotydilserine. Analysis of each tube was performed using flow cytometry.

2.2.8 Cell uptake of gold nanorods

ARH-77 and U266 cells at 80% confluency were collected in Falcone tubes and centrifuged at 800 rpm for 5 minutes. The supernatant was removed and pellets were suspended in RPMI 1640 medium. Cells were then plated in 24 well plates at a concentration of 10^5 cells/ well / 1ml. Cells were incubated with PEG modified gold nanorods at a final concentration of 10 or 25 μg/ml for 1.5 or 3 h. Cells in medium without nanorods were cultivated as a negative control group. Each experiment was performed in triplicate. After the incubation time, cells were collected in Falcon tubes and centrifuged at 800 rpm for 5 minutes and washed with PBS three times.. Finally, pellets were dispersed in 500 μl of concentrated nitric acid (HNO_3) solution in order to obtain cell lysates. After incubation overnight, the cells were diluted with UP water as all Falcon tubes contained 2% nitric acid (volume %) and stored at +4

^oC for further analysis using inductively coupled plasma mass spactroscopy (ICP-MS)

2.2.9 Photothermal therapy

To evaluate the efficiency of surface chemistry in laser ablation, U266 and ARH-77 cel lines were cultured in 96 well plates as each well included 10^4 cell. The final volume for each well was adjusted to 200 µl. Cells containing only RPMI-1640 was used as control group.
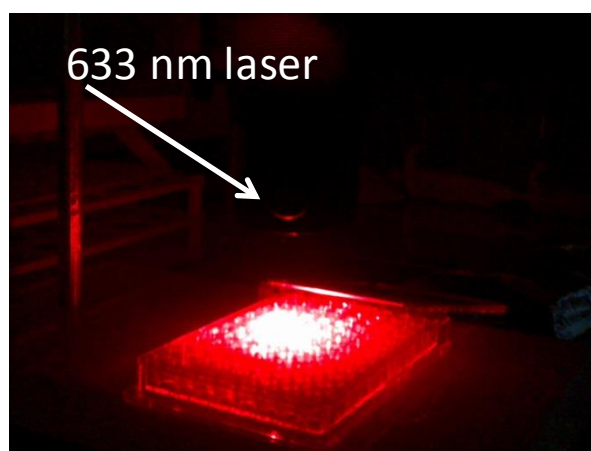
Figure 2.3 : Illustration of laser ablation on cells.

Following 3 hours incubation of U266 cells and ARH-77 cells with PEG-GNR and anti-CD138-PEG GNRs at 25 µg /ml of final gold atoms concentration for each well, both cell types were exposed to laser (20 mWatt, DRIEL Instruments, 79309, USA) operating at 633 nm which is in the near infrared region and does not effect the cell survival (Figure 2.3). After 10 min exposure to laser, cells were dyed with Trypan Blue with dilution ratio 1:1 (volume/volume). The number of living cells were counted under light microscope in 10x objective.

3. RESULTS and DISCUSSION

3.1 Synthesis Of Gold Nanorods

To find the optimal reaction conditions in order to generate high yielded gold nanorods via seed mediated method, different protocols were performed. In this study, gold nanorods were synthesized using seed mediated method. First, seed solution was prepared which enabled to produce gold nanorods. After preparation of seed solution, seed solution was kept at room temperature for at least two hours in order to reduce Na^+. Afterwards, growth solution was prepared and with the addition of seed solution at enough volume, the color of the growth solution turned into purple- grey colour which was the proof that seeds converted to gold nanorods. With changing the volume and concentrations of reducing agents such as silver nitrate, ascorbic acid, gold nanorods were fabricated with different aspect ratios. It should be taken into consideration that changing the concentration of weak or strong reducing agents for the fabrications of gold nanorods gives rise to obtain high or low yielded gold nanorods. It was also confirmed in previous published datas that changing concentration of silver nitrate and ascorbic acid could lead to produce high or low yielded gold nanorods (El Sayed et al.,2003).

Initially, gold nanorods fabricated by using method described previously by Nikoobaht et al. (Nikoobakht and El-Sayed 2003) were low yielded corresponding to UV-Visible spectrum (Figure3.1). Gold nanorods were obtained with 0,5 or 1 optic density. Figure 3.1 shows the absorption spectras of low and high yielded gold nanorods prepared depending on the methods decribed in detail in the experimental section. Extinction spectra for G1 exhibits a longitudinal peak at approximately 700 nm whereas spectras for G2 and G3 show longitudinal peaks at approximately 720- 760 nm respectively. By changing CTAB, ascorbic acid and silver nitrate concentrations, it was possible to generate high yielded gold nanorods corresponding to absorption spectra results. It was also visualized that low concentrated CTAB (0,1 M) added to $HAuCI_4$ enabled yellow color solution while high concentrated CTAB (0,2 M) enabled orange color. This results indicate that $AuCI_4^-$- CTAB interaction increases with increasing CTAB concentration. In other words, it could be resulted in the production of high concentrated gold nanorods.

Ultraviolet- Visible Spectroscopy of the Synthesized Gold Nanorods
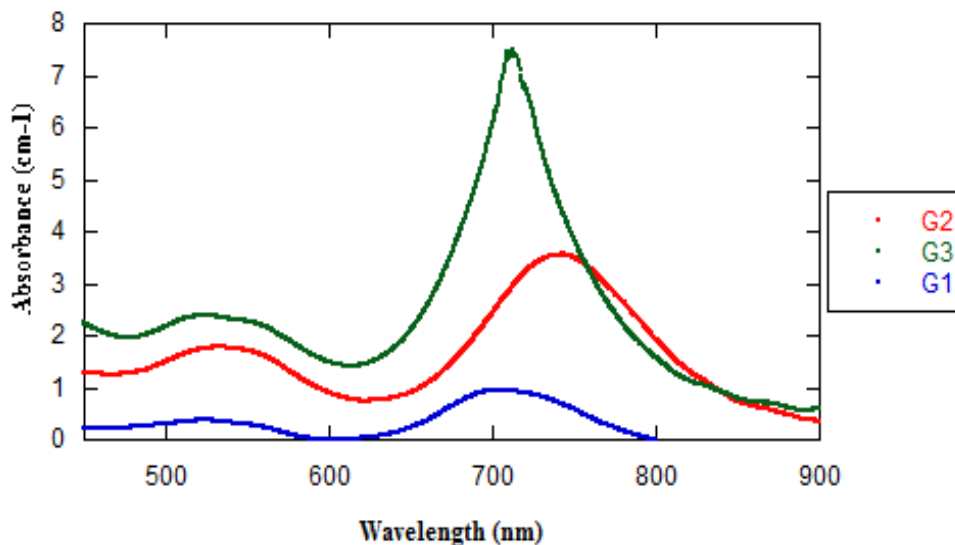
Figure 3.1 : Representation of Ultraviolet Visible Spectroscopy of Raw Gold Nanorods in water.

Figure 3.1 illustrates the longitudinal and transverse peaks of GNRs sythesized depending on different protocols described in experimental section. In general, the extinction spectra confirms that seed mediated approach enables the fabrication of gold nanorod by tuning the concentrations of constituents during growth process. The characteristic two peaks for gold nanorods observed in the extinction spectra indicate that it is possible to fabricate gold nanorods with tunable aspect ratios. As aspect ratio increases, the red shift occurs in the longitudinal plasmon resonance. Transverse peaks were aproximately observed at 520 nm whereas longitudinal plasmon resonances were in the transparency window (Gormley, Greish et al. 2011). UV results with comparison of absorbance values for each sample indicate that G3 sample can be more preferable than others to obtain high yielded gold nanorod production.

In order to evaluate the surface chemistry zeta potentials of the as prepared gold nanorods, PEG coated gold nanorods were measured by using Malvern Zeta Sizer.

Table 3.1 : Surface charge of CTAB coated GNRs dispersed in different dispartants.

Dispertant	Zeta Potentials
Water	58,6 ± 4,9
PBS	31,9 ±2.2
RPMI 1640	-

Table 3.1 shows the surface charges of CTAB capped Gold nanorods in different dispertants. Generally, surface charges of CTAB-GNRs for both dispertants were highly positive due to the cathionic surfactant, CTAB on the GNR surface (Alkilany, Thompson et al. 2012).

According to the results, zeta potential of CTAB-GNRs in PBS goes down to 31,9 ±2.2 mV. Because of the poor stability of CTAB coated gold nanorods in the high ionic strength culture medium, zeta potential of the CTAB coated gold nanorods could not be measured for RPMI 1640 (Huang, Barua et al. 2009)

Dynamic light scattering measurements were also performed for testing the stability of CTAB-GNRs in both water and PBS. As it is clearly seen in Figure 3.2, CTAB-GNRs are also stable in PBS.
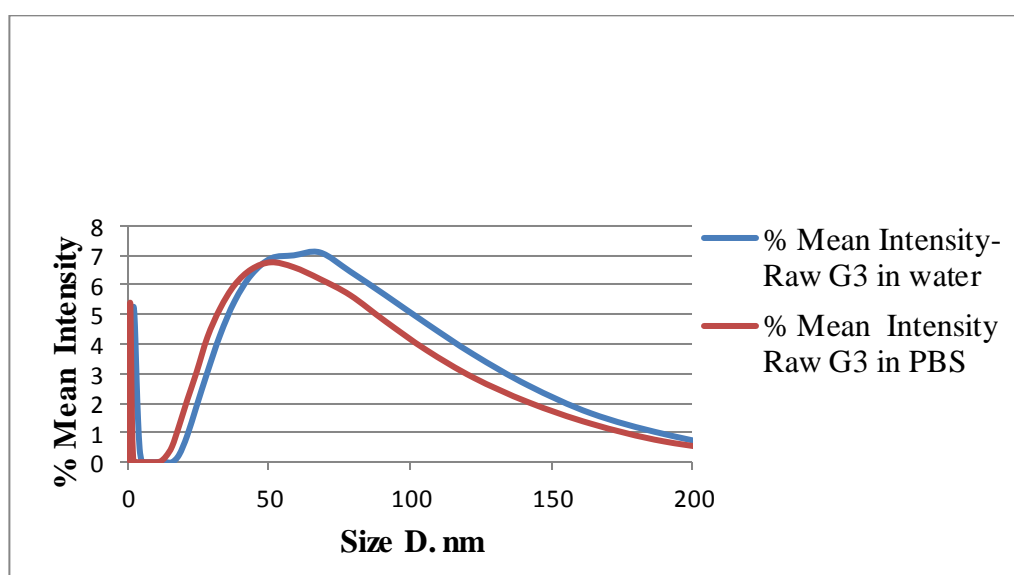
Figure 3.2 : Hydrodinamic Diameters of CTAB-Gold Nanorods in different dispertants prepared with G3 method described in the experimental section.

3.2 Surface Modification Of Gold Nanorods

Gold nanorods have been useful agents for several studies from drug delivery to cancer therapy selectively. In order to enhance the potential use of gold nanorods for biomedical applications, removal of CTAB from the surface of gold nanorods is required.

The most common application for the replacement of CTAB is the use of thiol groups because of the strong binding potential of gold to sulfur residues.

In this research, to replace CTAB molecules on the surface of gold nanorods with a mixture of bi- and mono-functional PEG molecules, i.e. monomethoxy-PEG-thiol (PEG-SH) and carboxy-PEG-thiol (COOH-PEG-SH) were performed. The reason why PEG mixture used was that PEG-SH prevents non-specific binding and the recognition by reticuloendothelial system whereas carboxy-PEG-thiol enables antibody to bind through its carboxylic sides (Eck, Craig et al. 2008).

The concentration of gold nanorods prepared according to the G3 method, was measured as 72.01 ppm by using ICP-MS. For PEG coating and cellular assays, gold nanorod solution was concentrated up to 1000 ppm.

The concentration of PEG molecule in 1 ml gold nanorod solution required for coating the gold nanorod surface was theoretically calculated assuming one PEG chain coats 0,07 nm^2 surface area (3.1), n refers to number of Au atoms per gold nanorod, $N_{avogadro}$ is avogadro constant, h is the height of gold nanord, r is diameter of a nanorod. The shape of gold nanorods was estimated as sylindirical with two hemispherical ends (see Figure 3.3). The diameter was recorded as 10 nm and height was recorded as 50 nm from SEM image.
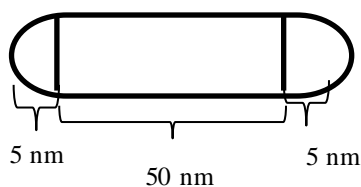
Figure 3.3 : Schematic illustration of a nanorod.

$$(4\pi + 2\pi rh)x\frac{0,07}{n \; x \; NAvogadro}$$

<div align="right">(3.1)</div>

From equation 3.1., the theoretical PEG concentration was found as 0,324 mg in 1 ml gold nanorod solution. Before *in vitro* cell culture experiments, optimizations through the molar ratios of PEG mixtures were tested. Mixed PEG solutions of COOH-PEG-SH/ PEG-SH in UP water were prepared at varying PEG-SH: COOH-PEG-SH molar ratios of 1:1 and 1:9.

The as prepared gold nanorods were incubated with mixed PEG molecules (MW 1000) overnight and next day dialysis was performed in order to avoid excess PEG molecules as described in detail in experimental section.

To compare the dose dependent effects of PEG molecules, gold nanorods were exposed to varying concentrations of PEG molecules after centrifugation process.

Figure 3.4 shows the extinction spectra of gold nanorods before and after PEGylation. After modifying the gold nanorods with PEG molecules at varying concentrations, longitudinal surface plasmone resonance slightly changed through red side. It is apperantly seen that the modifaction did not remarkably change the optical properties of gold nanorods. Decrease in the extinction intensity after modification was visualized (Niidome, Yamagata et al. 2006).
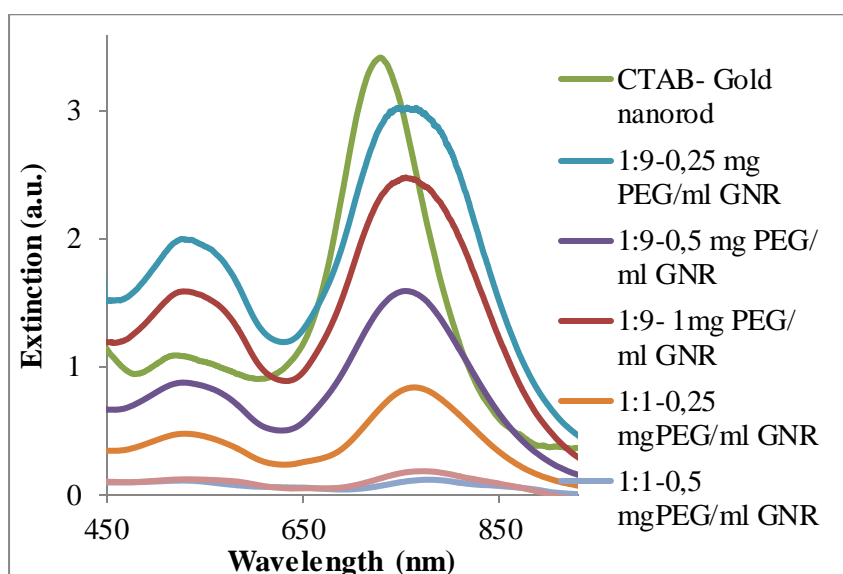
Figure 3.4 : Extinction spectra of gold nanorods before and after surface functionalization.

In order to find the optimum concentration required for overcoating the surface of gold nanorods with sufficient PEG molecules, mixed PEG solutions of COOH-PEG-SH/ PEG-SH in UP water at 1:9 molar ratio (200 µl, 300 µl, 400 µl, 800 µl, 10 mM) were prepared and gold nanorods were functionalized with PEG molecules at different concentrations. Figure 3.5 illustrates the hydrodynamic sizes of CTAB coated and PEG coated gold nanorods. After modifying with PEG, the increase in the hydrodynamic size of gold nanorods was observed.
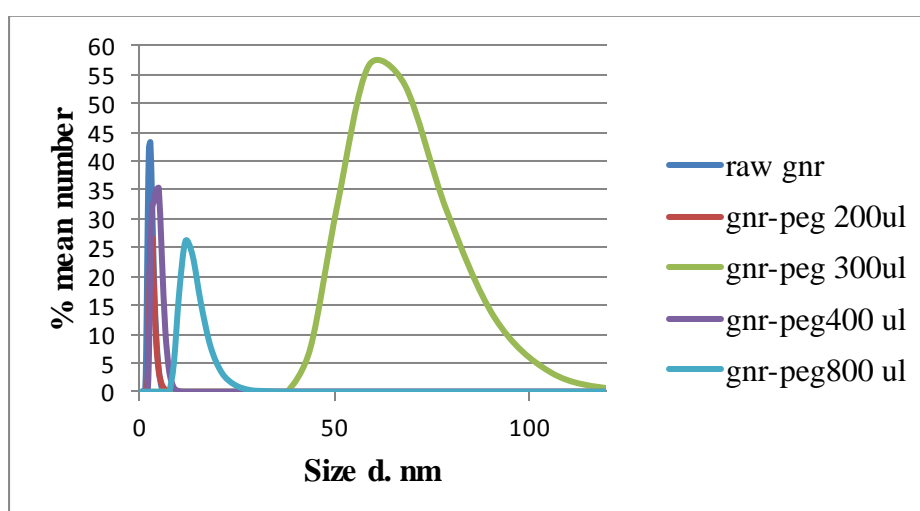
Figure 3.5 : Hydrodynamic diameter of CTAB-GNRs and PEG coated GNRs

Table 3.2 : Zeta potentials of PEGylated gold nanorods with varying concentrations

PEG volumes (10 mM at 1:9 molar ratio)	Zeta Potentials (mV)
CTAB-GNR	32,1
200	-19,1
300	-4,64
400	-12,3
800	-16,7

After PEGylation, the zeta potentials of PEG-gold nanorods in water were measured via Malvern Zeta Sizer. Table 3.2 shows the zeta potentials of CTAB-GNRs and PEG-GNRs. In comparison with CTAB-GNRs, the zeta potentials after surface modification go down to negative values (Rostro-Kohanloo, Bickford et al. 2009). These changes in the surface charge after modification of gold nanorod surface contributed to the ligand exchange was succeeded negative charged ligands. However, there was no saturation point observed in the zeta potentials of PEG-GNRs.

Although there were several concentrations tried to find the optimal range of the PEG concentration, previous experiments did not show the clear results. For this reason, mixed PEG solutions of COOH-PEG-SH/ PEG-SH in UP water were used by operating the molar ratios of COOH-PEG-SH/ PEG-SH at 1:1 and 1:9 respectively. For each molar ratios, gold nanorods (1ml, 1000 µg) were also treated with diffferent concentrations of PEG molecules in water (0,25 mg, 10 mM, 0,5 mg, 10 mM and 1 mg , 10 mM) in the gold nanorod solution.

Table 3.3 : Zeta Potential values of various PEG molecules

Samples	Zeta Potentials
GNR- CTAB	32,1 mV
GNR-PEG 1:1-0,25 mg PEG	-3.41 mV
GNR-PEG 1:1-0,5 mg PEG	-5,4 mV
GNR-PEG 1:1-1 mg PEG	-5 mV
GNR-PEG 1:9-0,25 mg PEG	0,5 mV
GNR-PEG 1:9-0,25 mg PEG	-2,62 mV
GNR-PEG 1:9- 1mg PEG	-1,13 mV

Table 3.3 illustrates the surface charges of the PEGylated gold nanorods at varying concentrations. Molar ratio of COOH-PEG-SH/ PEG-SH at 1:1 resulted in the sensitive values. For gold nanorod solution treated with 0,25 mg, 10 mM PEG molecules, the zeta potential of the PEGylated gold nanorod suspension was -3,41 meV. It is clearly seen from Table 3.3 that as PEG concentration in the gold nanorod solution increases, the zeta potential values goes down to approximataely -5,41 meV. Yet, the value did not change strongly when gold nanorods were treated with 1 mg, 10 mM PEG solution in water. It can be deduced that the gold nanorods' surface was saturated with PEG molecules respectively. The optimum concentration range of PEG molecules for ovorcoating the gold nanorods' surface was estimated between 0,25 mg and 0,5 mg for gold nanorod solution (1ml, 1000 μg). This results are also in good agreement with the theoretical calculations.
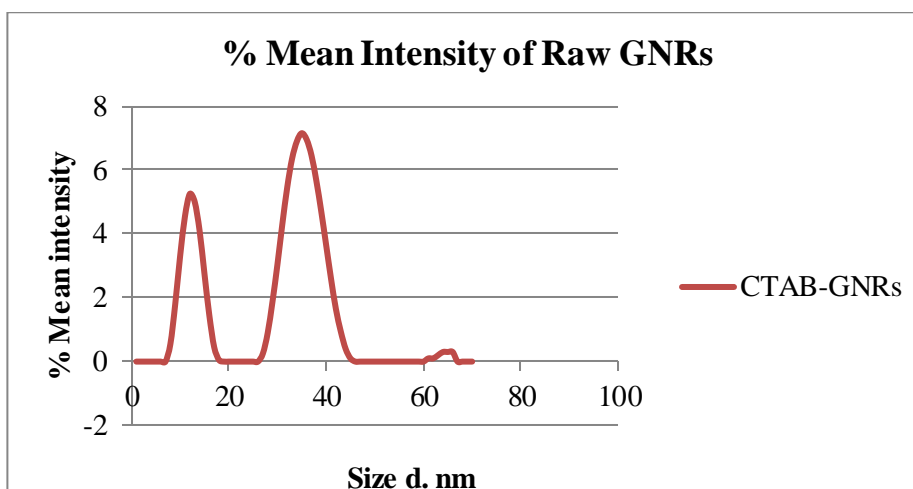
Figure 3.6 : DLS plot of CTAB-GNRs
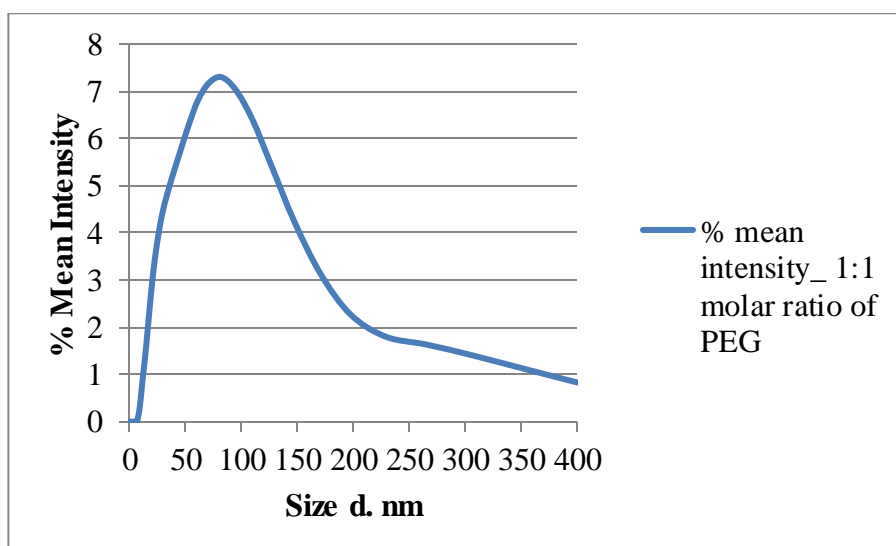
Figure 3.7 : DLS plot of PEGylated gold nanorods in water (Mixed PEG solution with a concentation 10 mM, 0,5 mg was used).

Figure 3.6 shows the hydrodynamic size of CTAB gold nanorods as 35,7 nm. After PEGylation, hydrodynamic diameter shifts up to ~71 nm respectively. Increase in the hydrodynamic diameter of GNRs after PEGylation indicates that Gold nanorods' surface was coated with PEG molecules (Figure 3.7).

Kopwitthaya et al. also performed DLS in order to determine the hydrodynamic size of the PEGylated gold nanorods. They also visualized that red shift occured after PEGylation step (Kopwitthaya, Yong et al. 2010).
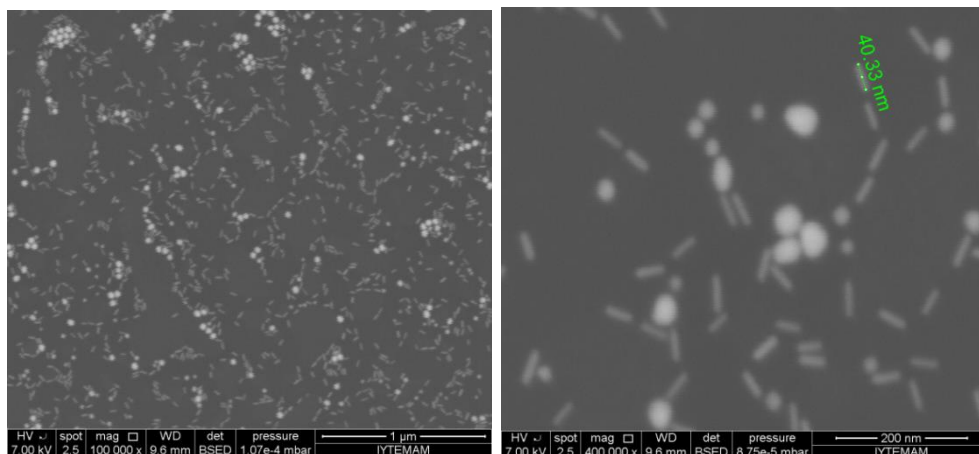
Figure 3.8 : SEM images of CTAB coated gold nanorods

The morphology of CTAB coated gold nanorods were visualized by using SEM operating at 7.00 kv. Figure 3.8 illustrates that it is possible to fabricate high yielded gold nanorods using G3 method described in detail in experimental section.

In order to support the results obtained from DLS and UV-Visible Spectroscopy, the morphology of the PEGylated gold nanords was also performed by SEM by operating at 4.00 keV with Zeiss Ultra Plus microscopy. Figure 3. 9 illustrates the gold nanorods coated with PEG molecule labeled with red arrow.
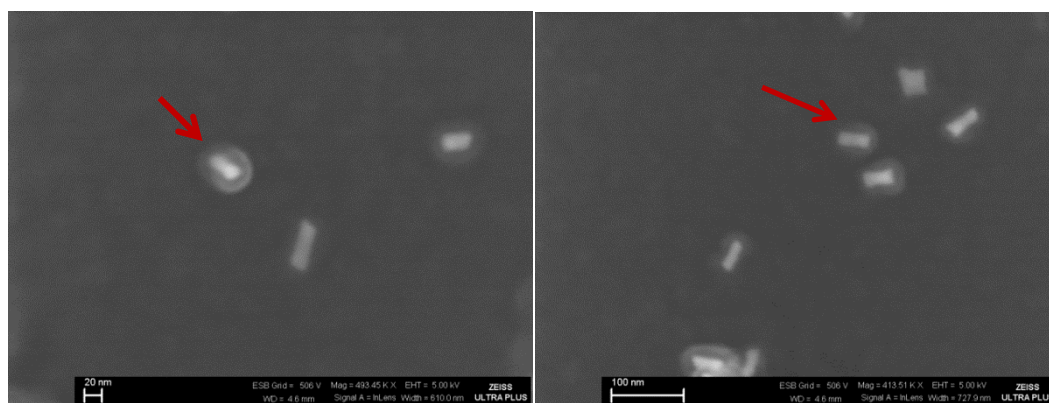
Figure 3.9 : SEM images of PEGylated gold nanorods (PEG molecules covered gold nanorod's surface is shown with red arrow).

3.3 Nanodrop Measurement

Prior to the conjugation of anti-CD138 to PEG coated gold nanorods, lysozyme was used as a model protein. In order to evaluate the binding efficiency of lysozyme, gold nanorods were treated with lysozyme due to the assumption that targeting of carboxylic groups of PEG was 100 % described in details in experimental section. Serial dilutions from lysozyme stock solution in PBS (1 mg, 200 μl) were performed to obtain standart curve.

Standart Curve of Lysozyme

y = 2,0709x + 0,0893
R² = 0,9972

◆ Standart Curve of Lysozyme

── Linear (Standart Curve of Lysozyme)
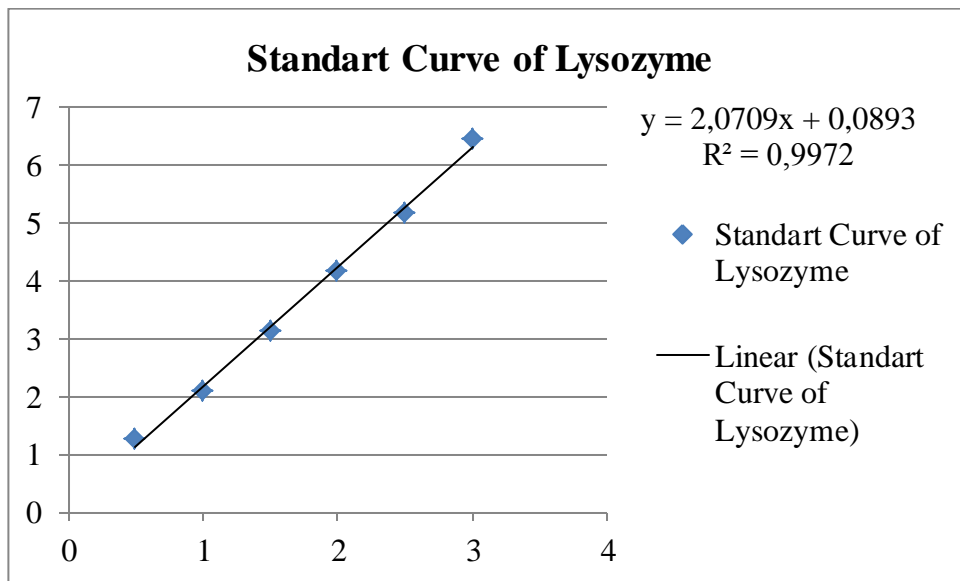
Figure 3.10 : Standart Curve Of Lysozyme As Model Protein

Absorbance values of each sample were converted to the concentration values equation 3.3 obtained from standart curve of lysozyme (See Figure 3.10).

$$y = 2,0709x + 0,0893$$

(3.3)

Table 3.4 shows the concentraions of the conjugation mixtures and protein concentrations of supernatant 1 and supernatant 2 after two washes with PBS.

The amount of protein conjugated with PEG coated GNR was calculated theoretically where C_0 refers to the concentration of control **(3.4).**

$$\text{Cprotein attached} = [C0 - [(A + B) - (C + D)]]$$

$$(3.4)$$

$$\frac{Cprotein\ attached \times Vreaction}{MA(Lysozyme) \times (mole\ of\ PEG - COOH\ in\ reaction\ solution)}$$

$$(3.5)$$

Table 3.4 : The Concentrations of samples calculated from standart curve of Lysozyme

Samples	Protein Concentrations (μg/ml)
Protein Stock Solution (C_0)	3,3
A-PEG-GNR plus Lysozyme (Supernatant after 1. wash)	5,85
B- PEG-GNR plus Lysozyme (Supernatant after 2. wash)	0,136
C- PEG-GNR (Supernatant after 1. Wash)	3,430
D-PEG-GNR (Supernatant after 2. Wash)	0,158

From the equation 3.4 and 3.5., percentage of targeted PEG-COOH with Lysozyme was found ~ 90 % respectively.

3.4 Polyacrylamide Gel Electrophoresis

SDS-PAGE has been a useful method for determinatio of the concentrations of protein mixtures several years Thus, the protein mixtures can be seperated easiliy due to their molecular weight or concentrations in samples (Cohen and Karger 1987). For this reason, to illustrate the presence of protein and the conjugation yield, SDS-PAGE was performed.
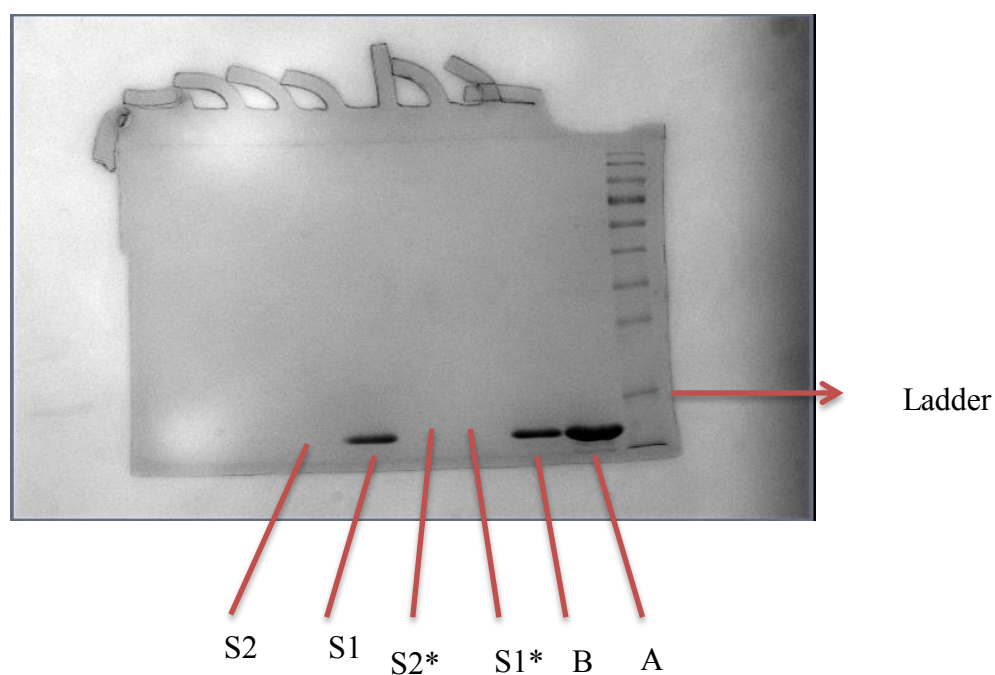
Figure 3.11 : The illustration of gel after coomassie blue staining. A) The original stock protein, B) The protein solution without nanorod. S1*: Supernatant 1 of PEG coated gold nanorod solution. S2*: Supernatant 2 of PEG coated gold nanords. S1: Supernatant 1 of lysozyme conjugated PEG-gold nanorods. S2: Supernatant 2 of lysozyme conjugated PEG-gold nanorods.

Figure 3.11 illustrates the appearance of bands loaded during gel electropharesis. To confirm the binding efficiency of lysozyme to PEG coated gold nanorods, apart from nanodrop measurement, SDS-PAGE gel electropharesis was performed with coomassie blue and silver staining. From image analysis program, the adjusted intensity values of the bands were visualized after staining. Table 3.5 shows the intensity of the bands obtained during analysis. Intensity of the bands is proportional to the concentration of protein. For this reason, the conjugation yield was calculated due to the intensity values of the bands **(3.6)**.

$$Conjugation\ \% = \frac{(A - (S1 + S2))}{B}$$

(3.6)

Table 3.5 : The adjusted volume intensity of bands visualized during image analysis

Samples	Adjusted Volume Intensity mm^2
A	185885
B	85142
S1	137920
S2	-

From this calculation, when targeted the 100 % of PEG coated gold nanorods with lysozyme, the binding yield was observed at 56,3 %. This is slightly correlated to the results obtained from nanodrop measurements. The difference between yields obtained from both nanodrop and electrophoresis may depend on inaccurate estimation of band intensities from image analysis program.

Nanodrop measurement and gel staining results, clearly confirm that, when targeted the total amount of COOH groups of PEG-coated gold nanorods, the targeting percentage is more than 50 %. This also supports that after the activation of COOH groups with reagents, the binding of protein or antibody through carboxylic sides of PEG molecules can be possible with more than 50 % binding efficiency.

3.5 Cytotoxicity assay of CTAB-GNRs and PEG GNRs via MTT

Cellular response to gold nanorods before and after modification has been shown by eaxmining the MTT assay in previously published datas (Rayavarapu 2010).

In this present work, cell survial was tested by using the conversion of MTT to purple formazan crysitals by metabolically active cells (Alkilany, Nagaria et al. 2009). Prior to handle cellular assays, GNRs were concentrated up to 1000 μg/ ml. Following 24, 48 and 72 hours exposure to the CTAB- gold nanorods and PEG-gold nanorods, dose dependent effects of CTAB-coated and PEG coated gold nanorods were assessed for CD138 (+) U266 cell line and CD138 (-) ARH-77 cell line. Initially, in order to show the toxic nature of CTAB-GNRs in cells, each cell line was exposed to the CTAB-GNRs at various concentrations (1, 2,5 , 5, 10, 25, 50 μg /ml (as Au atoms).
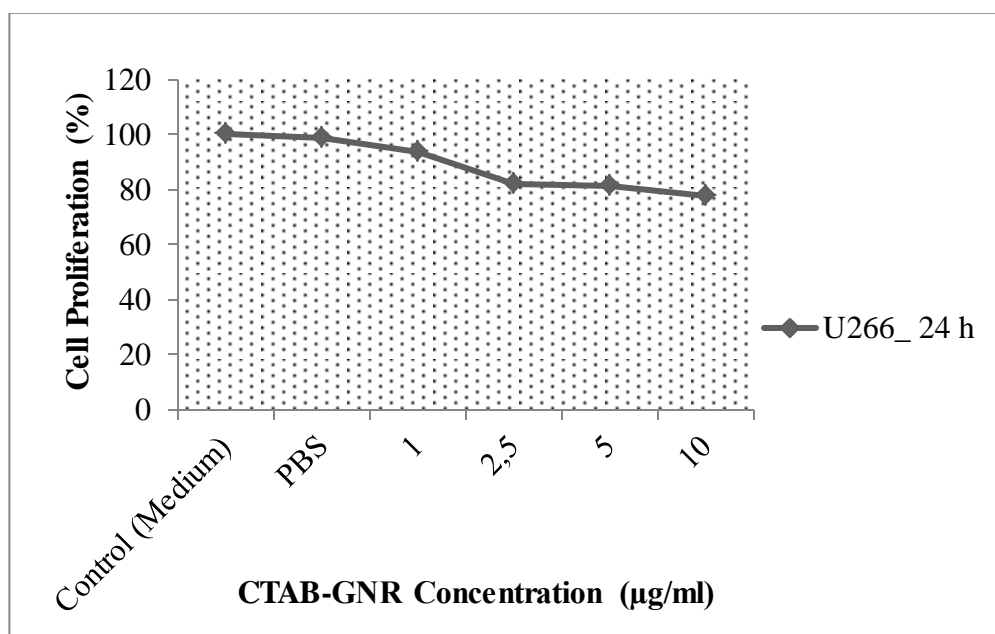
Figure 3.12 : Dose dependent response of U266 cell line following 24 hours exposure to CTAB-GNRs at 1, 2,5, 5 and 10 μg/ ml concentration.
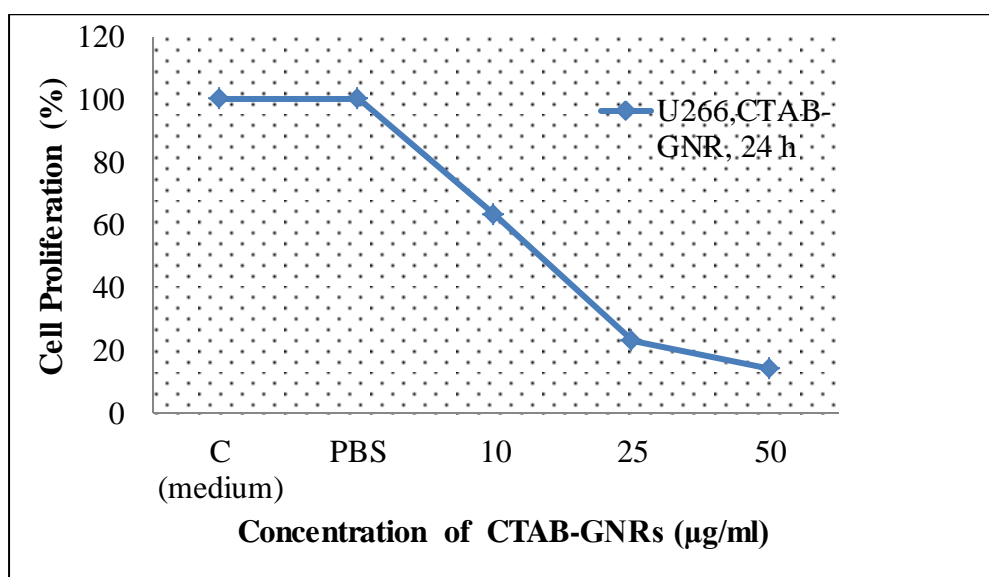
Figure 3.13 : Dose dependent effects of CTAB coated GNRs on U266 cell line. Cells treated with RPMI 1640 alone were used as control groups.

The average absorbance values for each cell samples were calculated and these values are shown as percentage of viable cells relevant to the absorbance values. All experiments were carried out more than triplicate. Error bars for each data are shown in plots. RPMI 1640 with 10 % FBS was used as control (LC_{100}). The cytotoxicity of PBS on cells was also tested.

The main point of the use of lower concentrations of CTAB-gold nanorods was to determine the LC_{50} (50 % cell survival- 50 % cell death) value range for each cell line. As it can be seen in Figure 3.12 and Figure 3.13 , it was observed that PBS is nontoxic to cells (LC_{100}).

In comparison with control groups (nontreated cells), after 24 hours incubation, mortality of U266 cells slightly decreases at low concentrations (See Figure 3.12) whereas the significant decrease in the cell viability was observed at 25 μg/ml (23%) and 50 μg /ml (14 %) (See Figure 3.13).
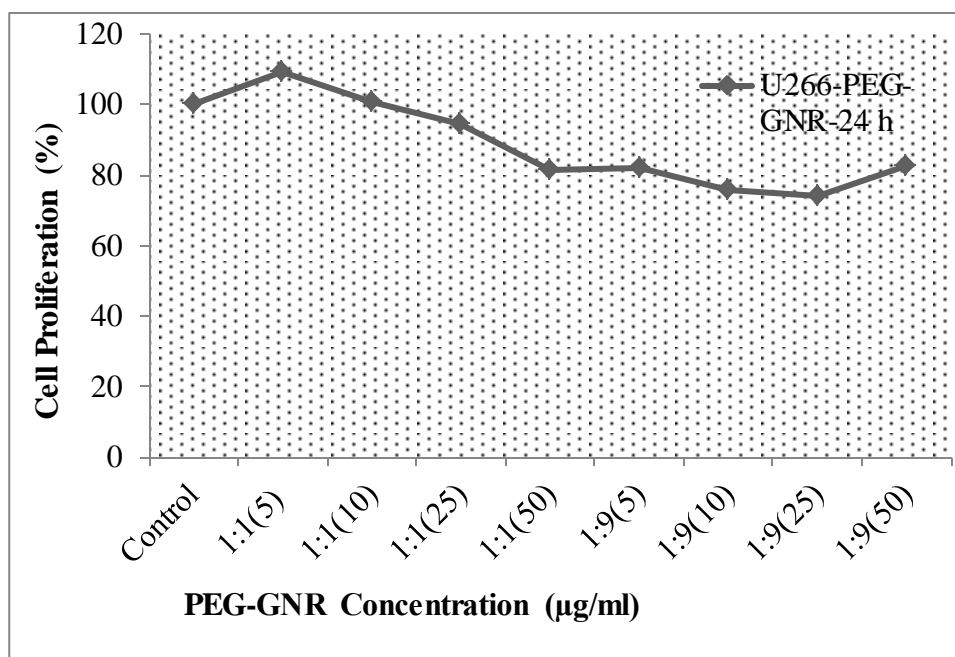
Figure 3.14 : Dose response curve of U266 cell line exposed to varying concentrations of PEG coated Gold nanorod. The molar ratio of COOH-PEG-SH/ PEG-SH 1:1 and 1:9 were tested. Furthermore, PEG coated gold nanorods at 5, 10, 25, 50 μg/ml (as Au atoms) concentration were evaluated.

Figure 3.14 shows the dose dependent effects of PEG coated gold nanorods folllowing 24 hours exposore. At the highest concentration of gold atoms (50 μg/ml) % cell viability comparison with control groups was observed at 81,4 % for the 1:1 molar ratio of SH-PEG/ COOH-PEG-SH and at 82,4 % for 1:9 molar ratio of SH-PEG/ COOH-PEG-SH. The results for PEG-gold nanorods were in contrast with CTAB- coated gold nanorods as expected (See Figure 3.13).

After 48 hours exposure to the CTAB-GNRs at low concentrations of gold atoms, negligible cell loss was observed (See Figure 3.15). After the increase in the concentrations of gold atoms treated with cells, the significant mortality of U266 cells was observed at the highest concentration (See Figure 3.16) whereas the cell viability observed for U266 treated PEG-GNRs is at ~ 109 % for 1:1 molar ratio of SH-PEG-COOH/ SH-PEG and 87,4% for 1:9 molar ratio of SH-PEG-COOH/ SH-PEG at the highest concentration of PEG-GNRs (See Figure 3.17)
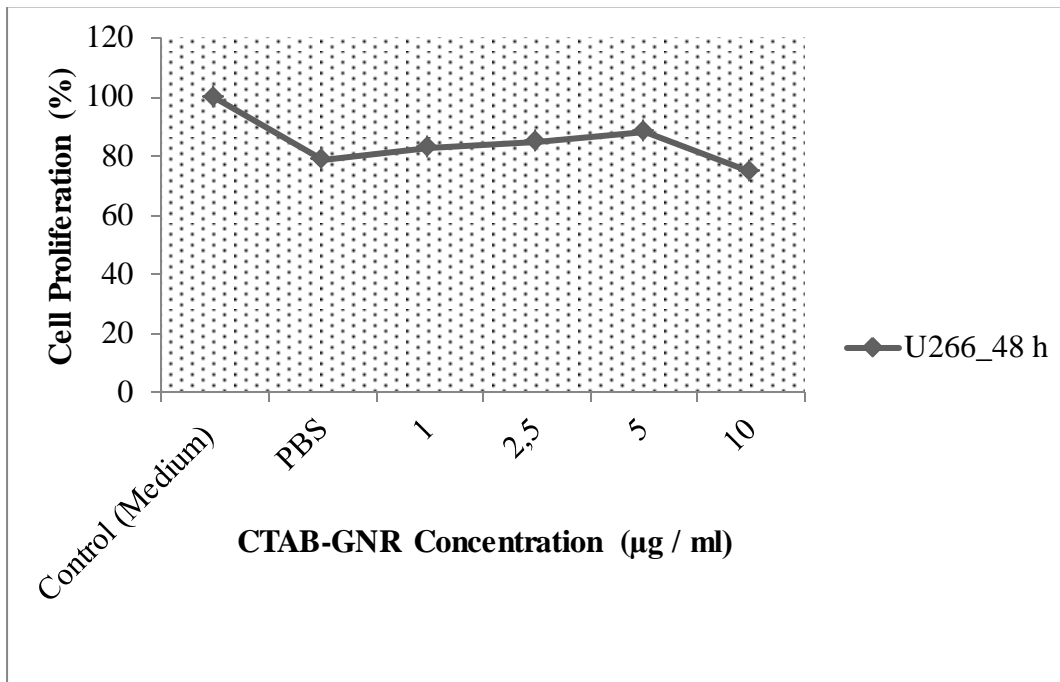
Figure 3.15 : Dose response curve of U266 exposed to CTAB- GNRs at increasing concentrations. Error bars are included in the plot area. Cells with only RPMI 1640 was used as contol groups. Cells with only PBS at the same volume with GNRs were assessed in order to see the cytotoxic effect on cells.
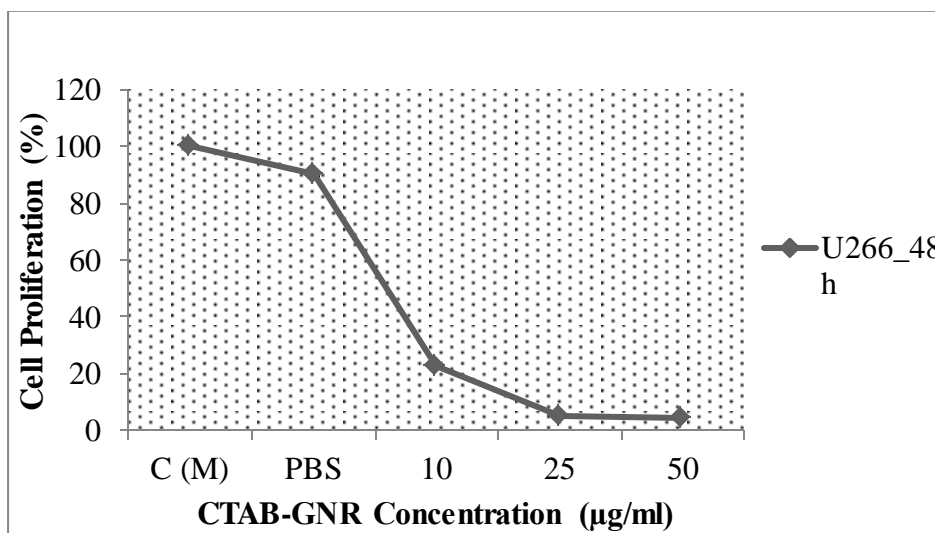
Figure 3.16 : Dose response cure of U266 exposed to CTAB- GNRs at increasing concentrations for 48 hours incubation period Error bars are included in the plot area. Cells with only RPMI 1640 was used as contol groups. Cells with only PBS at the same volume with GNRs were assessed in order to see the cytotoxic effect on cells.
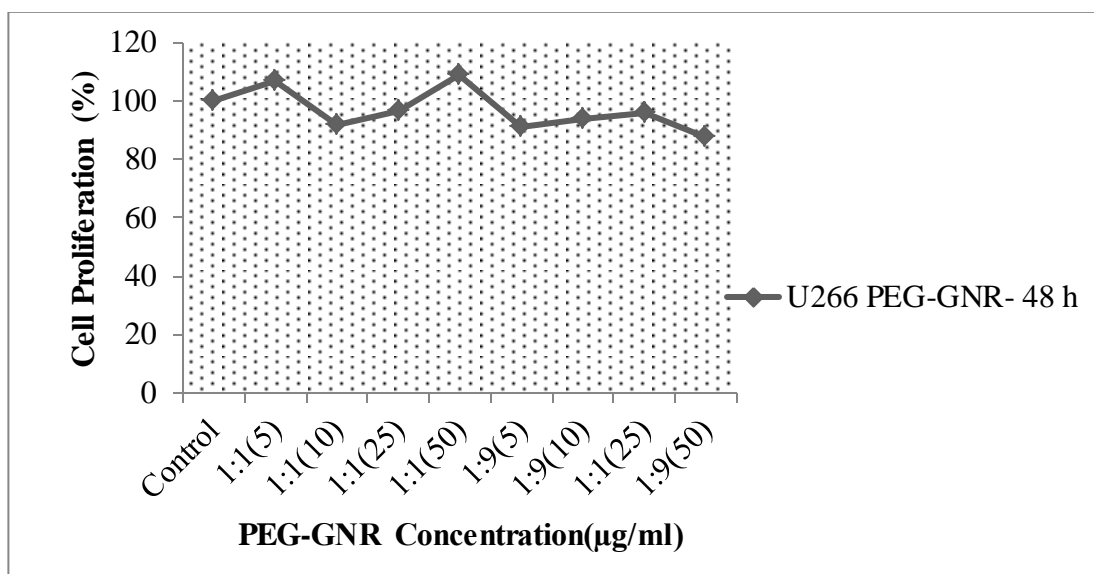
Figure 3.17 : Dose response curve of U266 exposed to PEG-GNRs at various concentrations with molar ratios 1:1 and 1:9 of SH-PEG-COOH/ SH-PEG increasing for 48 hours incubation period Error bars are included in the plot area. Cells with only RPMI 1640 were used as control groups.

On the other hand, after 72 hours exposure to the CTAB or PEG GNRs at increasing concentrations, it was resulted in the change of cell viability due to the surface chemistry as expected. The negligible cell loss was observed at lower concentrations of CTAB-GNRs (See Figure 3.18) in comparison with the higher concentrations of CTAB-GNRs.
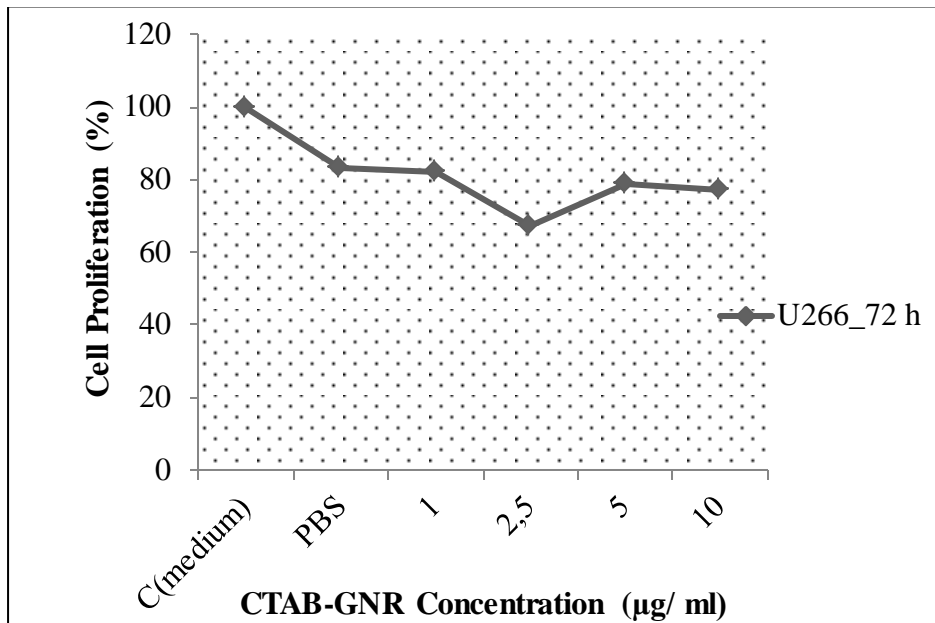
Figure 3.18 : Dose response curve of U266 cells treated with lower concentrations of CTAB-GNRs. Nontreated cells (only treated with RPMI 1640) were used as control groups.
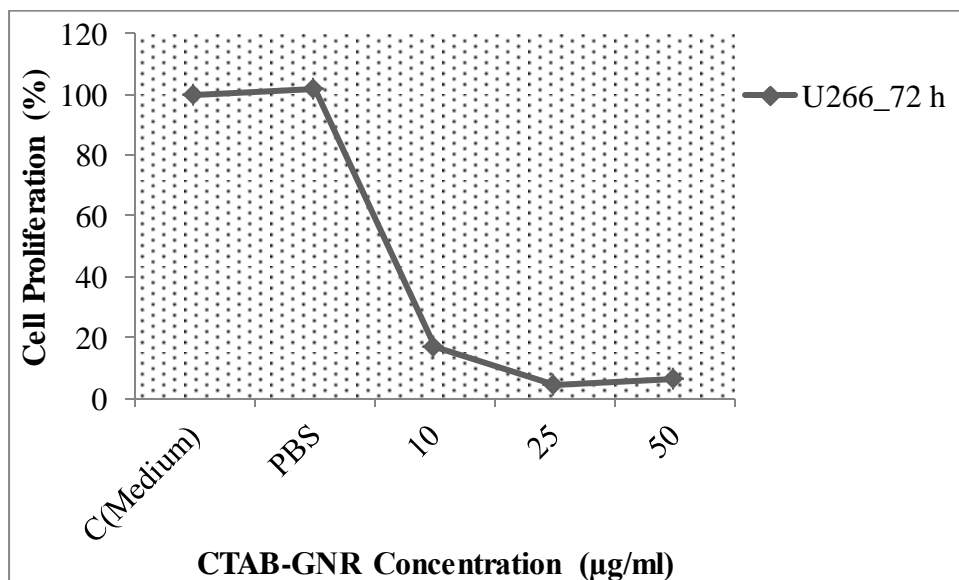
Figure 3.19 : Dose response cure of U266 exposed to CTAB- GNRs at increasing concentrations for 72 hours incubation period Error bars are included in the plot area. Cells with only RPMI 1640 was used as contol groups. Cells with only PBS at the same volume with GNRs were assessed in order to see the cytotoxic effect on cells.

Furthermore, following 72 hours incubation time for U266 cell line, the lethal dose for U266 cells was observed at the highest concentration of CTAB-GNRs (viable cells are ~6 % (See Figure 3.19). In contrast, as it can be visualized from Figure 3.20, at this concentration, PEG-GNRs eliminated the toxic effects on cells (viable cells for 1:1 molar ratio at 86 % , for 1:9 molar ratio at 88 %) respectively.
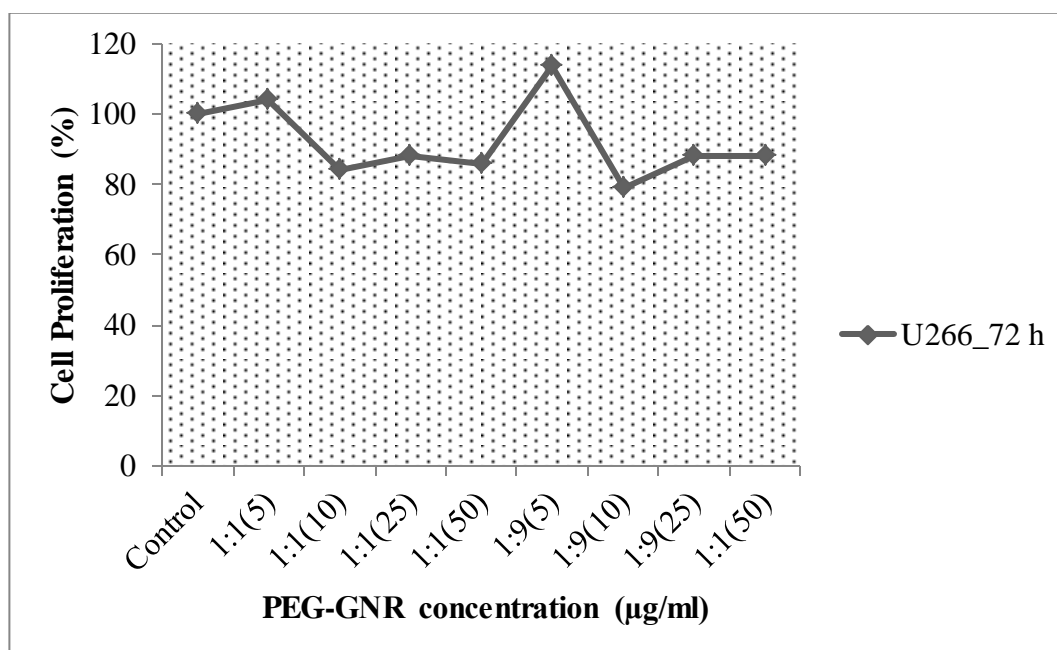
Figure 3.20 : Dose response curve of U266 exposed to PEG-GNRs at various concentrations with molar ratios 1:1 and 1:9 of SH-PEG-COOH/ SH-PEG increasing for 48 hours incubation period Error bars are included in the plot area. Cells with only RPMI 1640 was used as control groups.
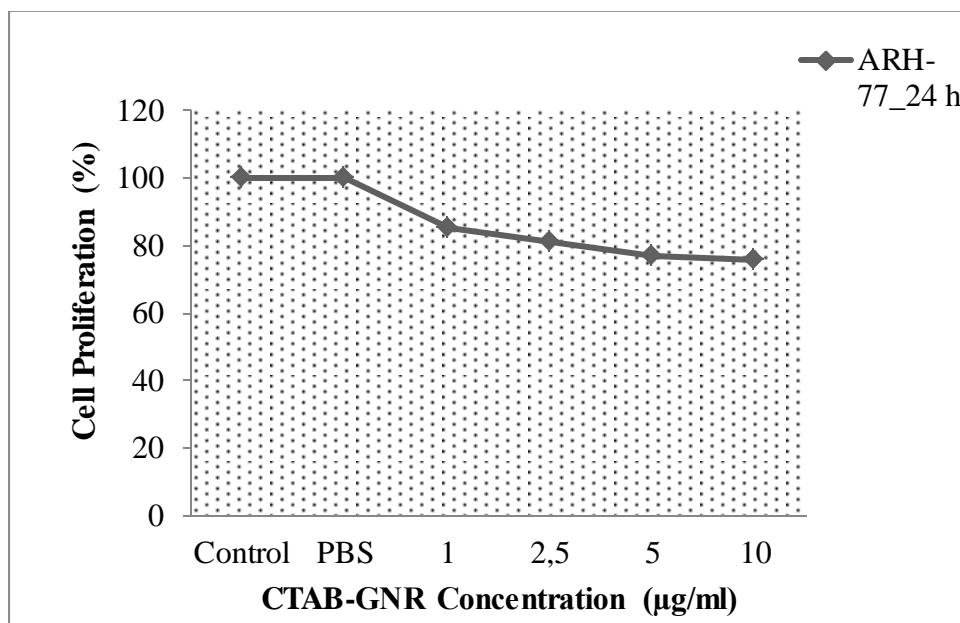
Figure 3.21 : Dose response curve of ARH-77 exposed to CTAB- GNRs at lower concentrations for 24 hours incubation period Error bars are included in the plot area. Cells with only RPMI 1640 was used as contol groups. Cells with only PBS at the same volume with GNRs were assessed in order to see the cytotoxic effect on cells.

Similar trends were also obtained for ARH-77 cell line for the case of CTAB-GNR and PEG-GNR. After 24 hours incubation period, as it can be seen in Figure 3.21, the IC50 value of cells treated with CTAB-GNRs is between 10 and 25 µg/ ml of gold atom concentrations. The highest cytoxicity of CTAB-GNRs is seen at 50 µg /ml (Cell viability, 10 %) in which concentration cells survival for PEG-GNRs is 87,5 % for 1:1 molar ratio of SH-PEG-COOH/ SH-PEG and 91,2 % for SH-PEG-COOH/ SH-PEG (See Figure 3.22).

Figure 3.22 : Dose response cure of ARH-77 exposed to CTAB- GNRs at increasing concentrations for 24 hours incubation period Error bars are included in the plot area. Cells with only RPMI 1640 was used as contol groups. Cells with only PBS at the same volume with GNRs were assessed in order to see the cytotoxic effect on cells.
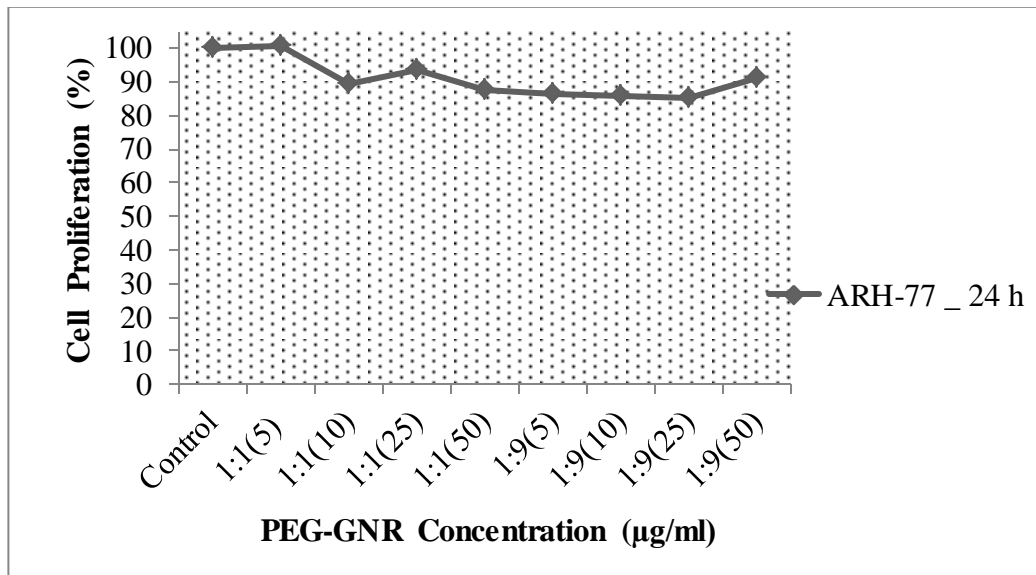

Figure 3.23 : Dose response curve of ARH-77 exposed to PEG-GNRs at various concentrations with molar ratios 1:1 and 1:9 of SH-PEG-COOH/ SH-PEG for 48 hours incubation period Error bars are included in the plot area. Cells with only RPMI 1640 was used as control groups.

69
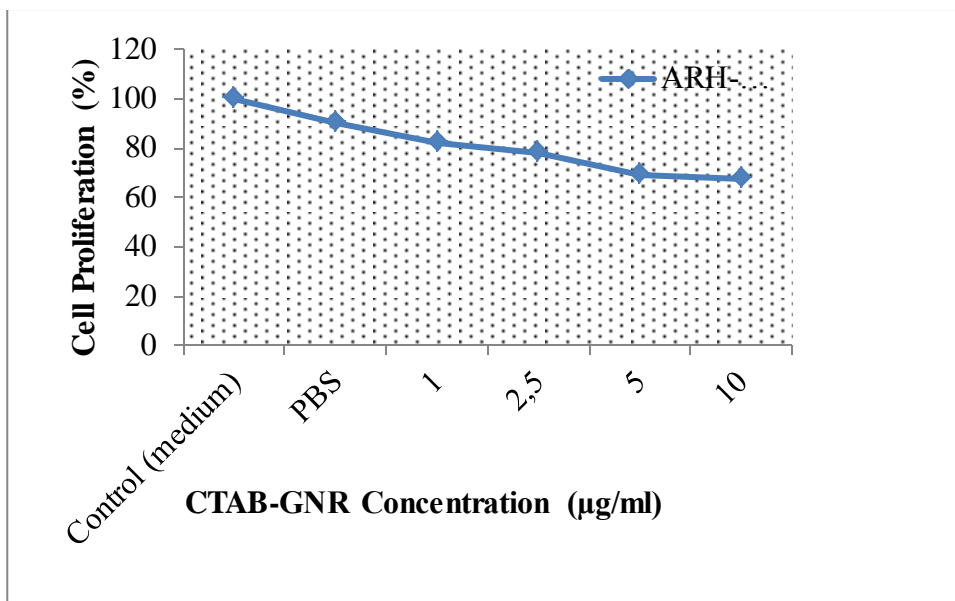
Figure 3.24 : Dose response curve of ARH-77 cells exposed to lower concentrations of CTAB-GNRs for 48 hours incubation period.

Figure 3.23 exhibits the cell respond to the lower concentration of CTAB- GNRs. In comparison with control groups, there is a little decrease in the cell viability even at these lower concentrations whereas Figure 3.24 shown at above, indicates that significant toxic effect of CTAB-GNRs increases proportional to concentation of CTAB-GNRs. Lethal dose for ARH-77 cells after 48 hours exposure, is 50 μg/ml of gold atoms concentration in CTAB-GNRs.
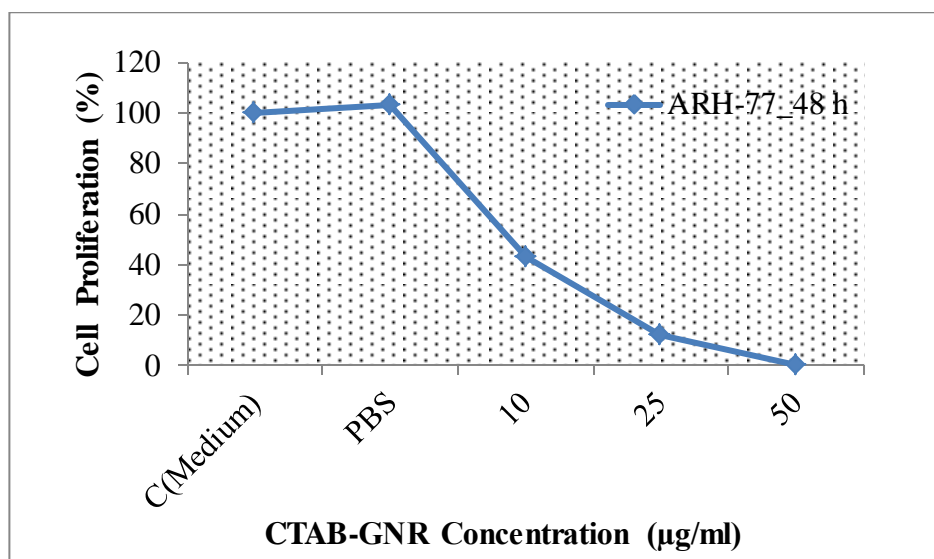
Figure 3.25 : Dose response curve of ARH-77 cells exposed to higher concentrations of CTAB-GNRs for 48 hours incubation period.

Figure 3.26 indicates that PEG-GNRs significantly reduces the toxicity on ARH-77 cells even at the highest dose in which CTAB-GNRs are lethal after 48 hours exposure time (See Figure 3.25).
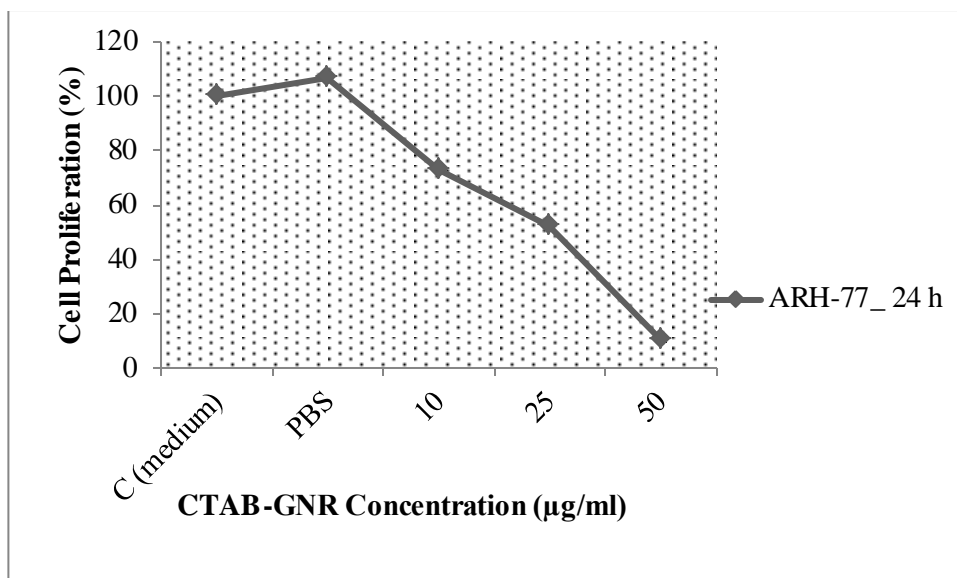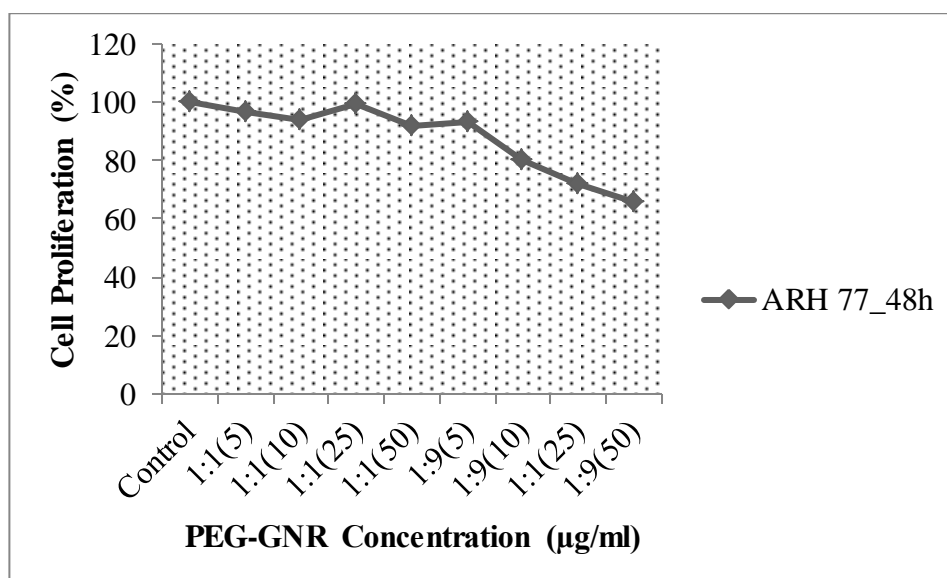

Figure 3.26 : Dose response curve of ARH-77 exposed to PEG-GNRs at various concentrations with molar ratios 1:1 and 1:9 of SH-PEG-COOH/ SH-PEG increasing for 48 hours incubation period Error bars are included in the plot area. Cells with only RPMI 1640 was used as control groups.
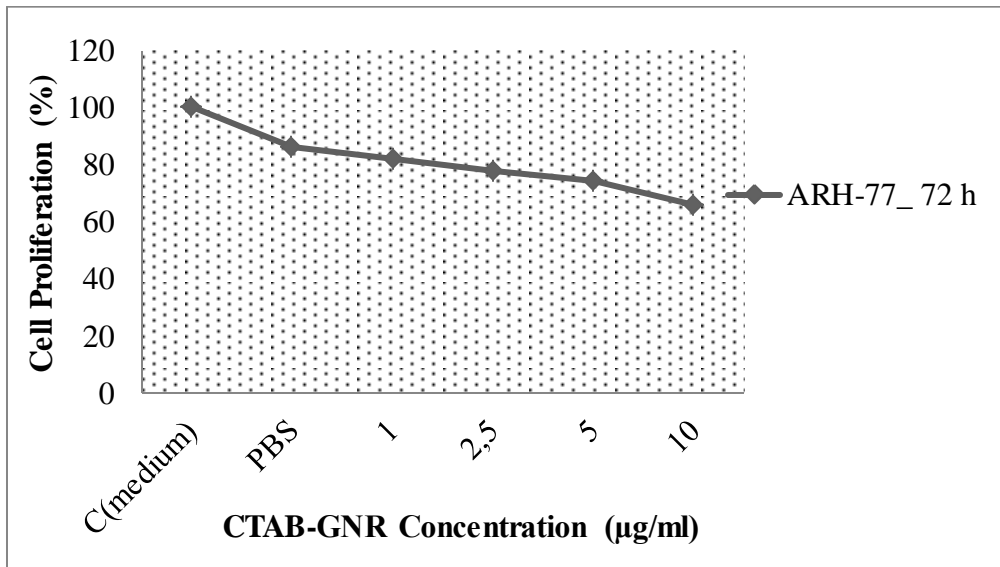
Figure 3.27 : Dose response curve of ARH-77 cells exposed to lower concentrations of CTAB-GNRs for 72 hours incubation period.
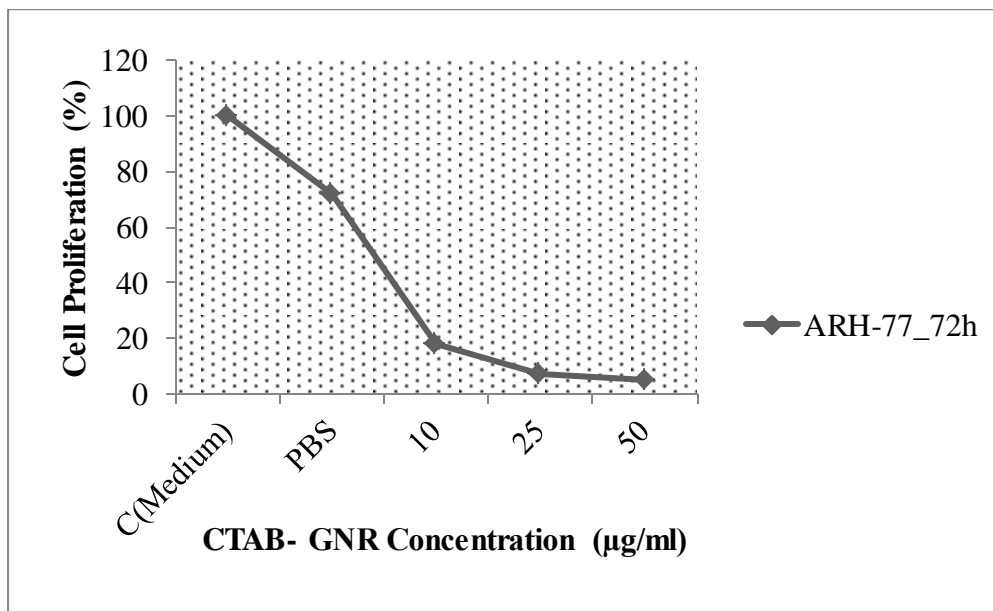
Figure 3.28 : Dose response curve of ARH-77 exposed to increasing concentrations of CTAB-GNRs. Cells with only RPMI 1640 was used as control groups.

For 72 hours incubation period, the lethal dose of CTAB-GNRs on ARH-77 cells seen in Figure 3.28 is at 50 μg / ml of GNR concentrations. However, PEG-GNRs even at high concentrations, lessen the toxic effect of GNRs corresponding to surface chemistry (See Figure 3.29).
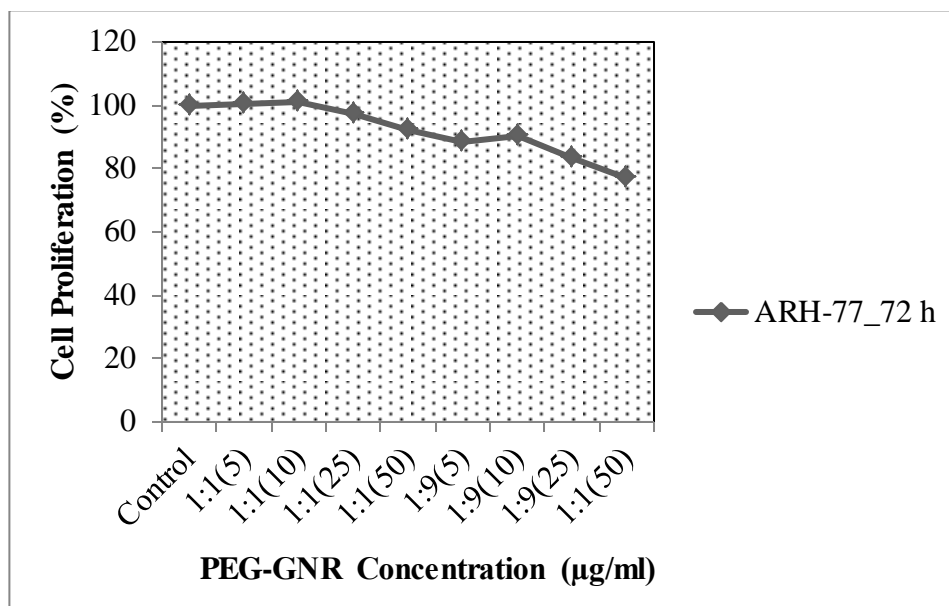
Figure 3.29 : Dose response curve of ARH-77 exposed to PEG-GNRs at various concentrations with molar ratios 1:1 and 1:9 of SH-PEG-COOH/ SH-PEG increasing for 72 hours incubation period Error bars are included in the plot area. Cells with only RPMI 1640 was used as control groups.

In general, it was visualized that ARH-77 cell line is more resistant than U266 cell line treated with CTAB-GNRs for 24, 48 and 72 hours respectively. The results obtained for both cell lines implicated that cytotoxicity occurs due to the presence of CTAB. Since after modification with PEG, the toxicity of gold nanords on cancerous cells remakably diminishes (Liopo, Conjusteau et al. 2012).

Although CTAB is required for the formation and stabilization, after shaping of GNRs, it is necessary to avoid the free CTAB residuals from GNRs to diminish the cellular mortality. Change in the surface chemistry regardless of surface charge, significantly effect the results on cells in conrast with original GNRs (Rayavarapu 2010)

Cytotoxic effects of CTAB gold nanorods are in concentration dependent manner. The results obtained in present study, strongly are in good agreement with the results found previously reported researchs (Cabada, de Pablo et al. 2012).

3.6 Annexin V Assay

Annexin V which is known as vascular protein with its quite strong anticoagulant properties (Reutelinsperger et al, 1985) has binding affinity to phospholipids which are located in plasma membrane. When cell death occurs, one of the phospholipids, phosphotydilserine is translocated from inner membrane to outer membrane. This is the sign of that cell death is occuring in a programmed way (Vermes, Haanen et al. 1995).

Phosphotydilserine is easily detected by staining fluorescent conjugate annexin V. Annexin V is therefore used to detect apoptotic cells in cell culture experiments.

Annexin V is used in conjuction with vital propidium iodide dye and fluorescent dye FITC for identification of early and late apoptoic cells. Damaged membranes are permeable to propidium iodide. In early phase of apoptosis; FITC is positive to cells while PI is negative. In the late apoptotic cells, FITC and PI are both positive to detect apoptotic cells. It enables us to illustrate how many percent of cultured cells are in the early apoptotic or late apoptotic phase.

In this present study, paralel to cell viability assay, U266 and ARH-77 cell lines were examined with CTAB-GNRs at concentration range where IC_{50} was observed in MTT assay. For this reason, from 2,5 μg/ml to 25 μg/ml of GNR concentrations were tested for 24, 48 and 72 hours incubation periods. Cells nontreated with CTAB-GNRs wre used as control groups.

Representative dot plots of annexin V staining are shown in Apendix A. Four quadrant plots show necrotic cells (Q1), late apoptotic cells (Q2), viable cells (Q3) and early apoptotic cells (Q4). Representative plots of fold increase in apoptotic cells were drawn depending on the total percentage of early apoptotic and late apototic cells.

Figure 3.30 illustrates the fold increase in programmed U266 cells death due to the increasing concentrations of CTAB-GNR after 24, 48 and 72 hours exposure. The effective induction of apoptosis was observed at 10 and 25 μg/ml of CTAB-GNRs on U266 cells for 24 h.
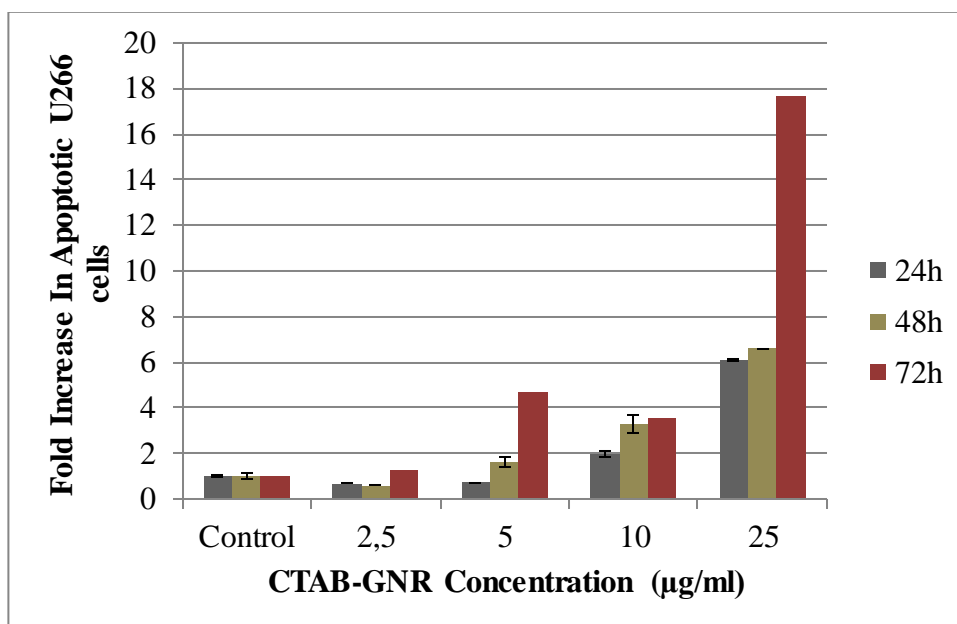
Figure 3.30 : Fold increase in the cell death for U266 cells after 24,48 and 72 h exposure to the CTAB-GNRs at various concentrations.

After 48 h and 72 h incubation time, CTAB-GNRs adversely effected the cell viability and induced apoptosis at higher concentrations. (See Figure 3.29).

Similar trends were also obtained for ARH-77 cell line after Annexin V staining. At 25 μg/ml, CTAB-GNR induced apoptosis ~1,4 order of magnitude higher than control groups (See Figure 3.31). Similarly after 48 and 72 h exposure to the CTAB-GNR, the apoptotic induction of CTAB-GNRs increase at 10 and 25 μg/ml concentrations in comparison with control groups.

In general, these results also confirm that U266 cells are more vulnarable to the increasing concentrations of CTAB-GNRs than ARH-77 cells. These results also support the results obtained from MTT assays that lower concentrations of CTAB-GNRs (2,5 and 5 μg/ml) are not effective on cell death whereas higher concentrations more effective on cell death. Moreover, induction of apoptosis in cells

is relevant to the surface chemistry of gold nanorods. Apoptotic effect of GNRs is due to the presence of CTAB (Lau, Chen et al. 2012).
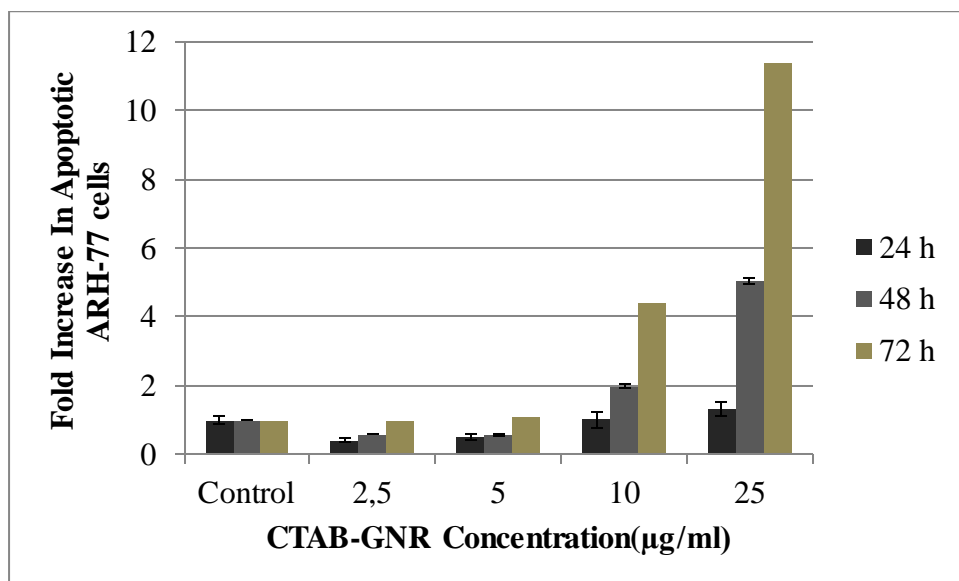
Figure 3.31 : Fold increase in the cell death for ARH-77 cells after 24, 48 and 72 hours exposure to the CTAB-GNRs at various concentrations.

3.7 Cell Uptake Of Gold Nanorods

Cell uptake of gold nanorods can be determined using different characterization techniques such as TEM, ICP-AES (Alkilany, Nagaria et al. 2009) or ICP-MS measurement. After the incubation of cells with gold nanorods, lysis of cell membranes via higly concentrated nitric acid, is resulted in the obtaining gold ions measured by ICP-MS.

In this work, ICP-MS measurement was performed in order to estimate the Au contents internalized by U266 and ARH-77 cells following the 1,5 and 3 hours exposure to the PEG-GNRs with 1:1 molar ratio (PEG-SH: COOH-PEG-SH) at two different concentrations (10, 25 μg/ml as Au atoms). These two concentration were determined corresponding to the cytotoxicity results and these concentrations were in

the range of IC_{50}. The numbers of GNRs taken per cell were calculated depending on the concentration of gold atoms coverted into the number of gold nanorods following the equations. The number of gold atoms (n) containing each gold nanorods was determined **(3.7)** where V is volume of one gold nanorod and ρ is the density of gold and M_A is molecular weight of gold. The number of gold nanorods (N)was calculated **(3.8)** where M refers the gold ions measured by ICP-MS.

$$n = \frac{V \; X \; \rho}{MA} \qquad\qquad\qquad (3.7)$$

$$N = \frac{M}{n} \qquad\qquad\qquad (3.8)$$
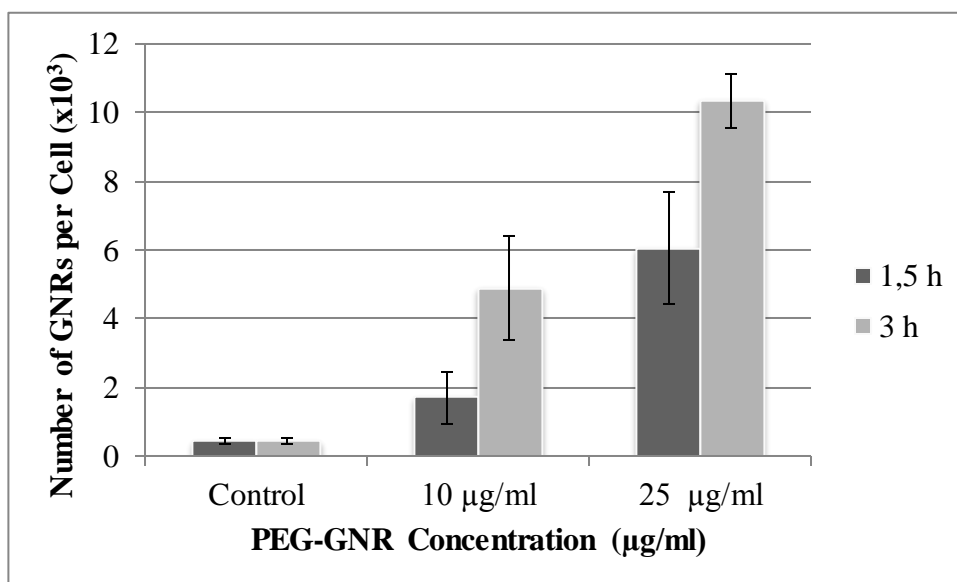
Figure 3.32 : Time and dose dependent uptake of PEG-GNRs by U266 cells. Concentration values indicate gold-atom concentrations.

Figure 3.31 shown at above, exhibits the cellular internalization of GNRs in different time periods. At a gold atom concentration of 25 μg/ ml, the highest upake by U266 cells was observed (6042,11 gold nanorods per cell for 1,5 h and 10936 gold nanorods per cell for 3 h).

Similar results were also obtained for ARH-77 cells. Figure 3.32 shows the time and dose dependent uptake of PEG coated gold nanorods by ARH-77 cells. This was also resulted in the increase in the uptake of gold nanorods in increasing time and dose.
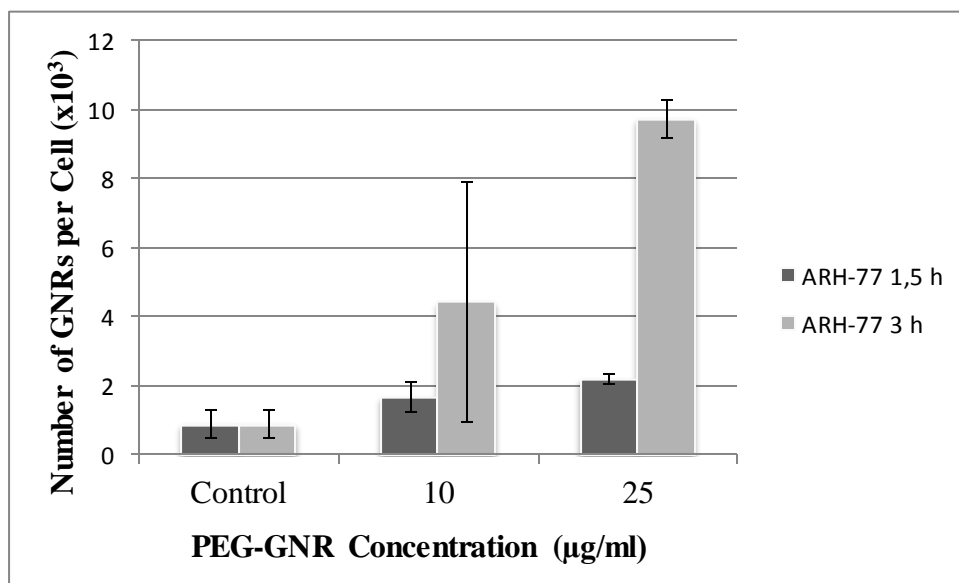
Figure 3.33 : Time and dose dependent uptake of PEG-GNRs by ARH-77 cells. Concentration values indicate gold-atom concentrations.

In comparison with the incubation time periods, following 3 hours incubation, the number of gold nanorods internalized by U266 and ARH cells was higher for both concentrations (see Figure 3.33). From these results, it can be withdrawn that gold nanorods can be internalized by mammalian cells (Alkilany, Nagaria et al. 2009). Meanwhile, this data also supports the time dependent uptake of gold nanorods (Gu, Cheng et al. 2009).

After the attachment of anti-CD138 to PEGylated gold nanorods, cellular uptake of anti-CD138 conjugated gold nanorods were carried out for 3h hours incubation time in which the highest uptake of PEGylated gold nanorods were observed for each cell

line. On the other hand, since the highest uptake of gold nanorods were obtained at 25 µg/ml concentration, the internalization of antibody conjugated gold nanorods were tested at this concentration.
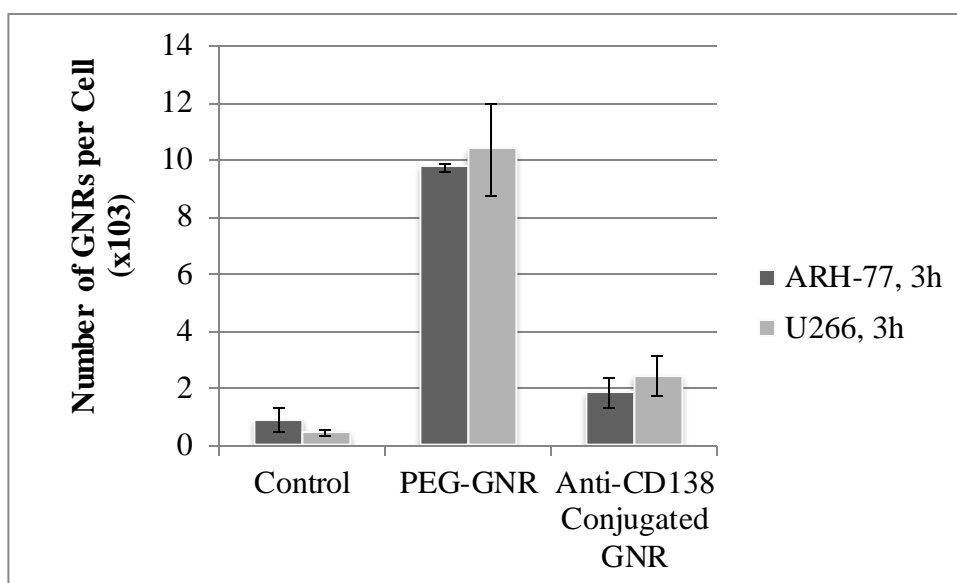
Figure 3.34 : Internalization of Gold nanorods at 25µg/ml concentration depending on the surface chemistry for 3 h incubation time for each cell line.

Figure 3.34 illustrates the comparison of the uptake of PEG coated gold nanorods and anti-CD138 conjugated gold nanords by U266 and ARH-77 cell line after 3 hours exposure.

In general, when compared to the uptake of anti-CD138 conjugated to the gold nanorods for each cell line, the higher uptake was observed for U266 cell line which is overexpressing CD138 antigen, as expected. However, contrary to the PEG-coated gold nanorods, the number of anti-CD138 conjugated gold nanorods internalized by U266 cells decreases. This may due to the non-equal distrubution of cells during experiment. In order to visualize precise results, cellular uptake should be repeated at least triplicate.

On the other hand, contrary to PEG coated gold nanorods the decrease in the uptake level for ARH-77 incubated with anti-CD138 conjugated gold nanorods confirms that ARH-77 does not express the CD138 (Seidel, Børset et al. 2000).

3.8 Photothermal Theraphy

Selectively targeting of cancer using photothermal therapy effects have been carried out for several year. Particulary, gold nanorods with their tunable aspect ratio scatter light in the near infrared region and are efficient to destroy cancerous cells without effecting the surrounding tissues. Since tissue penetration of light is lower than the light energy required to make gold nanorods (Weissleder 2001) convert light into heat, it is possible to use lasers at this wavelength.

In this current work, U266 and ARH-77 cells were irradiated with red laser at 633 nm with 20 mW power. Photodestruction of cancerous cells was assessed using Trypan Blue assay. Cell viability was calculated assuming the viability of control groups 100 %. Figure 3.35 shown at below indicates the cell viability after exposure to laser for 10 minutes respectively. Contrary to control groups, laser irradiation for PEG-GNR and anti-CD138 conjugated PEG-GNR exposured cells, was resulted in the decrease in cell viability. CD138 overexpressed on U266 cells, enhanced the efficiency of photodestruction using GNRs. In other words, it is easy to reach the cell membrane for anti-CD138 conjugated GNRs and more heat is transffered to the CD138 overexpressing cells.
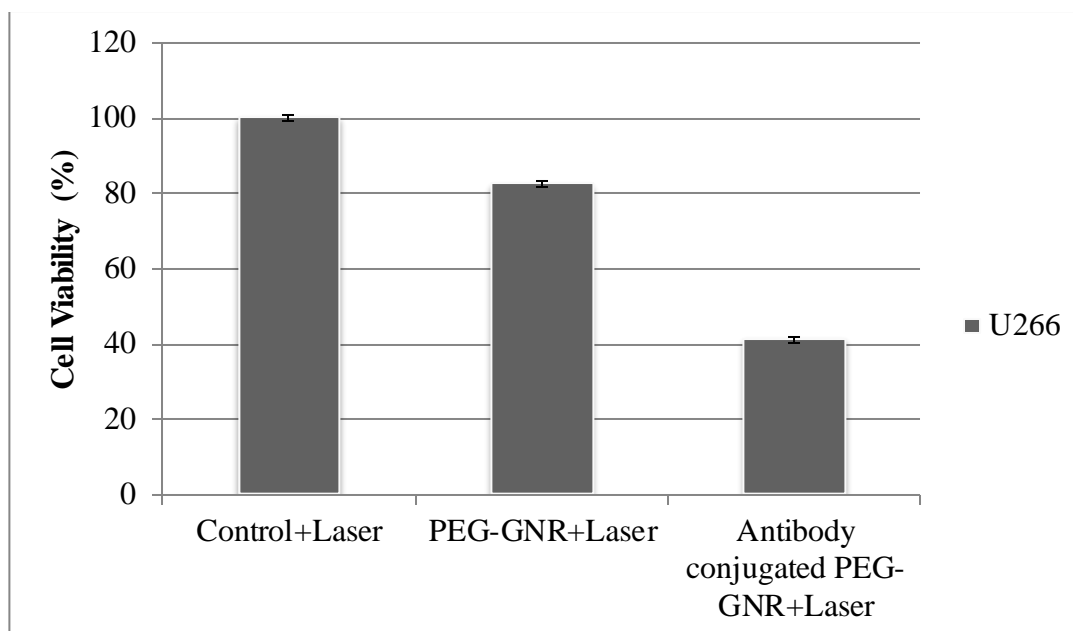
Figure 3.35 : Cell viability assay using Trypan Blue illustrates the percentage of cell survival in U266 cells after photothermal theraphy with laser only, PEG-GNR plus laser and laser plus PEG-GNR conjuagted to anti-CD138 antibody.

Similar results were obtained for ARH-77 cells. In comparison with the results observed in U266 cells, as it can be seen from Figure 3.36, the main difference was that, anti-CD138 conjugated PEG-GNRs does not greatly effect the ARH-77 cell survival as expected. Since CD138 is not expressed on ARH-77 cell line. As it is demonstrated in the previous works (Black, Kirkpatrick et al. 2008), gold nanorods are potential canditates for selectively targeting of cancer cells.
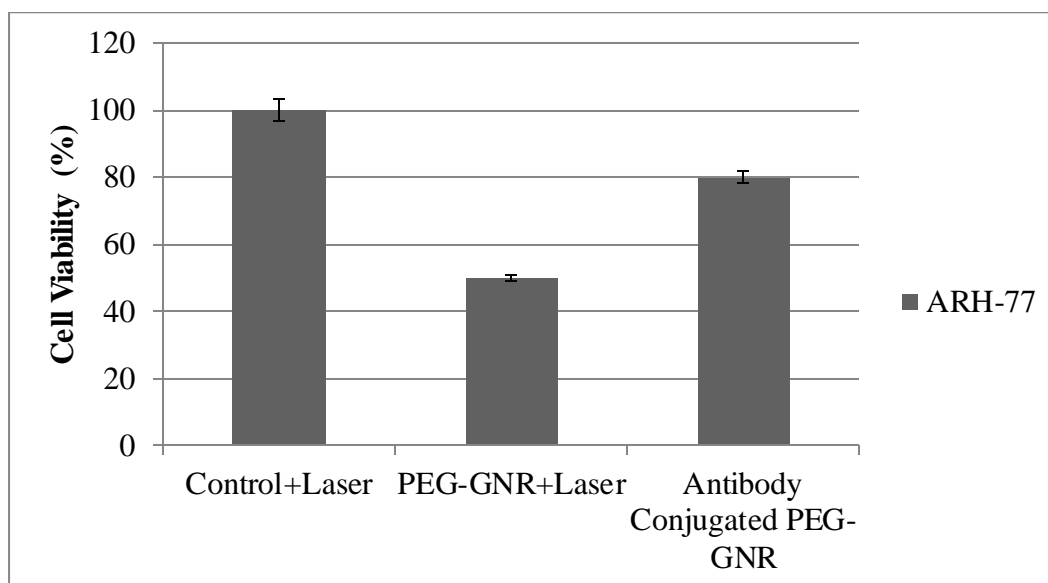
Figure 3.36 : Cell viability assay using Trypan Blue illustrates the percentage of cell survival in U266 cells after photothermal theraphy with laser only, PEG-GNR plus laser and laser plus PEG-GNR conjuagted to anti-CD138 antibody.

As it was demonstrated by Kumar et al. Caspase 3 activity proved that antibody conjugated gold nanorods enhance the pecentage of cell mortality relevant to bindigng efficiacy of antibody (Kumar and Abraham 2012). Our results match with the previous results that even at low wavelength laser, gold nanorods are effective for photodestruction of cancer cells. For future studies, irrradiation of cancer cells with increasing wavelentgths and increasing different powers of laser should be carried out to determine the energy thresold for completely destruction of cancer cells, respectively (Huang, El-Sayed et al. 2006). Furthermore, in order to monitor the cell mortality precisely after photothermal therapy, additional characterization techniques are required as well as Trypan Blue (Black, Kirkpatrick et al. 2008).

4. CONCLUSIONS AND RECOMMENDATIONS

The use of gold nanorods as photothermally targeting agents for cancer therapy, has been gaining a great deal of attention recently. Because of the potential use of gold nanorods as a strong and alternative candidates to the current diagnosis and cure techniques, we aimed to selectively target them for Multiple myeloma *in vitro*. First, in order to optimize the required concentration of gold nanorods for cellular assays, two different procedures of seed mediated method were carried out for synthesis. After the synthesis step, the surface coating of gold nanorod was performed using heterobifunctional PEG molecules. The surface chemistry of gold nanorods before and after modification was analysed by AFM, SEM, DLS and UV Spectroscopy. Results confirmed that surface was changed succesfully.

Dose dependent effects of CTAB coated gold nanorods and PEG-coated gold nanorods at different concentrations were tested. The apoptotic effects of CTAB coated gold nanorods were also investigated. Cytotoxicity results exhibited that in the presence of CTAB, gold nanorods were toxic to either U266 and ARH-77 cells. The lethal dose of CTAB coated gold nanorods was found between 25 and 50 μg/ ml of gold atoms concentration. After removal of CTAB via centrifugation and modification of gold nanorod surface with PEG, the toxicity was significantly diminished regarding to PEG molecules. The internalization of PEG- coated gold nanorods by U266 and ARH-77 cells were measured by ICP-MS for 1,5 and 3 h exposure time. The highest uptake was observed after 3 h incubation at the higher concentration. The results found in this study revealed that cellular uptake was time dependent manner. Furthermore, the uptake of anti-CD138 conjugated gold nanorods for each cell line was carried out. The result found for ARH-77 contributed to the fact that ARH-77 cells do not express CD138.

In order to assess the photothermallly treatment of multiple myeloma with gold nanorods, U266 and ARH-77 cells were firstly incubated with PEG coated gold nanorods and anti-CD138 conjugated gold nanorods at 25 μg /ml concentration of gold nanorods for 3 h. After exposure time, each cell was irradiated with 633 nm red laser for 10 minutes. In comparison with control groups, cell viability was reduced due to the photothermal effect of gold nanorods. After antibody conjugation, photothermal destruction of U266 cells were significantly increased contrary to PEG coated control groups. This was due to the delivery of heat coming from gold

nanorods to cellular membrane easily. On the other hand, photothermal effect of gold nanorods on cells was visiualized in comparison with control groups. Yet, the viability of ARH-cells incubated with anti-CD138 conjugated gold nanorods and PEG-coated gold nanorods was not greatly effected by surface chamistry . This also confirms that ARH-77 cells do not express the CD138. However, due to the wavelength and power of laser used in this work, cell viability did not significantly change. For further studies, it will be required to apply the laser with wavelength where gold nanorods strongly excite. Also, to enhance the power of laser more than 20 mW, can be more effective to increase the cell death *in vitro*. This preliminary study of this thesis will contribute to the novel treatment of multiple myeloma via gold nanorods *in vivo*. Furthermore, the use gold nanorods as contrast agents can be also alternative for the diagnosis of cancer in early phase as well as photothermal theraphy.

5. REFERENCES

Albrecht, M. G. and J. A. Creighton (1977). Anomalously intense Raman spectra of pyridine at a silver electrode. *Journal of the American Chemical Society* **99**(15): 5215-5217.

Alkilany, A. M., P. K. Nagaria, C. R. Hexel, T. J. Shaw, C. J. Murphy and M. D. Wyatt (2009). Cellular uptake and cytotoxicity of gold nanorods: molecular origin of cytotoxicity and surface effects. *Small* **5**(6): 701-708.

Alkilany, A. M., L. B. Thompson, S. P. Boulos, P. N. Sisco and C. J. Murphy (2012). Gold nanorods: their potential for photothermal therapeutics and drug delivery, tempered by the complexity of their biological interactions. *Advanced drug delivery reviews* **64**(2): 190-199.

Badr, G., M. K. Al-Sadoon, M. A. Abdel-Maksoud, D. M. Rabah and A. M. El-Toni (2012). Cellular and Molecular Mechanisms Underlie the Anti-Tumor Activities Exerted by Walterinnesia aegyptia Venom Combined with Silica Nanoparticles against Multiple Myeloma Cancer Cell Types. *PloS one* **7**(12): e51661.

Basiruddin, S., A. Saha, N. Pradhan and N. R. Jana (2010). Functionalized Gold Nanorod Solution via Reverse Micelle Based Polyacrylate Coating. *Langmuir* **26**(10): 7475-7481.

Black, K. C., N. D. Kirkpatrick, T. S. Troutman, L. P. Xu, J. Vagner, R. J. Gillies, J. K. Barton, U. Utzinger and M. Romanowski (2008). Gold nanorods targeted to delta opioid receptor: Plasmon-resonant contrast and photothermal agents. *Molecular Imaging* **7**(1): 50-57.

Boca, S. C. and S. Astilean (2010). Detoxification of gold nanorods by conjugation with thiolated poly (ethylene glycol) and their assessment as SERS-active carriers of Raman tags. *Nanotechnology* **21**(23): 235601.

Brown, D. M., C. Dickson, P. Duncan, F. Al-Attili and V. Stone (2010). Interaction between nanoparticles and cytokine proteins: impact on protein and particle functionality. *Nanotechnology* **21**(21): 215104.

C, S. R., J. Kumar, R. V, V. M and A. Abraham (2012). Laser immunotherapy with gold nanorods causes selective killing of tumour cells. *Pharmacol Res* **65**(2): 261-269.

Cabada, T. F., C. S. L. de Pablo, A. M. Serrano, F. del Pozo Guerrero, J. J. S. Olmedo and M. R. Gomez (2012). Induction of cell death in a glioblastoma line by hyperthermic therapy based on gold nanorods. *International journal of nanomedicine* **7**: 1511.

Chang, S.-S., C.-W. Shih, C.-D. Chen, W.-C. Lai and C. C. Wang (1999). The shape transition of gold nanorods. *Langmuir* **15**(3): 701-709.

Chen, H., L. Shao, Q. Li and J. Wang (2013). Gold nanorods and their plasmonic properties. *Chemical Society Reviews*.

Choi, W. I., J.-Y. Kim, C. Kang, C. C. Byeon, Y. H. Kim and G. Tae (2011). Tumor regression in vivo by photothermal therapy based on gold-nanorod-loaded, functional nanocarriers. *ACS nano* **5**(3): 1995-2003.

Cohen, A. and B. Karger (1987). High-performance sodium dodecyl sulfate polyacrylamide gel capillary electrophoresis of peptides and proteins. *Journal of Chromatography A* **397**: 409-417.

Connor, E. E., J. Mwamuka, A. Gole, C. J. Murphy and M. D. Wyatt (2005). Gold nanoparticles are taken up by human cells but do not cause acute cytotoxicity. *Small* **1**(3): 325-327.

Damiano, J. S., A. E. Cress, L. A. Hazlehurst, A. A. Shtil and W. S. Dalton (1999). Cell adhesion mediated drug resistance (CAM-DR): role of integrins and resistance to apoptosis in human myeloma cell lines. *Blood* **93**(5): 1658-1667.

Dickerson, E. B., E. C. Dreaden, X. Huang, I. H. El-Sayed, H. Chu, S. Pushpanketh, J. F. McDonald and M. A. El-Sayed (2008). Gold nanorod assisted near-infrared plasmonic photothermal therapy (PPTT) of squamous cell carcinoma in mice. *Cancer letters* **269**(1): 57-66.

Eck, W., G. Craig, A. Sigdel, G. Ritter, L. J. Old, L. Tang, M. F. Brennan, P. J. Allen and M. D. Mason (2008). PEGylated gold nanoparticles conjugated to monoclonal F19 antibodies as targeted labeling agents for human pancreatic carcinoma tissue. *Acs Nano* **2**(11): 2263-2272.

El-Sayed, I. H., X. Huang and M. A. El-Sayed (2005). Surface plasmon resonance scattering and absorption of anti-EGFR antibody conjugated gold nanoparticles in cancer diagnostics: applications in oral cancer. *Nano letters* **5**(5): 829-834.

Eliaz, R. E. and F. C. Szoka (2001). Liposome-encapsulated doxorubicin targeted to CD44 a strategy to kill CD44-overexpressing tumor cells. *Cancer research* **61**(6): 2592-2601.

Esumi, K., J. Hara, N. Aihara, K. Usui and K. Torigoe (1998). Preparation of anisotropic gold particles using a gemini surfactant template. *Journal of colloid and interface science* **208**(2): 578-581.

Fleischmann, M., P. Hendra and A. McQuillan (1974). Raman spectra of pyridine adsorbed at a silver electrode. *Chemical Physics Letters* **26**(2): 163-166.

Foss Jr, C. A., G. L. Hornyak, J. A. Stockert and C. R. Martin (1994). Template-synthesized nanoscopic gold particles: optical spectra and the effects of particle size and shape. *The Journal of Physical Chemistry* **98**(11): 2963-2971.

Fox, B. A., M. Drury, H.-M. Hu, Z. Cao, E. G. Huntzicker, W. Qie and W. J. Urba (1998). Lipofection indirectly increases expression of endogenous major histocompatibility complex class I molecules on tumor cells. *Cancer gene therapy* **5**(5): 307.

Frens, G. (1972). Particle size and sol stability in metal colloids. *Kolloid-Zeitschrift und Zeitschrift für Polymere* **250**(7): 736-741.

Gormley, A. J., K. Greish, A. Ray, R. Robinson, J. A. Gustafson and H. Ghandehari (2011). Gold nanorod mediated plasmonic photothermal therapy: a tool to enhance macromolecular delivery. *Int J Pharm* **415**(1-2): 315-318.

Grabinski, C., N. Schaeublin, A. Wijaya, H. D'Couto, S. H. Baxamusa, K. Hamad-Schifferli and S. M. Hussain (2011). Effect of gold nanorod surface chemistry on cellular response. *ACS Nano* **5**(4): 2870-2879.

Green, H. N., D. V. Martyshkin, C. M. Rodenburg, E. L. Rosenthal and S. B. Mirov (2011). Gold nanorod bioconjugates for active tumor targeting and photothermal therapy. *Journal of Nanotechnology* .

Gu, Y.-J., J. Cheng, C.-C. Lin, Y. W. Lam, S. H. Cheng and W.-T. Wong (2009). Nuclear penetration of surface functionalized gold nanoparticles. *Toxicology and applied Pharmacology* **237**(2): 196-204.

Harisinghani, M. G., J. Barentsz, P. F. Hahn, W. M. Deserno, S. Tabatabaei, C. H. van de Kaa, J. de la Rosette and R. Weissleder (2003). Noninvasive detection of clinically occult lymph-node metastases in prostate cancer. *New England Journal of Medicine* **348**(25): 2491-2499.

Hartland, G. V. (2011). Optical studies of dynamics in noble metal nanostructures. *Chemical reviews* **111**(6): 3858-3887.

Huang, H.-C., S. Barua, D. B. Kay and K. Rege (2009). Simultaneous enhancement of photothermal stability and gene delivery efficacy of gold nanorods using polyelectrolytes. *Acs Nano* **3**(10): 2941-2952.

Huang, X., S. Neretina and M. A. El-Sayed (2009). Gold nanorods: from synthesis and properties to biological and biomedical applications. *Advanced Materials* **21**(48): 4880-4910.

Huang, X. H., I. H. El-Sayed, W. Qian and M. A. El-Sayed (2006). Cancer cell imaging and photothermal therapy in the near-infrared region by using gold nanorods. *Journal of the American Chemical Society* **128**(6): 2115-2120.

Hubert, F., F. Testard, G. Rizza and O. Spalla (2010). Nanorods versus Nanospheres: A Bifurcation Mechanism Revealed by Principal Component TEM Analysis. *Langmuir* **26**(10): 6887-6891.

Huff, T. B., L. Tong, Y. Zhao, M. N. Hansen, J.-X. Cheng and A. Wei (2007). Hyperthermic effects of gold nanorods on tumor cells.

Ishii, Y., H.-H. Hsiao, G. Sashida, Y. Ito, K. Miyazawa, A. Kodama, J. H. Ohyashiki and K. Ohyashiki (2006). Derivative (1; 7)(q10; p10) in multiple myeloma. A sign of therapy-related hidden myelodysplastic syndrome. *Cancer genetics and cytogenetics* **167**(2): 131-137.

Jain, P. K., K. S. Lee, I. H. El-Sayed and M. A. El-Sayed (2006). Calculated absorption and scattering properties of gold nanoparticles of different size, shape, and composition: applications in biological imaging and biomedicine. *The Journal of Physical Chemistry B* **110**(14): 7238-7248.

Jain, R. K. (1999). Transport of molecules, particles, and cells in solid tumors. *Annual review of biomedical engineering* **1**(1): 241-263.

Jana, N. R., L. Gearheart and C. J. Murphy (2001). Wet chemical synthesis of high aspect ratio cylindrical gold nanorods. *The Journal of Physical Chemistry B* **105**(19): 4065-4067.

Jin, H., P. Yang, J. Cai, J. Wang and M. Liu (2012). Photothermal effects of folate-conjugated Au nanorods on HepG2 cells. *Applied microbiology and biotechnology* **94**(5): 1199-1208.

José Alonso, M. (2004). Nanomedicines for overcoming biological barriers. *Biomedicine & Pharmacotherapy* **58**(3): 168-172.

Kapp, D., G. Hahn and R. Carlson (2000). Principles of hyperthermia. *Cancer medicine* **5**(5).

Keblinski, P., D. G. Cahill, A. Bodapati, C. R. Sullivan and T. A. Taton (2006). Limits of localized heating by electromagnetically excited nanoparticles. *Journal of applied physics* **100**(5): 054305-054305-054305.

Kim, C. K., P. Ghosh, C. Pagliuca, Z.-J. Zhu, S. Menichetti and V. M. Rotello (2009). Entrapment of hydrophobic drugs in nanoparticle monolayers with efficient release into cancer cells. *Journal of the American Chemical Society* **131**(4): 1360-1361.

Kim, E. Y., R. Schulz, P. Swantek, K. Kunstman, M. H. Malim and S. M. Wolinsky (2012). Gold nanoparticle-mediated gene delivery induces widespread changes in the expression of innate immunity genes. *Gene Therapy* **19**(3): 347-353.

Kim, F., J. H. Song and P. Yang (2002). Photochemical synthesis of gold nanorods. *Journal of the American Chemical Society* **124**(48): 14316-14317.

Kiziltepe, T., J. D. Ashley, J. F. Stefanick, Y. M. Qi, N. J. Alves, M. W. Handlogten, M. A. Suckow, R. M. Navari and B. Bilgicer (2012). Rationally engineered nanoparticles target multiple myeloma cells, overcome cell-adhesion-mediated drug resistance, and show enhanced efficacy in vivo. *Blood Cancer Journal* **2**.

Kopwitthaya, A., K. T. Yong, R. Hu, I. Roy, H. Ding, L. A. Vathy, E. J. Bergey and P. N. Prasad (2010). Biocompatible PEGylated gold nanorods as colored contrast agents for targeted in vivo cancer applications. *Nanotechnology* **21**(31): 315101.

Kreibig, U. and M. Vollmer (1995). Optical properties of metal clusters.

Kumar, J. and A. Abraham (2012). Laser immunotherapy with gold nanorods causes selective killing of tumour cells. *Pharmacological Research* **65**(2): 261-269.

Kuo, T.-R., V. A. Hovhannisyan, Y.-C. Chao, S.-L. Chao, S.-J. Chiang, S.-J. Lin, C.-Y. Dong and C.-C. Chen (2010). Multiple release kinetics of targeted drug from gold nanorod embedded polyelectrolyte conjugates induced by near-infrared laser irradiation. *Journal of the American Chemical Society* **132**(40): 14163-14171.

KyuáLee, E., S. YoungáShin, S. WookáSon, C. HwanáOh, J. MyongáSong and S. HoáKang (2009). SERS imaging of HER2-overexpressed MCF7 cells using antibody-conjugated gold nanorods. *Physical Chemistry Chemical Physics* **11**(34): 7444-7449.

Lau, I. P., H. Chen, J. Wang, H. C. Ong, K. C.-F. Leung, H. P. Ho and S. K. Kong (2012). In vitro effect of CTAB-and PEG-coated gold nanorods on the induction of eryptosis/erythroptosis in human erythrocytes. *Nanotoxicology* **6**(8): 847-856.

Lee, K.-S. and M. A. El-Sayed (2006). Gold and silver nanoparticles in sensing and imaging: sensitivity of plasmon response to size, shape, and metal composition. *The Journal of Physical Chemistry B* **110**(39): 19220-19225.

Leontidis, E., K. Kleitou, T. Kyprianidou-Leodidou, V. Bekiari and P. Lianos (2002). Gold colloids from cationic surfactant solutions. 1. Mechanisms that control particle morphology. *Langmuir* **18**(9): 3659-3668.

Li, P.-Y., P.-S. Lai, W.-C. Hung and W.-J. Syu (2010). Poly (l-lactide)-vitamin E TPGS nanoparticles enhanced the cytotoxicity of doxorubicin in drug-resistant MCF-7 breast cancer cells. *Biomacromolecules* **11**(10): 2576-2582.

Link, S. and M. El-Sayed (2000). International Rev. *Phys. Chem* **19**: 409-453.

Link, S. and M. A. El-Sayed (1999). Spectral properties and relaxation dynamics of surface plasmon electronic oscillations in gold and silver nanodots and nanorods. *The Journal of Physical Chemistry B* **103**(40): 8410-8426.

Liopo, A. V., A. Conjusteau, O. V. Chumakova, S. A. Ermilov, R. Su and A. A. Oraevsky (2012). Highly purified biocompatible gold nanorods for contrasted optoacoustic imaging of small animal models. *Nanoscience and nanotechnology letters* (Print) **4**(7): 681.

Martin, C. R. (1996). Membrane-based synthesis of nanomaterials. *Chemistry of Materials* **8**(8): 1739-1746.

Matsumura, Y. and H. Maeda (1986). A new concept for macromolecular therapeutics in cancer chemotherapy: mechanism of tumoritropic accumulation of proteins and the antitumor agent smancs. *Cancer research* **46**(12 Part 1): 6387-6392.

McCarthy, J. R., K. A. Kelly, E. Y. Sun and R. Weissleder (2007). Targeted delivery of multifunctional magnetic nanoparticles. *Nanomedicine* **2**(2): 153-167.

Medarova, Z., W. Pham, C. Farrar, V. Petkova and A. Moore (2007). In vivo imaging of siRNA delivery and silencing in tumors. *Nature medicine* **13**(3): 372-377.

Niidome, T., M. Yamagata, Y. Okamoto, Y. Akiyama, H. Takahashi, T. Kawano, Y. Katayama and Y. Niidome (2006). PEG-modified gold nanorods with a stealth character for in vivo applications. *J Control Release* **114**(3): 343-347.

Niidome, Y., K. Nishioka, H. Kawasaki and S. Yamada (2003). Rapid synthesis of gold nanorods by the combination of chemical reduction and photoirradiation processes; morphological changes depending on the growing processes. *Chem. Commun.*(18): 2376-2377.

Nikoobakht, B. and M. A. El-Sayed (2003). Preparation and growth mechanism of gold nanorods (NRs) using seed-mediated growth method. *Chemistry of Materials* **15**(10): 1957-1962.

Norman, R. S., J. W. Stone, A. Gole, C. J. Murphy and T. L. Sabo-Attwood (2008). Targeted photothermal lysis of the pathogenic bacteria, Pseudomonas aeruginosa, with gold nanorods. *Nano letters* **8**(1): 302-306.

Pal, T., De, N. R. Jana, N. Pradhan, R. Mandal, A. Pal, A. Beezer and J. Mitchell (1998). Organized media as redox catalysts. *Langmuir* **14**(17): 4724-4730.

Papavassiliou, G. C. (1979). Optical properties of small inorganic and organic metal particles. *Progress in Solid State Chemistry* **12**(3): 185-271.

Patel, P. C., D. A. Giljohann, W. L. Daniel, D. Zheng, A. E. Prigodich and C. A. Mirkin (2010). Scavenger receptors mediate cellular uptake of polyvalent oligonucleotide-functionalized gold nanoparticles. *Bioconjug Chem* **21**(12): 2250-2256.

Pelicano, H., D. Martin, R. Xu, and and P. Huang (2006). Glycolysis inhibition for anticancer treatment. *Oncogene* **25**(34): 4633-4646.

Perez-Juste, J., I. Pastoriza-Santos, L. M. Liz-Marzan and P. Mulvaney (2005). Gold nanorods: synthesis, characterization and applications. *Coordination Chemistry Reviews* **249**(17): 1870-1901.

Picot, J., K. Cooper, J. Bryant and A. Clegg (2011). The clinical effectiveness and cost-effectiveness of bortezomib and thalidomide in combination

regimens with an alkylating agent and a corticosteroid for the first-line treatment of multiple myeloma: a systematic review and economic evaluation.

Placido, T., R. Comparelli, F. Giannici, P. D. Cozzoli, G. Capitani, M. Striccoli, A. Agostiano and M. L. Curri (2009). Photochemical synthesis of water-soluble gold nanorods: the role of silver in assisting anisotropic growth. *Chemistry of materials* **21**(18): 4192-4202.

Prasad, V., A. Mikhailovsky and J. Zasadzinski (2005). Inside-out disruption of silica/gold core-shell nanoparticles by pulsed laser irradiation. *Langmuir* **21**(16): 7528-7532.

Qiu, Y., Y. Liu, L. Wang, L. Xu, R. Bai, Y. Ji, X. Wu, Y. Zhao, Y. Li and C. Chen (2010). Surface chemistry and aspect ratio mediated cellular uptake of Au nanorods. *Biomaterials* **31**(30): 7606-7619.

Ramos, J. and K. Rege (2012). Transgene delivery using poly (amino ether)-gold nanorod assemblies. *Biotechnology and bioengineering* **109**(5): 1336-1346.

Rayavarapu, R. G. (2010). Gold nanorods as molecular probes for light-based imaging techniques, University of Twente.

Reuveni, T., M. Motiei, Z. Romman, A. Popovtzer and R. Popovtzer (2011). Targeted gold nanoparticles enable molecular CT imaging of cancer: an in vivo study. *International journal of nanomedicine* **6**: 2859.

Roberts, M., M. Bentley and J. Harris (2012). Chemistry for peptide and protein PEGylation. *Advanced drug delivery reviews*.

Rostro-Kohanloo, B. C., L. R. Bickford, C. M. Payne, E. S. Day, L. J. Anderson, M. Zhong, S. Lee, K. M. Mayer, T. Zal and L. Adam (2009). The stabilization and targeting of surfactant-synthesized gold nanorods. *Nanotechnology* **20**(43): 434005.

Sanz-rodríguez, F. and J. Teixidó (2001). VLA-4-dependent myeloma cell adhesion. *Leukemia & lymphoma* **41**(3-4): 239-245.

Sau, T. K. and C. J. Murphy (2004). Room temperature, high-yield synthesis of multiple shapes of gold nanoparticles in aqueous solution. *Journal of the American Chemical Society* **126**(28): 8648-8649.

Seidel, C., M. Børset, Ø. Hjertner, D. Cao, N. Abildgaard, H. Hjorth-Hansen, R. D. Sanderson, A. Waage and A. Sundan (2000). High levels of soluble syndecan-1 in myeloma-derived bone marrow: modulation of hepatocyte growth factor activity. *Blood* **96**(9): 3139-3146.

Singh, S., H. Grossniklaus, S. Kang, H. Edelhauser, B. Ambati and U. Kompella (2009). Intravenous transferrin, RGD peptide and dual-targeted nanoparticles enhance anti-VEGF intraceptor gene delivery to laser-induced CNV. *Gene therapy* **16**(5): 645-659.

Strickland, A. D. and C. A. Batt (2009). Detection of carbendazim by surface-enhanced Raman scattering using cyclodextrin inclusion complexes on gold nanorods. *Analytical chemistry* **81**(8): 2895-2903.

Takahashi, H., T. Niidome, T. Kawano, S. Yamada and Y. Niidome (2008). Surface modification of gold nanorods using layer-by-layer technique for cellular uptake. *Journal of Nanoparticle Research* **10**(1): 221-228.

Takahashi, H., Y. Niidome, T. Niidome, K. Kaneko, H. Kawasaki and S. Yamada (2006). Modification of gold nanorods using phosphatidylcholine to reduce cytotoxicity. *Langmuir* **22**(1): 2-5.

Toernblom, M., U. Henriksson and M. Ginley (1994). A field dependent 2H nuclear magnetic relaxation study of the aggregation behavior in micellar solutions of CTAB and SDS. *The Journal of Physical Chemistry* **98**(28): 7041-7051.

Turkevich, J., P. C. Stevenson and J. Hillier (1951). "A study of the nucleation and growth processes in the synthesis of colloidal gold." <u>Discussions of the Faraday Society</u> **11**: 55-75.

van der Zande, B. M., M. R. Böhmer, L. G. Fokkink and C. Schönenberger (2000). Colloidal dispersions of gold rods: synthesis and optical properties. *Langmuir* **16**(2): 451-458.

Vermes, I., C. Haanen, H. Steffens-Nakken and C. Reutellingsperger (1995). A novel assay for apoptosis flow cytometric detection of phosphatidylserine expression on early apoptotic cells using fluorescein labelled annexin V. *Journal of immunological methods* **184**(1): 39-51.

Vigderman, L., B. P. Khanal and E. R. Zubarev (2012). Functional Gold Nanorods: Synthesis, Self-Assembly, and Sensing Applications. *Advanced Materials* **24**(36): 4811-4841.

Wang, X., Y. Q. Wang, Z. Chen and D. M. Shin (2009). Advances of Cancer Therapy by Nanotechnology. *Cancer Research and Treatment* **41**(1): 1-11.

Wang, Y. W., X. Y. Xie, X. D. Wang, G. Ku, K. L. Gill, D. P. O'Neal, G. Stoica and L. V. Wang (2004). Photoacoustic tomography of a nanoshell contrast agent in the in vivo rat brain. *Nano Letters* **4**(9): 1689-1692.

Wei, Z., A. J. Mieszawska and F. P. Zamborini (2004). Synthesis and manipulation of high aspect ratio gold nanorods grown directly on surfaces. *Langmuir* **20**(11): 4322-4326.

Weissleder, R. (2001). A clearer vision for in vivo imaging. *Nature biotechnology* **19**(4): 316-316.

Woodle, M. C. and P. Y. Lu (2005). Nanoparticles deliver RNAi therapy. *Materials Today* **8**(8): 34-41.

Wust, P., B. Hildebrandt, G. Sreenivasa, B. Rau, J. Gellermann, H. Riess, R. Felix and P. Schlag (2002). Hyperthermia in combined treatment of cancer. *The lancet oncology* **3**(8): 487-497.

Xiao, Y., H. Hong, V. Z. Matson, A. Javadi, W. Xu, Y. Yang, Y. Zhang, J. W. Engle, R. J. Nickles and W. Cai (2012). Gold nanorods conjugated with doxorubicin and cRGD for combined anticancer drug delivery and PET imaging. *Theranostics* **2**(8): 757.

Zhang, W., J. Meng, Y. Ji, X. Li, H. Kong, X. Wu and H. Xu (2011). Inhibiting metastasis of breast cancer cells in vitro using gold nanorod-siRNA delivery system. *Nanoscale* **3**(9): 3923-3932.

Zhang, Z., J. Wang and C. Chen (2013). Gold nanorods based platforms for light-mediated theranostics. *Theranostics* **3**(3): 223.
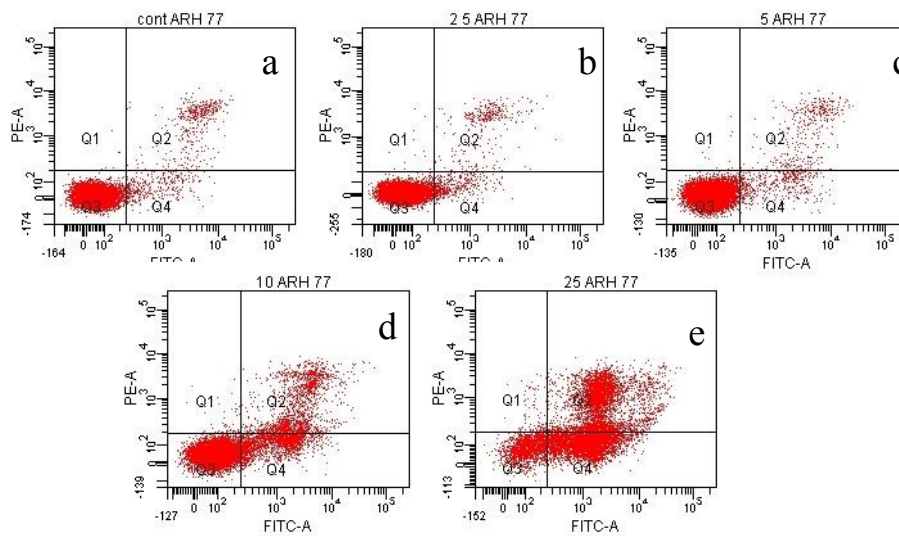
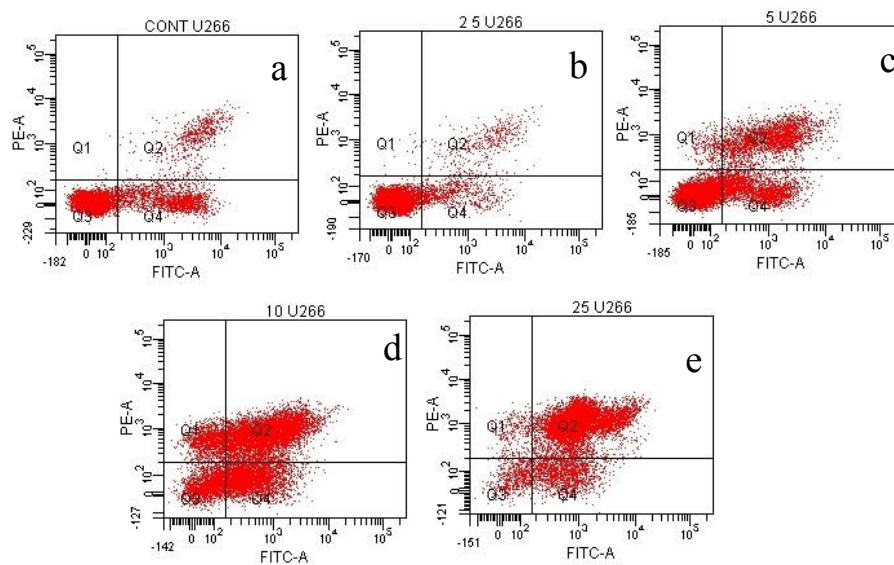**APPENDIX A: Illustration Of Dot Plots After Annexin V Staining**
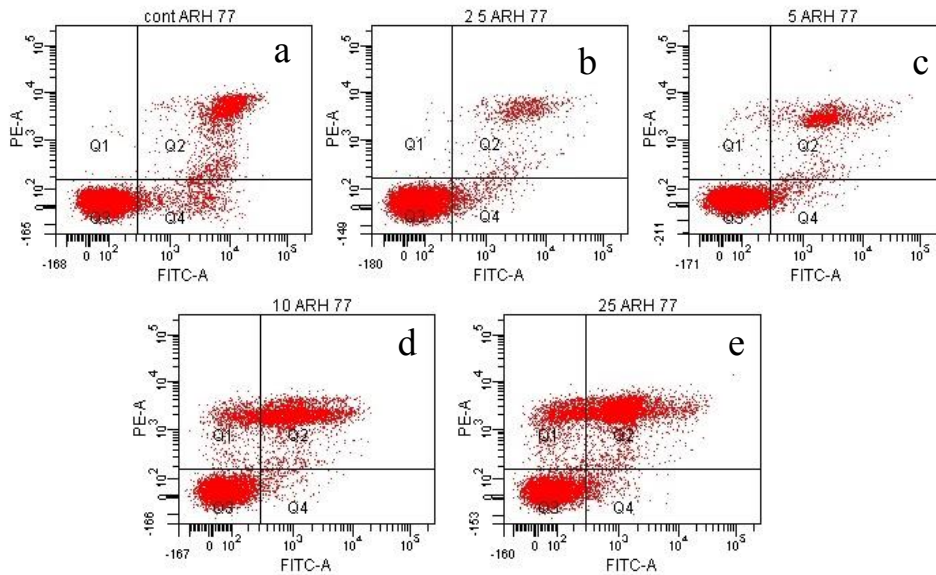
Figure A.1 : Representation of dot plots of annexin V staining for U266 cells exposed to CTAB-GNRs for 24 h incubation period. a) Control. b) 2,5 μg/ml.c) 5 μg/ml d) 10 μg/ml e)25 μg/ml .
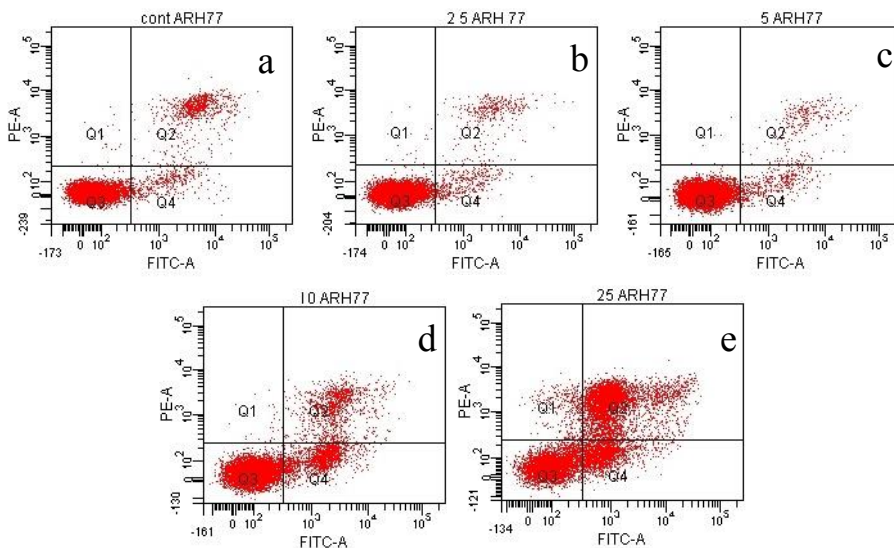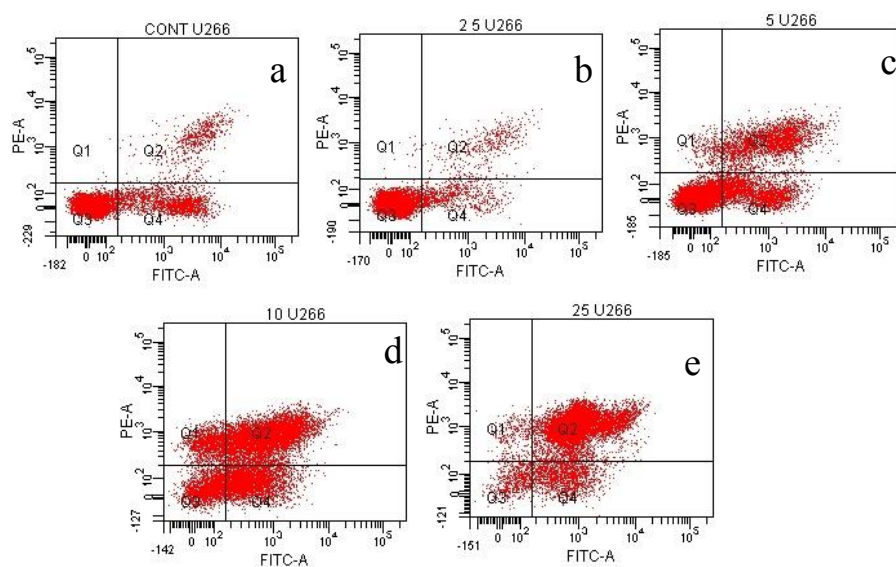

Figure A.2 : Representation of dot plots of annexin V staining for ARH-77 cells exposed to CTAB-GNRs for 48 h incubation period. a) Control. b) 2,5 μg/ml c) 5 μg/ml d) 10 μg/ml e)25 μg/ml.
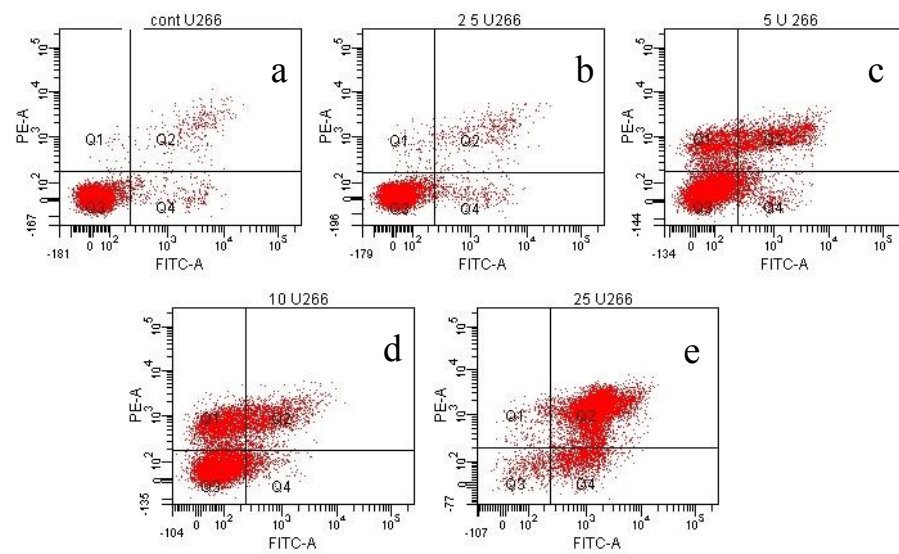
Figure A.3 : Representation of dot plots of annexin V staining for ARH-77cells exposed to CTAB-GNRs for 72 h incubation period.a) Control. b) 2,5 μg/ml c) 5 μg/ml d) 10 μg/ml e)25 μg/ml.

Figure A.4 : Representation of dot plots of annexin V staining for U266 cells exposed to CTAB-GNRs for 24 h incubation period. a) Control. b) 2,5 μg/ml c) 5 μg/ml d) 10 μg/ml e)25 μg/ml.

Figure A.5 : Representation of dot plots of annexin V staining for U266
cells exposed to CTAB-GNRs for 48 h incubation period. a)
Control. b) 2,5 μg/ml c) 5 μg/ml d) 10 μg/ml e)25 μg/ml.

Figure A.6 : Representation of dot plots of annexin V staining for U266 cells exposed to CTAB-GNRs for 72 h incubation period. . a) Control. b) 2,5 µg/ml c) 5 µg/ml d) 10 µg/ml e)25 µg/ml.

CURRICULUM VITAE

Name Surname: Gülşah MALGIR

Place and Date of Birth: ALAŞEHİR, 28.09.1987

Address: İstasyon Mh. Gecit Sk. Alaşehir-MANİSA

E-Mail: gulsah_malgir@gmail.com

B.Sc.: Bioengineering

M.Sc.: Nanotechnology

Research Interests

Bioengineering	Gene Theraphy
Nanobiotechnology	Cancer
Drug Delivery	Biomaterials

Work Experience

(July-August, 2008) Plant Genetics and Molecular Biology Laboratory, Ebiltem, Ege University

(15th June- 15th July 2010) Molecular Diagnostic Laboratory , Genetic & Bioengineering Department, Yeditepe University

(3th August-26th August 2010) Genetic Diagnostic Center, Pamukkale University Medical School

(2012-present) Helping Project Management Office, Gediz University

Lab Skills and Techniques

Cell culture, MTT assay, PCR, DNA extraction, AFM, Dynamic Light Scattering, Surface Plasmon Resonance, Localized Surface Plasmon Resonance, SDS-PAGE

Certificates

- Advances in Applied Physics and Material Science Congress, Antalya, 2012

- II.Stem Cell symposium, İzmir, 2010

- Cancer Workshop, Ege University Medical School, İzmir, 2010

- Certificate of Training on plant genetic, Ege University, İzmir, 2009

- I.Stem Cell Symposium, Ege University, İzmir, 2009

- ITU 3. International Student Congress, İstanbul, 2009

Honours and Awards

- **2011- -** Admitted to Gediz University Nanotechnology Program **with full scholarship** with the **highest** ranking among applicants.

- **2005-present-** Scholarship that is given for successful students from Turkish Government

- **2002-** awarded as **honoured student of the year** by Alasehir High School Administration

- **2001-** awarded in the Secondary School assay competition **ranked as 3rd** around city.

References

Available upon request